BUDAPEST UNIVERSITY OF TECHNOLOGY AND ECONOMICS
FACULTY OF CHEMICAL AND BIOENGINEERING
GEORGE OLAH DOCTORAL SCHOOL

SYNTHESIS AND STUDY OF GOLD CATALYSTS IN CO OXIDATION AND SELECTIVE OXIDATION OF GLUCOSE

Ph.D. Dissertation

Author: Tímea Benkó
Supervisor: Prof. Zoltán Schay, D.Sc.
Consultants: Andrea Vargáné Beck, C.Sc.
Anita Nagyné Horváth, Ph.D.

Department of Surface Chemistry and Catalysis
Centre for Energy Reserarch
Hungarian Academy of Sciences

Budapest – 2014

Köszönetnyilvánítás

Szeretném megköszönni témavezetőmnek, Schay Zoltánnak a munkám során nyújtott segítséget, iránymutató tanácsait és támogatását. Köszönettel tartozom Vargáné Beck Andreának szakmai támogatásáért és a mindennapok problémáinak megoldásában nyújtott segítségéért. Köszönöm Nagyné Horváth Anitának a szakmai segítséget, a publikációim alapos lektorálását és a baráti beszélgetéseket. Köszönöm Frey Krisztinának a munkám során nyújtott segítséget.

Hálával emlékszem Guczi László Professzor úrra, akinek szakmai tanácsai és jó szándékú kritikái segítették doktori munkámat.

Köszönöm Tungler Antal Professzor úrnak a hasznos tanácsokat, amellyel munkámat segítette.

Köszönöm Geszti Olgának a TEM mérések elvégzését és a kiértékelésben nyújtott rengeteg segítséget. Köszönöm Sáfrán Györgynek az együttműködést és a HRTEM méréseket. Köszönöm továbbá Srankó Dávid Ferencnek az XPS méréseket, Stefler Györgyinek a CO oxidációs méréseket, Kocsonya Andrásnak az XRF méréseket, Maróti Boglárkának a PGAA méréseket, Katona Róbertnek és Varga Zsoltnak az ICP-MS méréseket és Gubicza Jenőnek az XRD méréseket.

Köszönettel tartozom opponenseimnek Valyon József Professzor úrnak és Somodi Ferencnek az építő kritikáért és javaslatokért, melyek hozzájárultak jelen dolgozat végső formájának létrejöttéhez.

Köszönöm a Felületkémiai és Katalízis Laboratórium vezetőjének és összes dolgozójának, különösen Szabados Erikának, mindennemű segítségét és kedvességét, amellyel kellemes légkört teremtettek munkám elvégzéséhez.

Köszönöm az Energiatudományi Kutatóközpontnak és elődjének az Izotópkutató Intézetnek, hogy lehetővé tette doktori munkám végzését.

Köszönöm a Közigazgatási és Igazságügyi Hivatal Nemzeti Kiválóság Program TÁMOP-4.2.4.A/2-11/1-2012-0001 anyagi támogatását.

Köszönöm családomnak és barátaimnak, különösen Szüleimnek, Férjemnek és Kisfiamnak, hogy támogatásukkal, türelmükkel és bátorításukkal hozzájárultak e disszertáció létrejöttéhez.

Table of contents

Summary

In gold catalysis the performance of a supported catalyst is affected by the size, the distribution of the gold nanoparticles, the type and the structure of the support material and the different types of additives. The knowledge obtained about the behavior of gold as catalyst is not consistent and complete.

Based on the need for better understanding the activity – structure relationship of nanostructured gold, which leads us to improve the catalysts performance, modified supported gold catalysts were developed for CO oxidation and glucose oxidation reactions in this work.

First, unmodified gold catalysts of two different gold particle sizes supported on reducible (TiO_2, CeO_2) and irreducible (SiO_2) oxides were prepared and their catalytic behaviors were compared in CO and glucose oxidation (Chapter 5.1). A correlation was found between the temperature required for 50% CO conversion and the glucose oxidation reaction rate, the activity order of the catalysts was reverse in the two reactions. This result revealed that the known support and size effect in CO oxidation is not valid for glucose oxidation. In the latter reaction weak metal – support interaction is favored, the silica supported catalysts showed higher activity than the ceria or titania supported ones. The higher activity of the larger gold particles found in glucose oxidation is explained by the different

surface geometry needs for the larger glucose molecule compared to CO.

In CO oxidation further development of the most active Au/CeO_2 catalysts was carried out. For this purpose Au/SiO_2 catalysts modified by different amount of CeO_2 in a special way, when nanosize Au decorated with CeO_2 patches were prepared (Chapter 5.2). High resolution transmission electron microscopy (HRTEM) measurements revealed thin, nanosize CeO_2 moieties over gold already at extremely low 0.04wt% CeO_2 loading, which decreased the temperature of 50% CO conversion by 280°C compared to Au/SiO_2 reference. 0.16wt% CeO_2 was enough to approach the activity of the Au/CeO_2 reference sample. At 0.6wt% CeO_2 content the catalyst greatly exceeded the activity of the pure Au/CeO_2 used as reference. Further increase of the CeO_2 content above 0.6wt% did not change the activity significantly. HRTEM proved that up to this concentration ceria is attached onto gold surface and further increase in Ce-loading caused CeO_2 spread over the support surface as well. Strong interaction of Ce species with stabilizer ligands located around Au is suggested as the reason for CeO_2 localization on gold.

For the development of the most active Au/SiO_2 catalysts in selective glucose oxidation the addition of silver to Au nanoparticles was decided. Addition of a second metal to gold resulted synergetic activity increase in many oxidation reactions. AgAu bimetallic nanoparticles also have shown increased activity in glucose oxidation but supported AgAu nanoparticles were firstly applied in this work.

SiO_2 supported AgAu bimetallic catalysts were prepared by sol adsorption method with 10/90, 20/80, 33/67 and 50/50 Ag/Au molar

ratios (Chapter 5.3). UV-visible spectroscopy and HRTEM proved that the reduction of $HAuCl_4$ in Ag sol resulted in alloyed AgAu colloid particles and their alloyed structure remained after calcination and reduction treatment. The AuAg bimetallic effect and its dependence on the Ag/Au molar ratio were studied in glucose oxidation. Synergistic activity increase was observed compared to the Au/SiO_2 reference sample in case of the bimetallic samples up to Ag/Au=33/67 molar ratio. Maximum activity was reached at Ag/Au=20/80. Oxidation/reduction pretreatment slightly affected the activity of the catalysts; however the sequence of the samples remained the same. A reaction mechanism was proposed for glucose oxidation over our silica supported silver – gold catalysts, which is consistent with our experimental results and based on previous studies for alcohol oxidation and glucose oxidation on gold catalysts. The higher activity of the bimetallic samples is suggested to be caused by the improved O_2 activating ability provided by Ag sites. The further increase of Ag loading above the optimal concentration may dilute or cover the Au to such an extent that the number of gold ensembles necessary for glucose activation decreases deteriorating the activity.

Characterization of the parent monometallic Ag sol by HRTEM and Selected Area Electron Diffraction (SAED) showed the coexistence of the commonly known face centered cubic crystal phase of Ag nanospheres with the rarely observed hexagonal *4H–A*g structure in the same concentration. This hexagonal polytype of Ag has been observed, to date, only in nanocrystalline and continuous

films or nanorods; in nanospherical form it was reported, to the best of my knowledge, for the first time.

Összefoglalás

Arany katalizátorokon az elérhető aktivitást és szelektivitást alapvetően befolyásolja az arany nanorészecskék mérete és eloszlása, a szemcséhez kapcsolt oxid fázis szerkezete és mérete és a különböző módosítók hatása. Az arany nanorészecskék katalitikus tulajdonságairól a szakirodalomban közzétett tudás nem teljes és nem egységes. A katalizátorok szerkezete és aktivitása közötti összefüggések jobb megértése révén egyre jobb katalizátorokat fejleszthetünk.

Ebben a munkában arany nanorészecskéket tartalmazó katalizátorok szerkezet – aktivitás összefüggéseinek kutatásával foglalkozom, melyet egyfémes oxidhordozós és módosított kétfémes illetve oxid promoveált hordozós arany katalizátorok előállításával, CO oxidáció és glükóz oxidáció reakciókban mutatott viselkedésének vizsgálatával valósítottam meg.

Először módosítatlan, redukálható (TiO_2 és CeO_2) és nem-redukálható (SiO_2) oxid–hordozós két különböző méretű arany nanorészecskéket tartalmazó katalizátorokat állítottam elő és aktivitásukat hasonlítottam össze CO oxidációban és glükóz oxidációban (Chapter 5.1). Ellentétes sorrendet állapítottam meg a minták aktivitása között CO oxidációban és glükóz oxidációban. A katalitikus aktivitást CO oxidációban az 50%-os CO konverzió eléréséhez szükséges hőmérséklet tükrözi, míg glükóz oxidációban a kezdeti reakciósebességből számítottam.

Megállapítottam, hogy a CO oxidációban ismert méret– és hordozó– hatás nem érvényes glükóz szelektív oxidációjában, ebben a reakcióban ugyanis az inert szilícium–oxid hordozós katalizátorok jóval aktívabbnak bizonyultak, mint a cérium–oxid ill. titán–oxid hordozós minták. A nagyobb Au részecskeméretű minták nagyobb aktivitást mutattak glükóz oxidációban, ami azzal magyarázok, hogy a szén-monoxidhoz képest nagyobb glükóz molekula aktiválásához eltérő felületi geometriájú aktív centrumok szükségesek.

CO oxidációban a vizsgált egyfémes minták közül az Au/CeO_2 katalizátort találtam az egyik legaktívabbnak. A katalizátor aktivitásának növelését és a cérium–oxid szerepének vizsgálatát tűzve ki célul, ú.n. inverz katalizátorokat állítottam elő, amit inert–hordozós Au katalizátor cérium-oxiddal történő módosításával valósítottam meg. Nagy felbontású transzmissziós elektronmikroszkópos (HRTEM) vizsgálatok nanoméretű CeO_2-ot mutattak az arany felületén már 0,04wt% CeO_2 koncentrációnál, ami 280°C-al csökkentette az 50%-os CO konverzió hőmérsékletét az Au/SiO_2 referenciához viszonyítva. A 0,16wt% CeO_2-ot tartalmazó katalizátor aktivitása elérte az Au/CeO_2 referencia aktivitását, és a 0,6wt% CeO_2 tartalmú minta már jóval aktívabb volt, mint a cérium-oxidot hordozóként tartalmazó katalizátor. 0,6wt% CeO_2 tartalom fölött az aktivitás nem változott jelentősen, és sokkal nagyobb volt, mint a referencia Au/CeO_2 aktivitása. HRTEM mérések azt mutatták, hogy eddig a koncentrációig a CeO_2 inkább az arany felületén helyezkedik el, 0,6wt% fölött azonban már a hordozó SiO_2 felületén stabilizálódik. A Ce specieszek és az arany körüli stabilizátor ligandumok erős kölcsönhatása lehet az oka, hogy a CeO_2 inkább az

arany felületén helyezkedik el. Az Au–CeO_2 aktív periméter a promoveált mintában nagyobb fajlagos aktivitású, mint a CeO_2 hordozós arany katalizátorban.

Glükóz szelektív oxidációjához a reakcióban legaktívabb minta módosításával kívántam aktívabb katalizátort előállítani és vizsgálni a módosítás hatását. Az arany nanorészecskéket ezüsttel módosítottam, amivel az arany oxigén–aktiváló képességét kívántam befolyásolni. A szakirodalom szerint a hordozó nélküli AgAu kétfémes nanorészecskékkel glükóz oxidációban jelentős aktivitás növekedés érthető el az egyfémes aranyhoz képest, a gyakorlati szempontból előnyösebb hordozós AgAu katalizátorok alkalmazása azonban ebben a munkában jelenik meg először glükóz oxidációban.

A SiO_2 hordozós AgAu kétfémes katalizátorokat szol adszorpciós módszerrel állítottam elő; 10/90, 20/80, 33/67 és 50/50 Ag/Au mól arányban. UV-látható spektroszkópiás és HRTEM mérések igazolták, hogy a $HAuCl_4$ prekurzor nátrium-borohidrides redukciója Ag szolban ötvözet AgAu kolloid részecskéket eredményez és ötvözet szerkezetük a hordozóra helyezést követő oxidációs és redukciós kezelés után is megmaradt. Glükóz oxidációban az AgAu kétfémes hatást tanulmányoztam és annak függését az Ag/Au mól aránytól. Megállapítottam, hogy Ag/Au=33/67 alatt szinergikus aktivitás növekedés lép fel az egyfémes Au/SiO_2 és Ag/SiO_2 referencia katalizátorokhoz képest. Utóbbi minta a reakcióban inaktívnak mutatkozott. Maximális aktivitás–növekedést 20/80 Ag/Au aránynál találtam. Mérési eredményeimmel összhangban, az irodalomban Au katalizátorokon lejátszódó glükóz– és alkoholok oxidációjára ajánlott mechanizmus alapján javaslatot tettem a reakció mechanizmusára

$AgAu/SiO_2$ katalizátorok alkalmazása esetén. Eszerint a kétfémes katalizátorok nagyobb aktivitása a minták Ag által megnövelt O_2 aktiváló képességével magyarázható. Az optimális Ag/Au arány elérése után a további ezüst már annyira szétszabdalja vagy befedi az Au felületét, hogy a glükóz aktiválásához szükséges kiterjedtebb Au felület nem lesz elérhető ezáltal csökken az aktivitás.

Az ezüst szolt HRTEM és elektron diffrakciós (SAED) módszerekkel vizsgálva az ezüst lapon centrált köbös kristályrácsán kívül a ritkán előforduló hexagonális *4H*–Ag fázist sikerült azonosítani, melyet közel egyenlő mennyiségben tartalmazott az Ag szol. Az ezüst hexagonális (*4H*) kristály–módosulatát eddig csak Ag filmekben és pálcika alakú nanorészecskékben figyelték meg.

1 Introduction

Catalytic reactions play important roles in our life. Catalysts are used in all area of life from households to industry. Catalysis contributes to sustainable development through decreasing the energy consumption of the processes and eliminating or at least dramatically decreasing pollution from chemical and refining processes. The development of selective, highly active catalysts working under mild conditions meets the requirements of green chemistry. The importance of nanoparticles and nanostructures to the performance of catalysts has stimulated wide efforts to develop methods for their synthesis and characterization, making this area of study an integral part of nanoscience.

Gold – the most stable among all metals – was thought to be inactive in catalysis until Haruta's discovery[1] of the catalytic power of gold in carbon monoxide oxidation when its size is in the nanometer range. Later high activity of gold nanoparticles was demonstrated in several oxygen–transfer reactions such as CO oxidation, propene oxidation, water gas shift reaction, synthesis of H_2O_2, selective oxidation of alcohols and aldehydes.[2] Gold catalysts have many advantages compared to platinum group metals; it is resistant to oxidative atmosphere, moreover gold has greater price stability.[3] Though, in gold catalysis tremendous work deals with the mechanism, it is not fully understood, especially the activation of oxygen by gold.

Nowadays supported gold nanoparticles are used in the catalytic converter of vehicles, respiratory protectors, in fuel cells operating in electric vehicles and in chemical processes.[2,4]

In a catalytic system the performance of the catalysts is affected by the size, the distribution of the nanoparticles, the type and the structure of the support material; and the different types of additives.[2] Through controlled synthesis of nanostructured catalysts better understanding of the activity – structure relationship can be achieved leading to development of high performance catalysts.

In my dissertation supported gold catalysts are synthesized and characterized in order to investigate structure – catalytic activity relationship. Two different reactions are chosen for testing the activity of the catalysts: CO oxidation as a gas phase, total oxidation reaction; and glucose selective oxidation to gluconic acid as a liquid phase partial oxidation reaction. My aim is to study the gold-based catalysts in the different reactions to understand better the nature of the active sites and develop more efficient reaction specific catalysts for the two reactions.

2 State of the art

The summary of the most important preparation methods for supported gold catalysts and gold catalyzed reactions will be presented in this chapter with special attention to CO oxidation and glucose oxidation. Despite of the tremendous work found in the literature about heterogeneous gold catalysts the nature of the active site and the reaction mechanisms are not fully understood; in many cases the results are inconsistent.

2.1 Preparation methods

The success of gold in catalysis is based on the proper preparation method. The preparation method has a significant effect on the properties of supported gold catalysts thereby results in different particle size and geometry, different oxidation state of Au and different metal – support interaction. Moreover these parameters are in correlation with each other. Many preparation methods have been developed which fall into two main categories[2]:

1.) the gold precursor and the support are formed at the same time during the synthesis (*coprecipitation*)

2.) the gold or gold precursor is deposited on a preformed support. Many techniques belong to this category such as *impregnation, ion-adsorption, deposition – precipitation, deposition*

of organogold complex, chemical vapour deposition and colloidal gold deposition. The most important methods are detailed below.

2.1.1 Coprecipitation

In this method the support and gold nanoparticles are formed simultaneously. During the preparation process sodium-carbonate was added to the solution of gold precursor ($HAuCl_4$) and metal nitrate ($Fe(NO3)_2$) under controlled pH.[2] The formed hydroxide precipitates transformed to supported gold catalysts during calcination. This method is easy to carry out but its applicability is limited to metal hydroxides that can be co-precipitated with $Au(OH)_3$.[5]

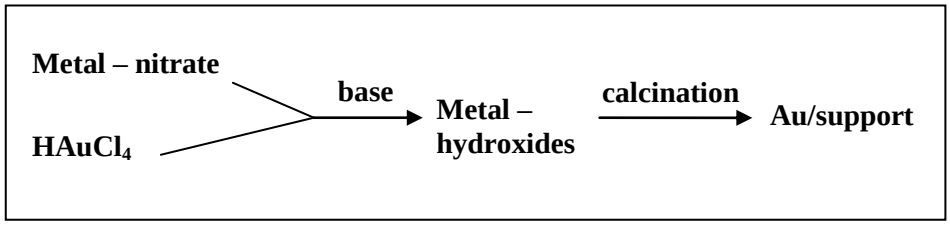

2.1.2 Impregnation

This is the simplest method for catalysts preparation. The support is mixed with the solution of the gold precursor followed by aging, drying and calcination. The most frequently used precursors are $HAuCl_4$,[6,7,8] $AuCl_3$[9] and ethylenediamine ($[Au(en)_2]Cl_3$)[10] complex. Silica, magnesia, alumina, titania and ferric oxide are used as supports. The method has two types: when the volume of the gold precursor solution corresponds to the pore volume of the support, the

method is called *impregnation to incipient wetness.* In the other process an excess of precursor solution is used then the solvent has to be evaporated. The efficiency of this method is poor: large gold particle sizes (10–35nm) and low activity were produced maybe due to the presence of the chloride ion of the precursor, which promotes mobility and agglomeration of gold species during thermal treatment.[5]

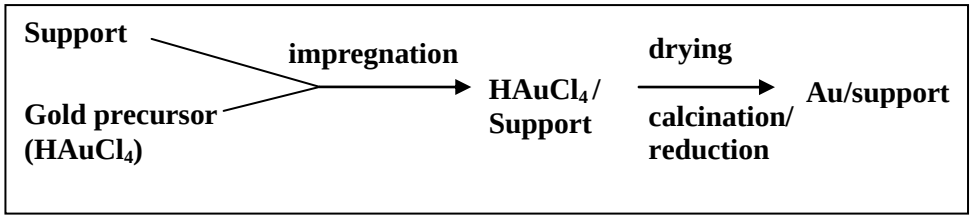

2.1.3 Ion adsorption

This method is based on the ion exchange between the gold precursor and the hydroxyl groups of the support in aqueous solution. The gold precursor, $HAuCl_4$ gives anionic complexes in aqueous solution if the pH of the solution is lower than the point of zero charge of the support, then the support surface is positively charged. The process was studied for the preparation of Au/TiO_2 at pH 2 under various conditions,[11] at which the main species in solution were $AuCl_3(OH)^-$ and $AuCl_4^-$; and these can interact electrostatically with the TiO_2 surface (point of zero charge: 6).

$$TiOH_2^+ + AuCl_4^- \rightarrow [TiOH_2^+ AuCl_4^-]$$

The performance of the catalysts prepared by this method is influenced by the temperature of preparation, the concentration of gold precursor solution and the type of the washing agent.

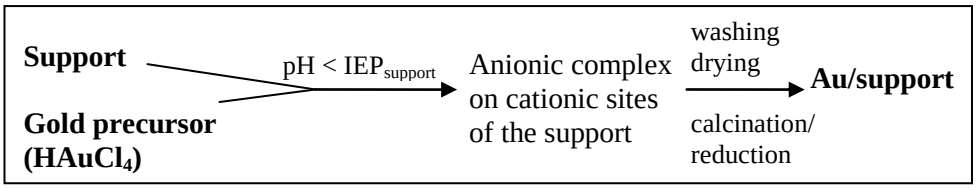

2.1.4 Deposition – precipitation

Deposition-precipitation (DP) is the method where metal hydroxide is supposed to precipitate on the oxide support.[12] By using this method base (sodium hydroxide or carbonate) is added to the suspension of oxide support and the aqueous solution of $HAuCl_4$, in order to raise the pH to 7 or 8 of the suspension. Then it is heated at 70 – 80°C with stirring for 1 hour. In order to remove the sodium and chlorine washing with water at ~50°C is applied. The product is filtered and dried at 100°C and calcined in air at higher temperatures to decompose the gold hydroxide complex to metal.[2]

Other version of this basic process was also applied. Using urea ($CO(NH_2)_2$) during the procedure was the first described DP method.[13] In this case no reaction takes place at room temperature in the solution of gold precursor, support and urea. The hydrolysis only starts when the solution is heated above 60°C:

$$CO(NH_2)_2 + 3H_2O \rightarrow CO_2 + 2NH_4^+ + 2OH^-$$

There is a gradual release of hydroxyl ions and increase of pH in the solution. Using urea 100% gold deposition can be reached from the solution onto the support unlike in the case of NaOH where the maximum efficiency of gold deposition is 60%.[14] If the preparation time is long enough (at least ~4 hour), small gold particles can be achieved.

DP method can be used only with support having isoelectric point (IEP) higher than 5 (MgO, TiO_2, Al_2O_3, ZrO_2, CeO_2) and it does not work with silica (IEP~2) and silica-alumina (IEP~1).[2]

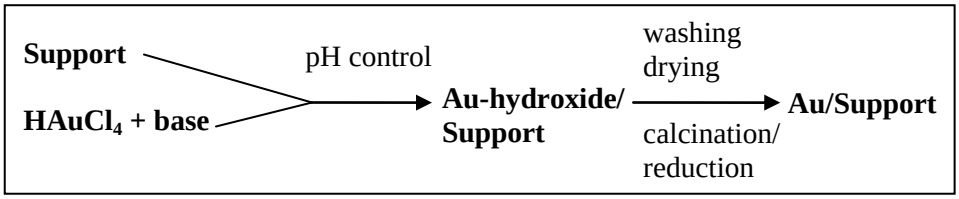

2.1.5 Colloid adsorption

With this technique stabilized gold colloids can be deposited on the support. The size, shape and surface charge of gold colloids can be tailored according to the desired catalysts. The proper choice of the reducing and stabilizing agent of gold is very important to control the properties of the catalysts.

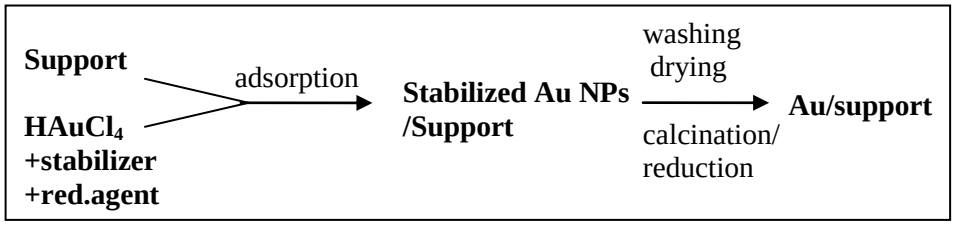

Gold colloids

Colloidal gold first appeared in Egypt and China at the 5th and was used to make ruby glass and color ceramics.[15] The most famous example is the pigment "Purple of Cassius" produced by reduction of $HAuCl_4$ with stannous chloride. Michael Faraday was the first who published a scientific paper on gold colloids. In 1857 he reported the formation of deep red solution of colloidal gold.[15]

Gold colloids have a strong adsorption band in the visible region, which is the origin of the observed red/purple colors of gold nanoparticles (NPs) in solution. This absorption band results from the collective oscillation of the conduction electrons in resonance with the frequency of the incident electro-magnetic field and is known as surface plasmon resonance (SPR) absorption.[15] The SPR frequency (and the color of the gold nanoparticle) depends on the particle size, shape and the nature of the surrounding medium.[15] Gold nanoparticles have been synthesized in various shapes like spheres, rods, cubes, plates, polyhedrons and wires. All shape has different physical properties (e.g. optical, electronic, and mechanical). The most thermodynamically favored shape is spherical. Spherical gold NPs can be synthesized in various sizes from 1nm to hundreds of nanometers.[15] **Figure 2.1** shows the color of gold colloids with different sizes and the change of the SPR band with the NP size.

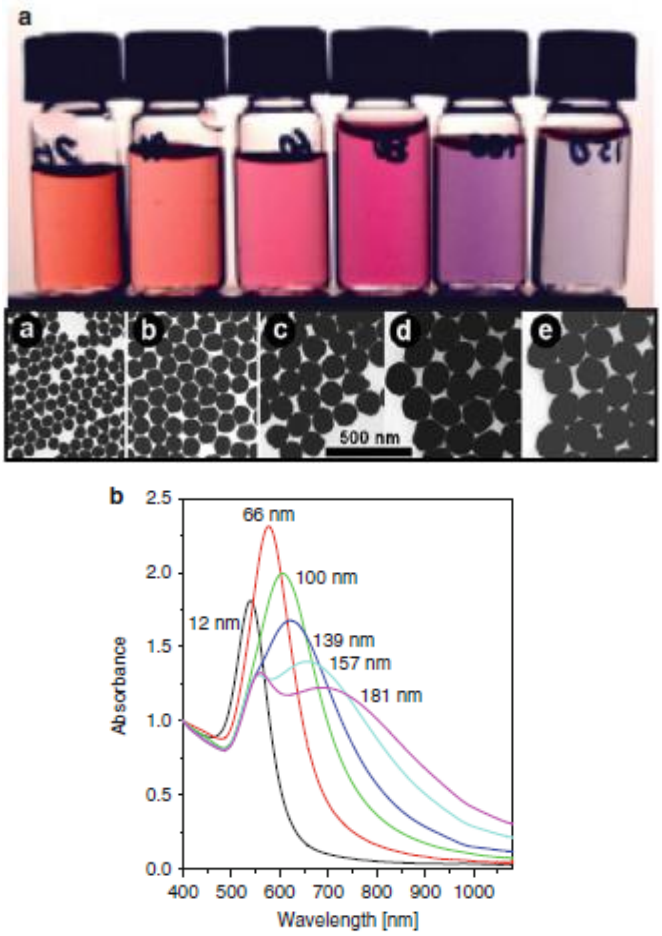

Figure 2.1.a) Different colors of spherical gold colloids according to their particle size and **b)** the corresponding visible spectra.[15]

In 1951 Turkevich reported the most frequently used preparation method for the synthesis of spherical colloidal gold NPs.[16] In his method $HAuCl_4$ was used as gold precursor and reduced by citrate in water, where citrate also served as a stabilizer. This method resulted 15 nm gold NPs with narrow size distribution. Other colloidal methods can be derived from the Turkevich method by changing the stabilizing and reducing agent, the preparation

conditions, the type and the concentration of the gold precursor producing gold NPs with many different sizes.[16]

In catalysis the main advantage of the use of colloidal NPs is that the mean size and size distribution can be controlled by the proper choice of the reagents and conditions. **Table 2.1** shows some examples on the effect of different stabilizers and reducing agents in the size of the gold NPs and the nature of the shell. The relative rates of nucleation and growth of the nanoparticles determine the size and size distribution. For small size and narrow size distribution needs rapid creation of large number of nuclei before growth starts. During the growth process the nucleation must be finished. Strong chemical reducing agent (e.g. sodium borohydride) generates small spherical nanoparticles.[15]

Table 2.1. Examples of gold NPs with different sizes and shells depending on the stabilizer and reducing agent.

Reducing agent	**Stabilizer***	**NPs size (nm)**	**Nature of the stabilizing shell**	**Ref.**
$NaBH_4$	PVA	2-3	pH dependent surface charge, bulky ligand	17
Sodium-citrate	Tannic acid	6-7	anionic surface charge, bulky ligand	18
$NaBH_4$	PDDA	2-3	cationic surface charge, bulky ligand	19
Sodium-citrate	Citrate	15-20	anionic surface charge, non–bulky ligand	16

*PVA: polyvinylalcohol; PDDA: poly(diallyldimethylammonium) chloride.

Catalyst preparation via colloid adsorption

Gold colloids can be immobilized on a support by mixing the stabilized colloidal suspension with the support followed by filtering, washing and drying. Colloids without immobilization may also be used as catalyst in liquid phase reactions if there is free surface for the reactants.

Using preprepared colloidal particles is advantageous because particle size is independently controllable, the size distribution is narrow and the gold already reduced.[2] This preparation process can be used on all type of support. The disadvantage of the method is the need of thermal treatment before catalytic use to remove the organic stabilizing shell which resulted particle sintering in most cases. **Table 2.2** shows some examples of catalysts prepared on various support with different stabilizer and the resulted gold particle sizes in the sol and after immobilization and thermal treatment.

Table 2.2. Examples of supported catalysts prepared by gold sol deposition. d_{Au}: mean diameter of Au nanoparticles.

Support	Stabilizer*	d_{Au} in the sol (nm)	d_{Au} on support after calcination (nm)	Reference
Carbon	THPC	2.9	4.3	20
Al_2O_3	THPC	3.5	3.8	20
SiO_2	TC	6.5	6.7	21
CeO_2	PVA	2.7	5.6	17
TiO_2	PDDA	15.1	15.0	19
TiO_2	PVA	2.2	5.3	17

*THPC: tetrakis(hydroxymethyl)phosphonium chloride; TC: tannic acid – sodium citrate; PDDA: poly(diallyldimethylammonium) chloride; PVA: polyvinylalcohol.

We have chosen this method, because we wanted to prepare gold catalysts with different particle sizes and this method allows us to use the same method for all the reducible and non-reducible supports. With this method also Au/SiO_2 catalyst can be synthesized so it makes easy the comparison of the catalysts with different support materials.

2.1.6 Preparation of gold containing bimetallic catalysts

The catalytic properties of gold can be improved by combining it with a second metal. Bimetallic catalysts appeared promising in activity enhancement in many reactions through forming

new active sites and inducing synergistic effects. The preparation methods of gold containing bimetallic catalysts may be divided into three categories:[2]

1) no interaction between the two metal precursors in solution (co-impregnation,[22,23] co-adsorption of cations,[24] deposition-precipitation,[25] photoreduction[26]);

2) interaction between the two metal precursors through surface reactions (redox methods);[27]

3) utilization of bimetallic precursors (molecular cluster compounds,[28] colloidal particles,[16,29] dendrimer–stabilized particles[30]).

Bimetallic nanoparticles may result in different type of structure: Au core–metal shell, metal shell–Au core, alloyed structure and transition structures between them. The final structure of the catalyst depends on the type of the second metal, the sequence of the reduction and the further treatments. Bimetallic gold containing colloids can be prepared in similar way like gold colloids alone. The most often used metal combined with gold are Pt,[28,30] Pd,[16,22,23,26,27] but we can find some Cu,[31] Ag[25] and Rh[32] containing catalysts, as well.

2.2 Reactions catalyzed by gold

Gold was thought to be inactive metal in catalysis. In 1823 Dulong and Thenard have published the first study about the catalytic power of gold in the decomposition of ammonia.[33,34] Then in 1834 Michael Faraday has reported the reaction of hydrogen with oxygen at room temperature catalyzed by gold.[35] In 1906 Bone et al. has

studied again this reaction using gold gauze and later gold powder.[36] The first report about the oxidation of carbon monoxide catalyzed by gold gauze at 573K was published[37] in 1927 but the big breakthrough in gold catalysis came in 1987 with the work of Haruta et al.[38] who has proved that supported gold nanoparticles are active at low temperatures in CO oxidation. Since then gold catalysts was proved to be efficient in many other type of reactions from gas phase to liquid phase. The most important reactions in which heterogeneous gold catalysts can be applied, besides total oxidation of CO and VOC, are the hydrogenation reactions of alkenes, water gas shift reaction and selective oxidations. The latter types of reactions can be divided into gas phase oxidation of hydrocarbons (alkanes and alkenes) to oxygenated product which is important in environmental protection and petrochemical industry; and partial oxidation of oxygen–containing organic molecules (mostly alcohols, aldehydes and sugars) typically in liquid phase, which is important in fine chemical industry.[39] Molecular oxygen, air or hydrogen peroxide can be used as oxidizing agent.

2.2.1 CO oxidation

It is widely accepted that the activity of gold catalysts in this reaction depends on:

— the particle size[40]

— the oxidation state of Au[41]

— the type and structure of oxide support[42]

— the interaction between gold particle and the support,[43]

and these effects are not separable from each other.

2.2.1.1 The effect of the particle size

Figure 2.2 shows the effect of the particle size on the CO oxidation activity. One can see that the activity/ surface Au atom (turn over frequency, TOF) of gold catalyst increases exponentially with the reducing size of the nanoparticles below 5nm. There is a sharp rise in activity beginning at ~5nm, as the gold particle size is lowered from 20nm. The optimum size for gold particles is 2–3nm.[44]

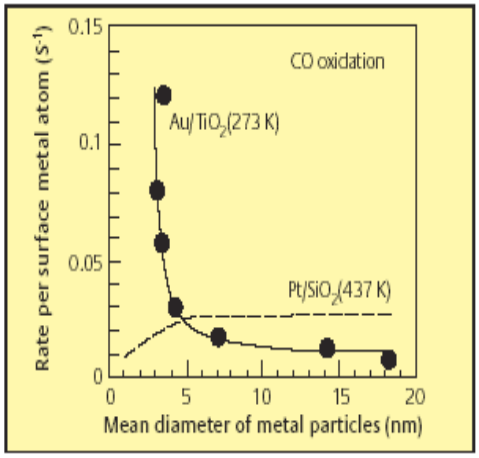

Figure 2.2. The effect of metal mean particle size on the CO oxidation reaction rate normalized by surface metal atom. Comparison of gold and platinum based catalysts.[5]

2.2.1.2 The effect of the support

The chemical nature of the support plays important role determining the activity. Oxide supports are divided into two groups according to their reducibility. Generally, the reducible oxides CeO_2, TiO_2, Fe_2O_3 etc. are considered to be "active supports" since they provide good activity for Au, while the irreducible ceramic oxides

SiO_2, Al_2O_3 can be regarded as inactive or much less active supports;[45] showing moderate activity if the particles are small enough. However many exceptions can be found due to the different preparation method which results different metal-support interactions.

In the case of the inactive supports the oxygen adsorption was suggested to happen on the defect sites of Au that is why the activity shows stronger dependence on the dispersion. The reducible active oxides, which are able to act as oxygen reservoir, the microstructure of oxide and the nature of metal-support interface are of key importance, since the oxygen activated by the oxide active sites generated partly by the interaction with Au is suggested to react with CO adsorbed on gold in close vicinity of the gold-oxide perimeter.[46]

The crystalline form of the support also has an effect. Comparing gold nanoparticles supported on various TiO_2 polymorphs (anatase, rutile and brookite), the Au–anatase perimeter seems to be significantly more active than the Au–brookite perimeter.[19] The difference in activity should be originated from the different structural, physical and chemical properties of the uppermost oxide layer making interface with gold determined by the crystal structure of TiO_2. However, different results were also obtained using different pretreatment conditions and preparation methods.[47]

The defect structure of oxides has important role in the formation and stabilization of Au nanoparticles. The activity of the Au-oxid perimeter depends on the morphology of the oxide component regardless of whether it is supporting Au nanoparticles or decorating them. Gold on nanosized ceria prepared by DP is two orders of magnitude more active than gold on bulk ceria prepared by

coprecipitation. Possible explanation is based on Raman spectroscopy measurement which showed the presence of superoxide (O_2^-) and peroxide (O_2^{2-}) species only on the nanosized ceria support.[2]

In our laboratory Au sols for heterogeneous catalytic purposes have been studied and applied for the last few years.[16,16,48] Gold supported on mixed oxide supports such as TiO_2–SiO_2 and TiO_2–SBA15 or CeO_2–SBA15 was prepared with special regard to ensure intimate contact of the active oxide and Au on a high surface area amorphous and mesoporous SiO_2. A unique approach, the so-called localized oxide promotion of gold, has been established and developed producing Au/SiO_2 catalysts that contain TiO_2 moieties on Au particles due to the post-modification of preformed Au particles.[19] This post-modification was done before or after the sol adsorption step. It was concluded that these "inverse catalysts" with even as low as 0.2 wt% TiO_2 possess better CO oxidation activity than the parent Au/SiO_2, while at 4wt%TiO_2 content they are more active than Au/TiO_2, although the Au particle size for the latter sample was unfortunately higher (sintering on TiO_2 could not be prevented). At low TiO_2 concentration transmission electron microscopy (TEM) and energy-dispersive X-ray spectroscopy (EDS) measurements proved the presence of TiO_x patches on Au particles while at higher TiO_2 loading Ti appeared both on Au and SiO_2 support. The enhanced CO oxidation activity was interpreted as a result of large and especially active Au–TiO_2 interface.

The surface OH groups and the affinity of the support to water is another aspect which can modify the catalytic properties.[2]

2.2.1.3 Mechanisms

There is not a unique mechanism for CO oxidation. The mechanism may depend on the type of the catalyst and influenced by the reaction conditions and also the moisture level. The suggested mechanisms can be divided into two categories:[49]

1.) the reaction takes place only on metallic particles

2.) the support is involved in the reaction

In the first case CO oxidation proceeds on small, low coordinated Au clusters. The reaction takes place through cooperative adsorption of the reactants. The adsorption of the CO – which induces electron excess on gold – is followed by the adsorption of oxygen without dissociation, in O_2^- form. This type of mechanism could be applied for irreducible oxides (SiO_2, Al_2O_3) supported catalysts because these supports are thought to be not involved in the reaction.[2,50]

Another mechanism proposed for Au/Al_2O_3 requires Au^+ cation at the edge of the particle, carrying an OH^- group.[51] An oxygen molecule adsorbs dissociatively on steps or defect sites of metallic gold atoms. In the next step a CO molecule reacts via hydroxycarbonyl ion, liberating CO_2 and restoring the initial centre. (**Figure 2.3**) No kinetic evidence was shown for this proposal. The existence of the Au(I)OH at the interface was deduced from observations on the deactivation of the catalysts, the positive effect of water in the feed, the effect of chloride ion and TOF-SIMS measurements that detected AuO^- and AuO_2^-.[2, 52]

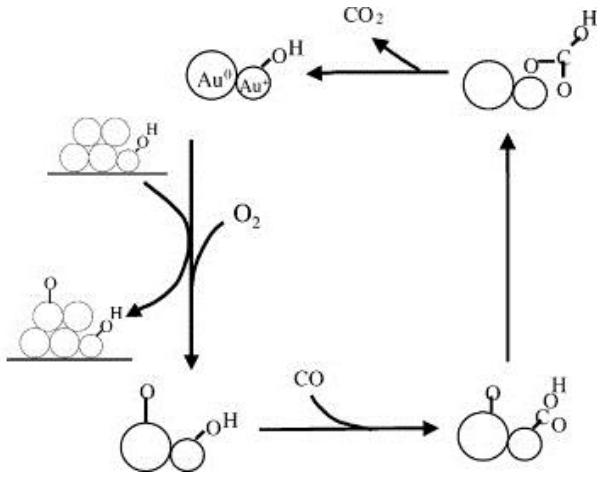

Figure 2.3. Reaction mechanism proposed for Au/Al_2O_3 catalyst by Kung et al.[11]

Theoretical studies on stepped Au(211) and Au(221) surfaces of Au_{12} and Au_{34} supported on MgO lead to the proposal of Eley-Rideal mechanism.[53] According to this proposal the gaseous oxygen reacts with CO adsorbed on gold, through the formation of the metastable O–O–CO intermediate complex; the surface oxygen atom adsorbed on gold reacts with a second CO molecule from the gas phase in a fast reaction.

The proposed mechanisms where the support plays an active role in the reaction are more complicated. In these mechanisms the role of the support is in oxygen activation, while CO is adsorbed on metallic gold. The adsorbed CO and O_2 can react at the perimeter of the particle, at the gold-support interface.[2,5] Some authors proposed that the gold particles are

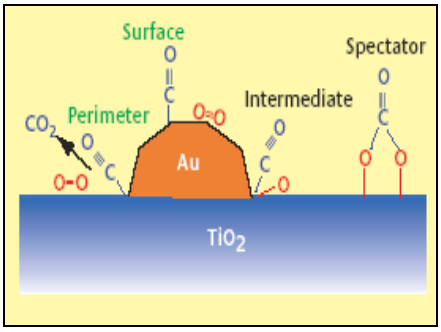

Figure 2.4. Mechanism proposed by Haruta *et al.*[5]

metallic[5,12,54] **(Figure 2.4)**, while others suggested that gold cations are also present.[55] All the supposed mechanism focus on the reaction between adsorbed CO and an oxygen molecule, as the rate-determining step.

Kinetic analysis on Au/TiO_2 suggested Langmuir – Hinshelwood mechanism, the non–competitive adsorption of the reactants and the particle edges have been proposed as active sites.[56] A proposal for the oxygen activation by the reducible oxide supposed that oxide ion vacancies exist on the surface where the O_2 can adsorb in O_2^- superoxide form near the gold surface. This model is reinforced by the deactivation of catalysts caused by "spectator" carbonate ions which block the surface anion vacancies; and also by deactivation caused by chloride ion.[57]

Bond and Thompson supposed cationic gold at the interface beside metallic gold which acts as a "chemical glue" and responsible for the stability of the small particles.[55]

Mechanism suggested for ceria supported catalysts involve more possibilities. Ceria can provide reactive oxygen via forming surface and bulk vacancies through redox processes involving the

Ce(III)/Ce(IV) couple (Mars–van Krevelen type).[58] The interaction is more complicated when there is possibility of incorporation of cationic Au into the ceria lattice forming $Ce_{1-x}Au_xO_{2-\delta}$ type solid solution.[59] Depending on the morphology (preparation method) of ceria, different catalytic activities can be obtained: Yi and co-workers[60] experienced using Au/CeO_2 that the CO conversion depended on the shape (polyhedra, cube or rod) viz. the crystal planes of CeO_2. The adsorption/desorption properties of CO and oxygen species were related to the nature of exposed crystal planes of ceria nanocrystals. The ceria rods with {100} and {110} dominant surfaces showed the best performance with higher concentrations of Au^+ and Au^{3+}.

2.2.2 Selective oxidation of D-glucose

Selective oxidation processes represent a large class of organic reactions where the development of clean and efficient "green" processes can have a significant positive economic and environmental impact. Catalytic oxidation of reducing sugars, like D−glucose, D−lactose and D−maltose over gold give products of greater value. The oxidation product of D−glucose, obtained by hydrolysis of sucrose, starch and cellulose; is gluconic acid (or its salts) which is used as water-soluble cleansing agents and as additives to food and beverages. The annual gluconic acid production is about 60 000 tonnes, that is made by fermentation despite problems with separation of the ferment, with control of by-products and disposal of waste water.[2,61,62] These problems can be avoided by heterogeneous

catalysts; moreover, utilization of gold catalysts has an environmental advantage – the reaction can be carried out using molecular oxygen or air as oxidizing agent at mild (30 – 90 °C) reaction conditions.

The selective oxidation of glucose to value added product is important in industry and also in environmental aspects since D-glucose – the most abundant monosaccharide in nature – can be derived from biomass. **Figure 2.5** shows the selective oxidation of the aldehyde group of glucose to carboxyl group. The reaction was extensively studied but the results are not consistent and many unclear questions have emerged.

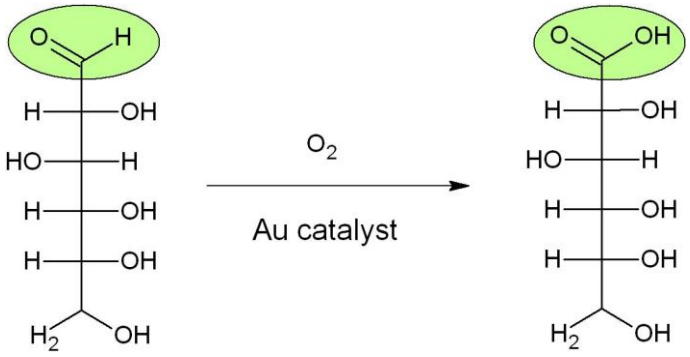

Figure 2.5. Selective oxidation of the aldehyde group of glucose to gluconic acid with molecular oxygen.

First, Biella et al. published[61] the highly efficient utilization of gold catalyst in the reaction. In contrast with the Pt and Pd based catalysts (**Figure 2.6**) (exhibiting high activity but low selectivity), using gold catalysts gluconate was obtained with 100% selectivity moreover self-poisoning and metal leaching were also avoided.[63,64]

Alkaline condition was essential for high activity but the reaction proceeded also under uncontrolled pH.[61,65]

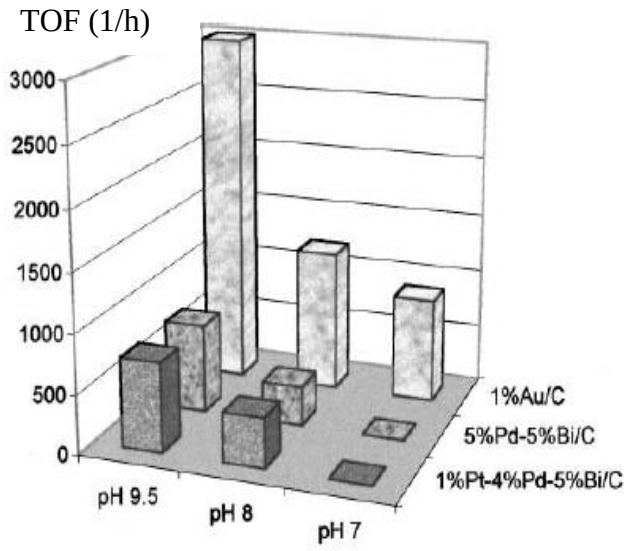

Figure 2.6. Comparison of glucose oxidation activities of Pt and Au catalysts and the effect of the pH.[61]

The highest reaction rate with total selectivity to gluconic acid was achieved at 50°C and pH 9.5, at higher temperature and pH value side products (fructose, sorbitol, mannose, glycolaldehyde, maltose) were formed.[66] Kinetic studies on glucose selective oxidation resulted in different conclusions on the reaction mechanism. Önal at al. published zero order reaction with respect to glucose. However, further investigation showed increased reaction rate with increasing oxygen pressure from 1.5 to 9 bar and glucose concentration dependence with a maximum reaction rate at 20 – 30wt% [67]. The results fitted a Langmuir – Hinshelwood model. Rossi and his

coworkers[68] found that the reaction rate is proportional to the oxygen pressure and increased with glucose concentration in the range of 0.05mol/L to 0.2mol/L, the estimated activation energy was 47 kJ/mol and Eley-Rideal mechanism was proposed.[68]

The mechanism suggested afterwards involved O_2 reduction to hydrogen peroxide, which was experimentally detected by Rossi and coworkers.[69] A study on the poisoning effect of different molecules on Au catalysts concluded that soft bases have high poisoning effect and hard bases (e.g. OH^-) have promoting effect on the activity in aerobic glucose oxidation. A molecular model for the electronic interactions has been suggested: soft and hard nucleophiles interact with the gold clusters in a different way and influence the oxygen reduction step of glucose oxidation.[69,70,71]

Structure sensitivity of the reaction was studied by Comotti et al.[72] Catalytic activity of Au colloids inversely proportional to the diameter of Au nanoparticles in the size range of 2.5 to 6 nm and a sudden loss of activity above 10 nm in size were observed. The stability of the colloid particles was low, coagulation occurred after about 400 sec. To improve the stability, gold colloids were deposited on carbon support. The initial rates of the reaction were unchanged compared to the rates observed with non-supported particles operated under the same conditions, hence it was concluded that the support is of limited importance in the origin of the catalyst activity in the oxidation of glucose. However the gold - support interaction was declared to be essential for the formation of a stable catalyst system.[73,74,75] On the contrary other authors[66] reported different catalytic activity using different type of carbon supports with the

same Au particle size indicating a specific metal - support interaction. Ishida et al. observed that gold particle size influences the catalytic effect more significantly than the nature of the support comparing carbon and different metal oxide supports such as Al_2O_3, ZrO_2, TiO_2, CeO_2.[76,77]

2.3 Interaction of oxygen with gold

Chemisorption of oxygen on bulk gold surface does not take place under normal conditions, but it is possible if the temperature is high enough and the process may be helped by impurities.

In the case of supported gold catalysts molecular oxygen takes part in the reactions in four possible ways:[2]

1) adsorption on the support in an activated form next to gold particle where the other reactant can be adsorbed (TiO_2, CeO_x, Fe_2O_3 etc.)

2) direct reaction with the adsorbed reactant (Eley–Rideal mechanism)

3) formation of $Au^+ – O_2^-$ by extracting charge from gold atoms, on very small gold particles

4) dissociative chemisorption to atoms on Au of below 2nm in diameter

The often mentioned possibility for oxygen involvement is the first but strong reaction rate dependence on particle size supports the 3rd

and 4th possibilities. Little evidence supports the Eley–Rideal mechanism.[2]

2.4 Bimetallic gold catalysts in CO oxidation and glucose oxidation

The catalytic performance of gold can be modified by its combination with a second (third) metal. Numerous publication reports on activity enhancement of AuPd systems in different processes (as e.g. synthesis of hydrogen peroxide[78] and vinyl acetate[79]; selective oxidation of alcohols[80], styrene[81], toluene[82]). Other less intensively investigated bimetallic compositions as AuPt[83,84], AuAg[85], AuCu[86], AuNi[87], AuCo[88], AuRh[89], AuIr[90], AuRu[91] also presented superior catalytic properties to that of either component separately, mostly in oxidation reactions. In this section we focus on AgAu bimetallic system in selected reactions regarding that these were the subject of our investigations.

In oxidation reactions AgAu nanocatalysts have been reported to show synergism, higher activity has been reached in different oxygen transfer reactions such as CO oxidation, preferential CO oxidation in H_2 (PROX), oxidation of benzyl alcohol and glucose. The increased activity strongly depends on the silver content of the bimetallic catalysts in benzyl alcohol[92] and glucose oxidation.[93,94,95] While in the case of monometallic gold catalysts the activity is influenced by the particle size and the nature of the support, in the case of bimetallic AgAu nanoparticles (NPs) they have secondary importance in CO oxidation in presence and absence of hydrogen.[96,97]

Regarding the AgAu structure Mou et al. reported the relevance of the pretreatments: in oxidizing atmosphere Ag-O bond formation was detected by EXAFS and after reduction in H_2 the silver oxide disappears and realloying of Ag and Au was observed.[97,98] The calcination and reduction temperature also affected the catalytic activity in CO oxidation.[99] Zanella and coworkers have studied TiO_2 and SiO_2 supported Au-Ag catalysts in CO oxidation reaction and found that the support is not involved in the reaction as in the case of the monometallic gold catalysts.[100] Synergistic effect has been observed in CO oxidation between Ag and Au using mesoporous aluminosilicate as support and explained by improved adsorption and activation of oxygen on the catalysts.[101] The best activity was achieved when Ag/Au molar ratio was 3/1 and that was explained by the strongest intensity of the O_2^- species on the catalyst surface detected by electron paramagnetic resonance (EPR) technique.[102]

In glucose oxidation Comotti et al. have reported[103] higher activity of activated carbon supported AuPt and AuPd nanoparticles compared to monometallic gold NPs at low pH, whereas almost no effect has been detected at pH 9.5. Hermans et al. have reported[104] synergistic activity in glucose oxidation at high pH using carbon supported Au/Pd catalysts prepared by impregnation in aqueous solution. The synergistic effect was related to high Pd surface content. Zhang, Toshima and their co-workers have extensively studied unsupported, PVP–protected bimetallic AuPd, AuPt, AgAu and trimetallic AuPtAg nanoparticles in glucose oxidation.[105,106,107,108,109,110] Synergistic activity has been reported in all three systems at high pH. The “crown-jewel-structured” AuPd nanocluster

catalysts were prepared by galvanic replacement reaction method, they shown excellent activity in the reaction. The authors concluded that “the anionic charge on the top Au atoms is the direct cause for the high reactivity”, based on DFT calculation results and XPS measurement; namely 0.25eV of Au $4f_{7/2}$ binding energy decrease was detected compared to the corresponding Au nanocluster. In the case of Ag core/Au shell type bimetallic nanoparticles the highest activity was reached at Ag/Au = 1/4 atomic ratio. The synergistic activity increase was explained by the possible electronic charge transfer from Ag in the core to the Au in the shell originating from the ionization potential of Au and Ag (9.22 and 7.58eV, respectively), however the XPS results showed binding energies corresponding to zero valence Au and Ag in the AgAu NP (Au $4f_{7/2}$: 83.8eV and $Ag3d_{5/2}$: 367.8eV, respectively).[93,107] In the case of the trimetallic AuPtAg alloy NPs (atomic ratios: 70/20/10=Au/Pt/Ag) higher activity was reported than in the case of the corresponding Au-containing bimetallic NPs and correlated to small diameter of the NPs and the negatively charged Au atoms due to electronic charge transfer from Ag atoms and the PVP stabilizer. XPS results showed the binding energy of Au $4f_{7/2}$ in the AuPtAg NPs 0.2eV lower than that of in the pure PVP protected Au NPs (82.8eV). DFT calculations also confirmed the negatively charged Au atoms, and Ag atoms were found positively charged in the trimetallic NPs.[108,109]

The explanation of the higher activity of the bimetallic AgAu catalysts based on XPS measurements. The authors detected very small binding energy shifts which is not changed with the metal composition.

In the case of colloidal catalysts, which were applied in Zhang's works, the presence of stabilizing agent can affect on the reaction.

2.5 Preceding research in our research group

Professor Guczi initiated the research on nanosized gold catalysts around 1997 in the Institute of Isotopes. The investigations were focused on the Au particle size effect on the catalytic activity in relation with the modified electron structure of the nanodispersed gold, and the understanding the nature and role of the Au-reducible active oxide perimeter in the CO oxidation reaction. These questions were studied in SiO_2/Si(100) supported model systems prepared by physical methods and in high surface area oxide supported systems prepared by chemical methods, typically using colloid adsorption technique.[111] These studies emphasized the importance of the size of Au NPs not only in their own catalytic properties (as shown on Au/SiO_2/Si(100) samples, where SiO_2 can be regarded inactive support),[112,113] but its indirect influence on the own activity of active, reducible oxide overlayer on gold nanoparticle- and thinfilm (studied in MOx/Au/SiO_2/Si(100) type systems, where M: Fe, Ti and Ce).[114,115,116,117,118,119] The influence of the active oxide and Au-oxide interface morphology was studied in TiO_2 promoted Au/SiO_2 applying amorphous and ordered mesoporous silica supports.[16,48,19,120] Au sol deposition was applied for Au introduction for providing similar Au particle size and chemical state (vis. metallic) in the different systems. The decisive role of the stabilizer shell and the surface charge of Au NPs in the precursor colloid and the support

were demonstrated in directing the formation of the active perimeter. Moreover, the highly dispersed nanosized TiO_2 stabilized either on the surface of silica surface, then interacting with Au nanoparticles or deposited directly on the Au surface provided perimeter increased specific activity compared to that of present in TiO_2 supported gold catalyst.[121] The effect of TiO_2 morphology was observed also in case of Au supported on different well crystallised polymorphs of TiO_2.[19] Modifying the Au catalyst performance by combining Au with a second metal in bimetallic particles has also been investigated in the case of AuPd system on „inert" silica and „active" TiO_2 support in CO oxidation reaction.[16,122,123] On SiO_2 the activity of alloyed AuPd decreased compared to the common activity of the monometallic analogous, which may be in relation with the modified redox properties of palladium that may weaken the O_2 activation ability. On TiO_2 support this activity decrease was not detected, that was attributed to O_2 activation provided by the AuPd–TiO_2 perimeter.

The aims of the present work are significantly determined and based on the preceding activity of the Department summarized briefly above and naturally on the results published in the literature of the field. It is a continuation and extension of the preceding gold catalysis research. The results and deductions gained for the gold catalysts in CO oxidation as a model of total oxidation reactions is to be investigated how show up or alter in partial oxidation of organic substrates in the other big class of oxidation reactions. For first steps in this approach the glucose selective oxidation was chosen as a model reaction. The other issues relate to two of the most important modification possibilities of gold catalysts, as active oxide promotion

and interaction with another metal in bimetallic particles. After the investigation of TiO_2 promotion, modification with CeO_2 was chosen as another active co–operator of gold typically in total oxidation reactions, which was studied primarily in the form of CeO_2 supported Au systems earlier. On the other side Ag as second metal in supported Au–based bimetallic system was decided to investigate, because of the well–known own activity of Ag in oxidation reactions and oxygen activation and on the other hand the promising results on AuAg cooperation in selective oxidation reaction reported in literature on unsupported bimetallic AuAg colloids.

3 Aims of the work

The general aim of the work was the controlled preparation of different structure supported gold catalysts for study their catalytic activity – structure relationship to understand better the nature of the active sites and improve their catalytic performance in the desired reactions.

CO oxidation, as a gas phase, total oxidation reaction and liquid phase selective glucose oxidation reactions were selected as model reactions.

Supported gold catalysts were to be modified according to the chosen test reaction. The individual steps of this research work were as follows:

— Based on the comparison of the same catalysts in CO oxidation and glucose oxidation reaction, the selection of the catalysts modification was aimed to achieve improved activity in the relevant reactions.

— For CO oxidation the design of catalytically active Au-CeO_2 interface was planned in a special way, when nanosize CeO_2 is in intimate contact with silica supported gold (inverse catalyst).

— Investigation of this inverse catalyst structure and the effect of the active oxide (CeO_2) concentration on the CO oxidation were targeted.

— For glucose oxidation the preparation of supported bimetallic silver-gold catalysts with various Ag/Au molar ratios was aimed.

— In the bimetallic catalysts the effect of altering silver concentration on the structure and the glucose oxidation were planned.

The following methods were selected for the structural characterization of the catalysts:

— ICP-MS, XRF and PGAA techniques to determine the metal and CeO_2 content of the catalysts;
— TEM and XRD measurements to calculate the particle size of the metals and CeO_2;
— HRTEM and SAED techniques to discover the structure of metals and CeO_2 and the metal – oxide interface;
— UV-visible spectroscopy to observe the surface plasmon resonance of the metal nanoparticles;
— X-ray photoelectron spectroscopy to determine the surface concentration and the oxidation state of the metals and CeO_2.

4 Experimental

4.1 Materials

The following materials were used for catalysts preparations:

Solvent: Ultrapure Milli-Q water; resistivity: 18.2 MΩ cm at 25°C, conductivity: 0.056μS/cm at 25°C (Millipore)

Metal precursors:

$HAuCl_4 \cdot 3H_2O$ (Aldrich)

$AgNO_3$ (Aldrich)

cerium(III) nitrate hexahydrate (Merck)

Stabilizing and reducing agents:

polyvinylalcohol (PVA) (Aldrich) **Figure 4.1. (a)**

poly(diallyldimethylammonium) chloride (PDDA) 20 wt% in water (Aldrich) **Figure 4.1. (b)**

tannic acid, $C_{76}H_{52}O_{46}$; M=1701.20 g/Mol (Aldrich;Lot SZBA1240) **Figure 4.1. (c)**

sodium citrate (Aldrich)

$NaBH_4$ (Aldrich)

Supports:

silica (Degussa Aerosil 200, Davisil)

titania (Degussa P25 and Eurotitania from Tioxide International)

ceria nanopowder (Aldrich)

For glucose oxidation:

D-glucose (Aldrich)

Na_2CO_3 for the preparation of the buffer solution (Sigma-Aldrich)

$NaHCO_3$ for the preparation of the buffer solution (Sigma-Aldrich)

0.8 wt% Au/C catalyst reference (World Gold Council) is prepared at Milano University (Italy) by deposition of gold sols on high surface area carbon (X40S, 1200 m^2/g). Gold content is 0.8wt% with average particle diameter 10.5 nm (TEM) / 6.7 nm (XRD).

For CO oxidation:

CO and O_2 in He (Messer)

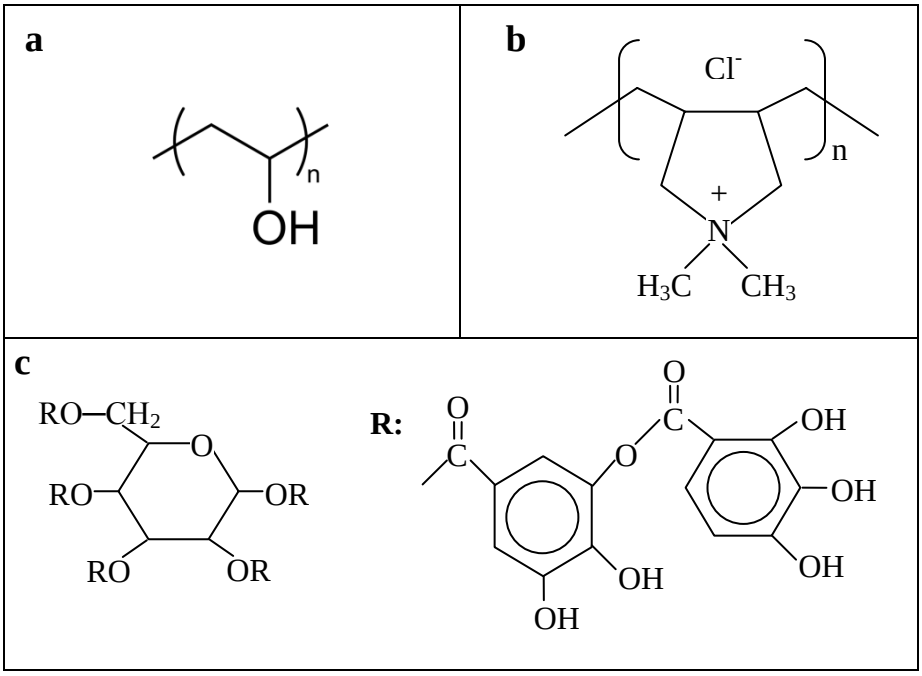

Figure 4.1. a) polyvinylalcohol (PVA) **b)** poly(diallyldimethylammonium) chloride (PDDA), **c)** tannic acid

4.2 Methods

4.2.1 Sample preparation

Colloid adsorption method was used for the preparation of all samples. The main steps of the preparation process:

— Preparation of the metal sol using metal – precursor, reducing agent and stabilizing agent.
— Adsorption of the sol on the support with or without further addition of PDDA polycation which can modify the surface charge of the support or the colloid.
— Filtering, washing and drying.
— Oxidation and (in several cases) reduction treatment.

4.2.1.1 Preparation of the metal sols

Tannin–citrate – stabilized gold sol

Tannin–citrate stabilized Au colloid (*Au–TC*) was prepared by reducing and stabilizing 16mL 0.32mM $HAuCl_4$ at 60°C with the mixture of 3.2mL 2 g/L sodium citrate and 0.8mL 0.5 g/L tannic acid and left at that temperature for 30 min under stirring. The immediate appearance of the red color of the sol evidenced the reduction of Au^{3+} ions.

PVA-stabilized gold and silver sols

Monometallic Au (*Au–PVA*) and Ag sols were prepared by addition of 12mL 25mM $NaBH_4$ solution to the mixture of 25 mL of

6.0 mM $HAuCl_4$ or $AgNO_3$ precursor and 30 mL of 0.2 wt% PVA solutions. All the sols were prepared at 273 K in solutions cooled by icy water.

Bimetallic Ag-Au sols

For formation of AgAu bimetallic nanoparticles consecutive reduction method was applied instead of co-reduction of the metal precursors in order to avoid AgCl precipitate formation during the preparation. For AgAu sols preparation different amount (2.5, 5.0, 10.0, 12.5 mL) of 6.0 mM $AgNO_3$ solution and 20 mL 0.2 wt% PVA was diluted by 400 mL MilliQ water and proper amount of freshly prepared 25mM sodium borohydride providing $BH_4^-/Ag^+=2$ molar ratio was added under vigorous stirring. The reduction of Ag^+ ions was indicated by the sudden appearance of yellow color that deepened during about 30 min stirring. When the Ag sol formation was completed and the $NaBH_4$ had been decomposed, the mixture of different amount (22.5, 20.0, 15.0, 12.5 mL) of 6.0 mM $HAuCl_4$ and 10 mL of 0.2 wt% PVA solution was added followed by freshly prepared 25mM sodium borohydride providing $BH_4^-/Au^{3+}=2$ molar ratio. This procedure resulted samples of various Ag/Au atomic ratios: 10/90, 20/80, 33/67, 50/50.

Table 4.1. The quantity of the reagents used for the preparation of the bimetallic sols.

Catalyst	**$AgNO_3$ 6mM (mL)**	**First part $NaBH_4$ 25mM (mL)**	**$HAuCl_4$ 6mM (mL)**	**Second part $NaBH_4$ 25mM (mL)**
10Ag90Au/SiO_2	2.5	1.2	22.5	10.8
20Ag80Au/SiO_2	5	2.4	20	9.6
33Ag67Au/SiO_2	10	4.8	15	7.2
50Ag50Au/SiO_2	12.5	6	12.5	6

4.2.1.2 Preparation of the supported catalysts

I. SiO_2, TiO_2 and CeO_2 supported gold catalysts

Two series of SiO_2, TiO_2 and CeO_2 supported Au samples were prepared by the adsorption of appropriate amount of the above described sols on the supports for 2wt% Au loading. *Au-PVA* sol was adsorbed on

- SiO_2 (Davisil) at pH 1.5 (*Au-SiO_2-PVA*)
- CeO_2 at pH 5 (*Au-CeO_2-PVA*)
- TiO_2 (P25) at pH 5 (*Au-TiO_2-PVA*) and

Au-TC sol was adsorbed on

- SiO_2 (Aerosil 200) (*Au-SiO_2-TC)*
- TiO_2 (Eurotitania) (*Au-TiO_2-TC*) at pH 1.5
- CeO_2 (*Au-CeO_2 -TC*) assisted by PDDA addition (0.4mL 20%).

The discoloration of the liquid phase indicated the complete adsorption of Au nanoparticles (NPs). All the preparation systems

were filtered, washed thoroughly with MilliQ water and dried at 60–80 °C. Different silica and titania supported samples were prepared to see that the different structure but same chemical composition could influence the activities. Table 4.2 summarizes the monometallic different oxide supported catalysts used in the first part of the work.

Table 4.2. The monometallic different oxide supported catalysts.

Catalyst	**Stabilizing agent**	**Reducing agent**	**Support**
Au–SiO_2–PVA	PVA	$NaBH_4$	SiO_2 (Davisil)
Au–TiO_2–PVA	PVA	$NaBH_4$	TiO_2 (P25)
Au–CeO_2–PVA	PVA	$NaBH_4$	CeO_2 (Aldrich)
Au–SiO_2–TC	Tannic acid	Sodium citrate	SiO_2 (Aerosil)
Au–TiO_2–TC	Tannic acid	Sodium citrate	TiO_2 (Eurotitania)
Au–CeO_2–TC	Tannic acid	Sodium citrate	CeO_2 (Aldrich)

II. "Inverse" CeO_2 – Au/SiO_2 catalysts

For the preparation of CeO_2 – Au/SiO_2 catalysts the above described tannin-citrate stabilized Au sols were used as "parent" sols in the next steps. We used appropriate amounts of the sol to give 2 wt% Au supported samples, while the cerium content of the samples was planned to be varied between 0.5wt% and 7.5 wt% CeO_2. The cerium precursor was introduced in two different ways.

In preparation **method A** (Ce–Au sol adsorption method), a calculated amount of aqueous solution of 20mM Ce-nitrate was added to the Au sols at room temperature under stirring, then the

temperature was increased to 60°C within 1 h and kept there for 4 hours. Finally, the sol was cooled down to room temperature. When the largest amount of Ce(III) nitrate was added to the Au sol, destabilization of the colloidal system happened and red precipitate with hardly observable tiny particles formed. Additional citrate seemed to dissolve this precipitate. Due to this experience blank experiment (using all components without gold) was taken in order to elucidate whether the precipitate formed only in the presence of gold, or the reaction media itself favors precipitate formation. Tannic acid-citrate solution at pH=8 was heated up to 60°C where the tannic acid started to hydrolyze as during the usual sol preparation, then HCl was added to set the pH=6.5 (the final pH of the parent gold sol). 20 mM Ce(III)-nitrate was added dropwise to the mixture at 60°C and white disperse precipitate was observed after addition of 0.6 ml of Ce(III)-nitrate to 16 ml of blank solution. This white precipitate seemed to dissolve by eyes upon addition of more Na-citrate (like in the case of Au-Ce composite sol described above). The next sample with less Ce-content was prepared with more care, thus, the addition of 20 mM Ce(III) nitrate solution to the Au sol was done drop by drop and finally some additional citrate was added (half of the volume of actual Ce–nitrate added) and no change of color was observed this time and the sol was stable on the following days as well.

The adsorption of Ce-containing Au sols (composite sol) onto Aerosil SiO_2 was accomplished with the aid of PDDA polycation. Without this additive the adsorption of the sols on silica could not be taken place. Certain amount of PDDA (depending on the actual sol, usually 1.5–1.7 ml 0.08 wt% aqueous PDDA solution per 100 mg of

SiO_2) was preadsorbed on Aerosil under stirring at room temperature. Next, the pure Au or the composite sol was added to the silica suspension and the white color of silica changed to red or reddish purple as a sign of the successful adsorption accompanied with discoloration of the liquid phase. In some cases additional amount of PDDA was necessary to complete the adsorption of the composite sol and/or to cause the flocculation of silica which facilitates filtration, because Aerosil silica contains loose aggregates of individual SiO_2 particles of 12 nm and so it is hard to filter. The suspension was stirred vigorously at room temperature for about 1 h then the solid was separated by filtration, washed thoroughly with water and dried for two days at 70^{o}C.

In preparation **method B** (Au/SiO_2 impregnated by $Ce(NO_3)_3$ method), the parent Au/SiO_2 was further processed. The dried sample was mixed with the appropriate amount of cerium nitrate solution at 50^{o}C for 40 min, then the temperature was raised to 60–65^{o}C and the water was allowed to evaporate (it took usually 4-5 hours). Finally, the Ce-loaded Au/SiO_2 samples were dried for 2 days at 70^{o}C.

Thus, catalysts with different CeO_2 content produced by method A and B contained more or less the same Au loading of about 2wt%. The samples prepared by method A are denoted for instance by ACe0.04, where the numbers at the end refer to CeO_2 content in wt%. The samples produced by method B are labeled in the same way but with starting letter B. As references, ~2 wt% Au/SiO_2 and ~2 wt% Au/CeO_2 were prepared the same way without addition of Ce precursor. However, in the case of CeO_2 support, the sol adsorption

step was done at pH~2–3 (to increase the positive surface charge of the support) without addition of PDDA polycation.

III. Bimetallic AgAu/SiO_2 catalysts

Adsorption of the above described Ag, Au–PVA and AuAg sols on SiO_2 (Aerosil 200) were assisted by PDDA addition. All suspensions were filtered, the filtered cake washed thoroughly and dried at 60°C. Before catalytic tests the supported catalysts were calcined in synthetic air flow at 400°C for 1 h and after that reduction treatment was carried out in hydrogen flow at 350°C for 30 min.

Scheme 1. Schematic illustration of the planned preparation process of the SiO_2 supported bimetallic AgAu catalysts.

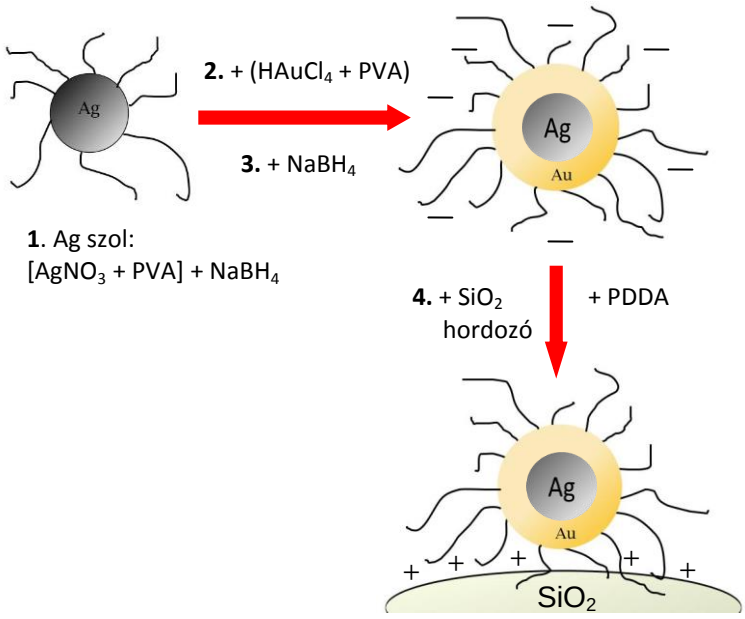

Scheme 1 shows the concept of the preparation process of the $AgAu/SiO_2$ catalysts; however the final structure of those is different from the illustration (see in Chapter 5.3).

4.2.2 Sample characterization techniques

Inductively Coupled Plasma – Mass Spectrometry

The Au and Ce content of the samples were firstly determined using a double-focusing inductively coupled plasma mass spectrometer (ICP-MS, ELEMENT2). All measurements were made using a Scott-type spray chamber operating at room temperature and a Meinhard concentric nebulizer. The dried catalyst sample was dissolved using a 1 ml HNO_3, 3 ml HCl and HF acid mixture and heated up to 80 ^{o}C in water bath for 20 minutes and cooled down to room temperature afterwards. Prior to the ICP-MS analysis the excess HF was removed. Au and Ce standards were used as reference. [a]

X-ray Fluorescence Spectrometry

The Ce content of three samples was determined using radioisotope induced X-ray fluorescence spectrometry (XRF) method[124] applying a very good correlation factor between ICP-MS and XRF measurements. The Ce content of the samples of about 50 mg was measured and ^{241}Am ring source with 3.65 GBq activity was used as excitation source. The emitted X-rays were detected by a Canberra 30165 type Si(Li) X-ray detector. The detector signals were processed by a standard NIM electronics and collected by a Canberra 35plus multichannel analyser. Measurement time was 1800 sec. The recorded spectra were evaluated by the AXIL software[125].

[a] Ezúton is köszönöm Katona Róbertnek és Varga Zsoltnak az ICP-MS méréseket.

CeO_2 contents of all samples were calculated from the Ce content obtained by the above techniques. (XRF and ICP-MS).[b]

Prompt–Gamma Activation Analysis

About 50-350 mg of the $AgAu/SiO_2$ catalyst was analyzed with prompt-gamma activation analysis (PGAA),[126] a nuclear analytical technique for non-destructive determination of elemental compositions. This way the dissolution of the sample, any loss or contamination during the sample handling could be completely avoided. The samples were irradiated in a guided neutron beam for 5-60 000 seconds at the PGAA facility[127] of the Budapest Neutron Center and the gamma-rays from the radiative neutron capture are detected with a Compton-suppressed HPGe detector. The energies and intensities of the peaks in the gamma spectrum were determined with the Hypermet-PC[128] program, whereas the element identification and the calculation of the concentrations was done with the program ProSpeRo[129], utilizing our prompt-gamma analysis library.[130] Every step of the measurement and the evaluation can be described with statistical methods; therefore the uncertainties of the results can be readily estimated from a single measurement.[c]

Transmission Electron Microscopy

The distribution and size of gold, silver, bimetallic gold-silver and CeO_2 particles were studied by a Philips CM20 transmission

[b] Ezúton is köszönöm Kocsonya András segítségét az XRF mérésekben.
[c] Ezúton is köszönöm Maróti Boglárkának a PGAA méréseket.

electron microscope (TEM) operating at 200 kV equipped with energy dispersive spectrometer (EDS) for electron probe microanalysis. The particle size distribution of the NPs was obtained by measuring the diameter of about 300 metal particles. High-resolution transmission electron microscopy (HRTEM) investigations were carried out by a JEOL 3010 microscope operating at 300 kV with a point resolution of 0.17 nm. The HRTEM was equipped with a GATAN Tridiem energy filter used for Electron Energy Loss Spectroscopy (EELS) elemental mapping. The sols and aqueous suspensions of the samples were drop-dried on carbon-coated microgrids for the investigations. In due cases Au–etalon was dropped onto the grids and used for HRTEM reference.[d]

X-ray Diffraction

The phase composition of crystalline components of selected samples was investigated by X-ray diffraction using a Philips Xpert powder diffractometer with CuKα radiation (λ = 0.15418 nm). The relative fraction of CeO_2 and Au phases was characterized by the ratio of the integrated intensities of the strongest peaks of CeO_2 (111) and Au (111) at $2\Theta = 28.7°$ and 38.3°, respectively. The crystallite size for each phase was determined from the full width at half maximum of the first peak using the Scherrer-equation.[e]

[d] Ezúton is köszönöm Geszti Olgának és Sáfrán Györgynek e méréseket.
[e] Ezúton is köszönöm Gubicza Jenőnek az XRD méréseket.

UV – Visible Spectroscopy

UV-visible absorption spectra of the sols and the supported samples were recorded at ambient temperature using a double-beam spectrophotometer (JASCO V-550). The aqueous suspensions of the catalysts samples were dropped on a glass plate and after evaporating water the UV-visible spectra of the samples were recorded.

X-ray Photoelectron Spectroscopy

Near surface composition and chemical state of the samples and before and after reactions were determined by XPS performed by a KRATOS XSAM 800 XPS machine equipped with an atmospheric reaction chamber. Al Kα characteristic X-ray line, 40 eV pass energy and FAT mode were applied for recording the XPS lines of Au4f, Ag3d, Ce3d, C1s, O1s, Si2p and Ti2p. The binding energies (BE) were determined relative to C1s at 285 eV in the case of CeO_2-Au/SiO_2 samples. Si2p binding energy at 103.3 eV was used as reference for charge compensation in the case of the bimetallic SiO_2 supported samples. The powdered samples were placed on the stainless steel sample holder without any fixation and pumped down very slowly to avoid dusting. Spectra were taken in the as received state and after 300^{o}C /400°C calcination *in situ* and in the case of the $AgAu/SiO_2$ samples after reduction *in situ* to get information about the surface concentrations and the oxidation state of the components.

Sensitivity factors given by the manufacturer were used for the quantification.[f]

High-performance liquid chromatography

Analysis of the reaction products of glucose oxidation was performed by HPLC on a JASCO instrument equipped with a Jasco UV 2075 and an ERC 7515A RI detector. A Hamilton HC-75H+ form cation exchange column was used with aqueous succinic acid 0.11 mM as the eluent with 0.4 ml/min flowing rate at 80°C. The conversion was calculated on the basis of the concentration of gluconic acid produced and glucose consumed. Under these conditions selectivity was always 100 %.

The determination of the glucose and gluconic acid concentrations was carried out using a joint calibration curve of glucose and gluconic acid; points of the calibration curve were recorded at known conversions, because of the superposition of the peak of glucose and gluconic acid at high conversions.

4.2.3 Catalytic tests

CO oxidation

The CO oxidation was measured in a quartz plug flow reactor of 4mm inside diameter at atmospheric pressure connected via a differentially pumped capillary inlet system to a Balzers Prisma

[f] Ezúton is köszönöm Schay Zoltánnak és Srankó Dávidnak az XPS méréseket.

quadrupole mass spectrometer (QMS) 200. 30 mg catalyst was used which was in situ calcined at 300°C and 450°C in 20%O_2 in He mixture for 1 h (10 °C/min heating rate, 30 ml/min gas flow). Temperature programmed reaction was performed with a gas flow of 0.54% CO and 9.1 % O_2 in He at 55 ml/min with 4°C/min ramp rate. The pretreatment of the catalysts were performed *in situ*. The conversion was calculated on the basis of the CO_2 production.[g]

Glucose oxidation

Oxidation of glucose was carried out in a thermostated, magnetically stirred batch reactor, bubbling oxygen at atmospheric pressure through the liquid phase (**Figure 4.2**). The reaction was started by adding the calcined (400 °C in air for 1 h) or calcined and reduced (350°C in hydrogen for 30 min) catalyst to the O_2 saturated solution. The oxygen saturation was checked by Hanna HI 9143 dissolved oxygen meter. pH was kept at a constant value 9.5 by using carbonate-bicarbonate (volume ratio: 2:3) buffer solution. Typical reaction parameters were: c_{buffer} = 0.1 M, T = 35 °C stirring rate = 1000 rpm, 30 mL aqueous solution of glucose: $c_{glucose}$ = 0.1 M, O_2 flow = 100 mL/min (1 atm).

[g] Ezúton is köszönöm Stefler Györgyinek a segítséget a CO oxidációs mérésekben.

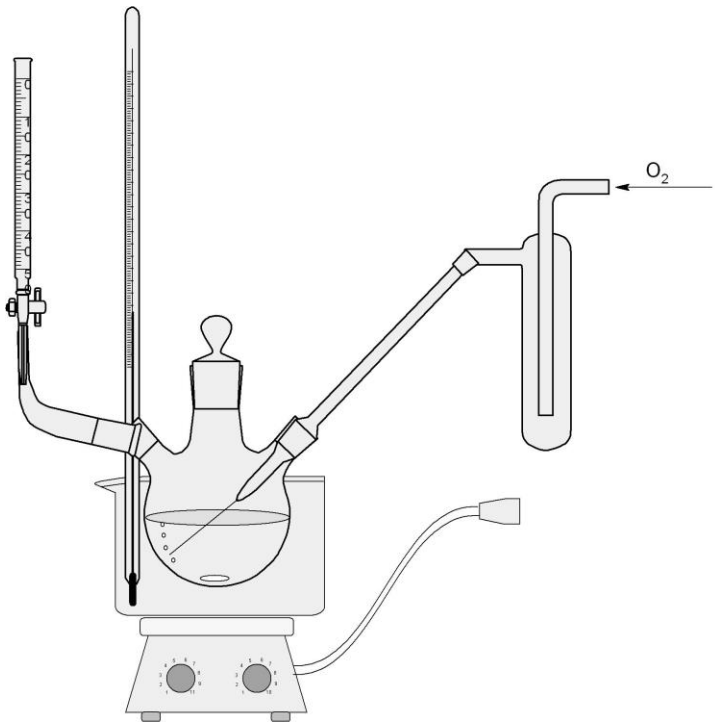

Figure 4.2. Illustration of the reactor used for glucose oxidation reaction

The reaction is carried out under alkaline conditions where silica support might have been dissolved. Experiment was made for checking the dissolution of silica as follows. 90 mg Davisil silica were mixed with 0.1 M carbonate-bicarbonate buffer then it was stirred for 3 hours. The mixture was filtered through a 0.2 μm porous diameter filter then the Si content of the filtrate was measured by ICP–MS. 13 wt% of the silica dissolved after 3 hours of reaction. If we consider a linear dissolution rate of silica, the amount of dissolved silica is less than 1 wt% in the first 10 minutes where the initial reaction rate was calculated for comparison of the samples.

Utilization of buffer solution is very convenient compared to titration with NaOH. The possible negative effect of the buffer was investigated. The buffer reduced the reaction rate when its concentration was above 0.1 M. Below this concentration (0.05 M) the reaction rate did not changed within the experimental error. For comparison the reaction was performed with NaOH titration and the reaction rate was slightly higher: we obtained 10% higher reaction rate in the first 10 minutes in the case of the most active sample.

5 Results and Discussion

5.1 Comparison of supported gold catalysts in CO oxidation and glucose oxidation

5.1.1 Introduction

Characterization and catalytic behavior of gold supported on different oxide catalysts are shown in the present chapter. Catalytic activities were investigated and compared in both CO oxidation and glucose selective oxidation reactions. The aim of this part of work was to answer weather the known size and support effect in CO oxidation valid for the oxidation of glucose in order to clarify the contradictions appeared in the literature. Further aims were to select the most active catalyst for further modification in order to achieve new catalysts with better performance.

5.1.2 Catalytic properties

Two series of catalyst samples were prepared by colloidal gold deposition on different supports (CeO_2, TiO_2 and SiO_2) with 2 wt% of nominal gold loading as it was detailed in Chapter 4. The catalysts were tested and their performance was compared in CO oxidation and glucose oxidation reactions. The catalytic results can be seen in **Table 5.1.**

Au supported on both TiO_2 and CeO_2 was very active in CO oxidation with a temperature of 50% conversion (T_{50}) of 30°C, 130°C and 57°C, 46°C in case of PVA and TC stabilized samples, respectively (**Table 5.1**). The behavior of Au-SiO_2 catalysts was different, they were less active. The Au/C catalyst in CO oxidation did not show activity until 190°C where the carbon support started to burn.

Table 5.1. Activities of the catalysts in CO oxidation and glucose oxidation. The catalysts were calcined at 400°C in air for 1 h.

Samples	**Catalytic activity**		
	CO oxidation	**Glucose oxidation**	
	T at 50% CO conversion (°C)	Reaction rate (μmol/min)	Spec. activity (μmol/mg_{Au}/min)
Au/C (WGC)	–	35	147
Au–SiO_2–PVA	400	34	66
Au–TiO_2–PVA	30	6	10
Au–CeO_2–PVA	57	6	10
Au–SiO_2–TC	308	25	42
Au–TiO_2–TC	130	12	18
Au–CeO_2–TC	46	14	23

5.1.2.1 Glucose oxidation

The evaluation of the results of liquid phase reactions is more complicated than that of the gas phase reactions. The required temperature is below 60°C, the appropriate pH is between 9 and 10. Under the actual reaction conditions only gluconic acid as product was observed in its gluconate form. No isomerization products were detected.

5.1.2.1.1 Effect of catalyst mass

In case of the most active Au/C catalyst the effect of catalyst amount was studied between 10 and 40 mg. Reaction parameters, such as buffer concentration, temperature, stirring rate, glucose concentration and oxygen flow rate were kept constant. **Figure 5.1** shows the effect of catalyst amount in terms of initial reaction rate. The rate increases linearly indicating that the reaction proceeds under kinetic control in the whole range. In further experiments 30 mg catalyst was used.

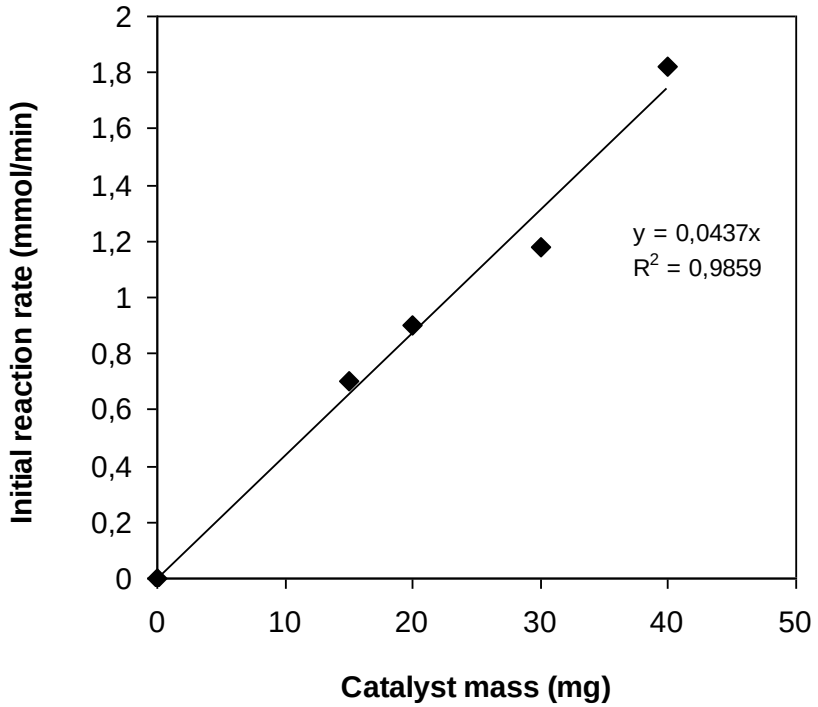

Figure 5.1. Effect of catalyst amount on glucose oxidation with Au/C, c_{buffer} = 0.1 M, pH = 9.5, T = 35°C, stirring rate = 1000 rpm, $c_{glucose}$ = 0.1 M, O_2 flow = 100 mL/min (1 atm).

5.1.2.1.2 Effect of oxygen concentration

The effect of oxygen concentration was studied by choosing two different values of oxygen concentration provided by using 20%O_2/N_2 and pure O_2 bubbling.[131] The experiments were carried out using c_{buffer} = 0.1 M, pH = 9.5, T = 35°C, stirring rate = 1000 rpm, $c_{glucose}$ = 0.1 M. The reaction rate increases with oxygen concentration as follows: 14μmol/min at 20% O_2/N_2; 35 μmol/min at 100% O_2.

Dissolved oxygen (DO) meter was used to estimate the rate of oxygen dissolution. The measurement was carried out in a separate

experiment (c_{buffer} = 0.1 M, pH = 9.5, T = 35°C, stirring rate = 1000 rpm, $c_{glucose}$ = 0.1 M) because it was not possible during the reaction due to the technical parameters of the DO meter. The rate of oxygen dissolution in the reaction media were estimated to be the same or higher than the rate of glucose oxidation reaction over the most active Au/C sample. This result confirms that the overall reaction rate is not limited by oxygen dissolution.

A typical glucose oxidation conversion curve is presented in **Figure 5.2.** The curve is linear up to 50 % glucose conversion then the rate started to decrease. This behavior can be interpreted either by a non-zero order reaction with respect to glucose or the buffer capacity is close to its maximum value at about 50 % conversion, the pH starts to decrease and for this reason the reaction rate also decreases. The initial reaction rate was determined from the linear initial part of the conversion curves.

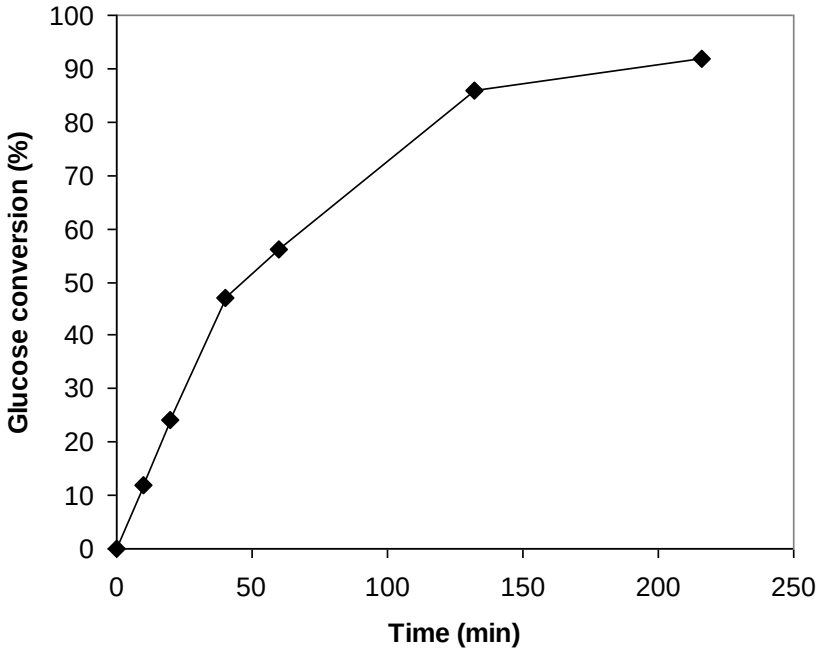

Figure 5.2. Glucose oxidation conversion curve, catalyst: 30mg 0.8 wt% Au/C, c_{buffer} = 0.1 M, pH = 9.5, T = 35°C, stirring rate = 1000 rpm, $c_{glucose}$ = 0.1 M, 30mL reaction mixture, O_2 flow = 100 mL/min (1 atm).

5.1.3 Comparison of the activity in CO oxidation and in glucose oxidation

Figure 5.3 shows correlation between the T_{50} in CO oxidation and reaction rate in glucose oxidation that demonstrates the relation between the activities in the two reactions. The higher the temperature of 50 % CO conversion the lower the activity of the sample is. The more active samples in CO oxidation are less active samples in glucose oxidation. The apparent linear relation has no physical explanation. The comparison of initial reaction rates of both reactions would be more meaningful kinetically; however the activity

differences in CO oxidation are so large, that there were no temperature found to measure all samples.

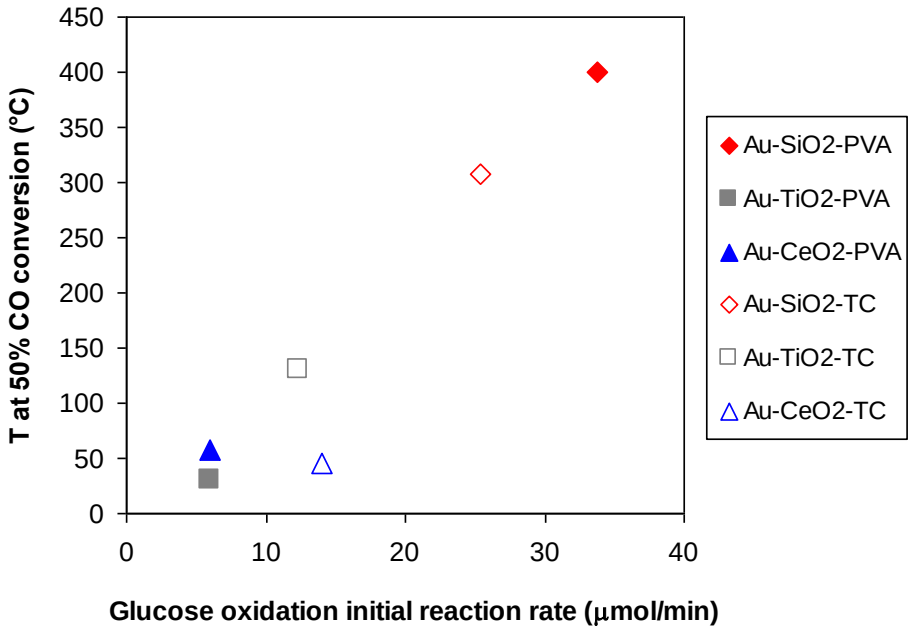

Figure 5.3. Comparison of activities in CO oxidation and glucose oxidation. The higher the *T* of 50 % CO conversion the lower the activity is.

Reducible oxides - ceria and titania - ensure the high activity in CO oxidation, whereas silica is much less effective support. In accordance with previous studies[2,77] the activity increases with decreasing particle size. In contrast, in glucose oxidation inverse activity order was found. Similar behavior was observed by Edwards et al.[22] in the oxidation of hydrogen, where a quite precise inverse correlation between the rates of hydrogen peroxide synthesis and carbon monoxide oxidation was established. In our case silica and carbon supported samples were more effective than the reducible oxide supported samples. For explanation of the observed behavior of

the catalysts in the two reaction structural characterization of the samples was carried out.

5.1.4 Structure of the catalysts

The diameter of the particles and the gold content of the samples were determined by TEM and ICP-MS, respectively (**Table 5.2**). After deposition on the support followed by calcination the particle sizes of the pre-prepared gold sols increased to 5-7 nm in case of the PVA stabilized samples and 7-13 nm in case of the tannin-citrate stabilized samples due to sintering (during calcinations). This sol adsorption preparation method allows us to use the same pre–prepared colloidal particles in case of all support. Although, the sintering during the calcination necessary for the removal of organic materials results in bigger size and broader size distribution compared to the size of the original colloid depending on the type of support and colloid.

Table 5.2. Sample properties

Samples	Support	Au content (wt %)	Surf.area/pore size (m_2/g)/nm	d_{Au} (TEM) after calcination (nm)
Sols				
Au-PVA		-	-	2.2 ± 0.9
Au-TC		-	-	6.7 ± 1.8
Catalysts				
Au/C (WGC)	Activated carbon	0.8	1200/0.8-0.9	10.5
Au-SiO_2-PVA	Davisil	1.7	300/15	7.8 ± 2.8
Au-TiO_2-PVA	P25	2.3	55/non porous	5.3 ± 2.1
Au-CeO_2-PVA	Aldrich	2.2	80-100/ non porous	5.6 ± 3.5
Au-SiO_2-TC	Aerosil	2	200/ non porous	6.8 ± 2.8
Au-TiO_2-TC	Eurotitania	2.3	125/3.6	13.0 ± 5.6
Au-CeO_2-TC	Aldrich	2	80-100/ non porous	8.0 ± 3.8

The effect of the catalytic reaction on the samples was tested. XPS spectra were recorded on the samples after calcination, before glucose oxidation and on the spent catalysts after glucose oxidation. The results confirmed the presence of gold on the surface of each samples. The surface atomic ratio of gold and the support cation were calculated and presented in **Table 5.3**. The binding energy of Au was

83±0.2 eV in the case all samples. The same amount of gold was found on the surface before and after glucose oxidation except Au-SiO_2-PVA (Davisil supported Au sample) and Au-TiO_2-TC (Eurotitania supported Au sample). Thus, we can suppose that there is neither metal-leaching nor sintering during liquid phase glucose oxidation except of those samples, where the surface Au/Si, Ti ratio decreased.

Table 5.3. Surface Au content of samples (measured by XPS).

Samples	**Surface atomic ratio Au/M (M=Ce, Si, Ti) (%)**	
	Before glucose oxidation	**After glucose oxidation**
Au-CeO_2-PVA	1.6	1.7
Au-CeO_2-TC	2.2	2.2
Au-SiO_2-PVA	1.2	0.6
Au-SiO_2-TC	0.5	0.5
Au-TiO_2-PVA	1.4	1.4
Au-TiO_2-TC	2.4	1.9

Regarding the silica supported samples the Au/Si ratio decrease was not observed in the case of Au-SiO_2-TC (Aerosil 200 supported) sample. The difference between the behaviors of the silicas might be due to their different structure. Aerosil 200 is a non-porous, very small particle-size (12 nm average primary particle size) support material which might be able to stabilize the gold particles via surrounding it. The gold could not move easily on its surface because of this steric effect. This explanation was supported by the negligible

change in the average particle size during calcination, too: In the case of Au-SiO_2-PVA (Davisil) the size increased from 2.2 to 7.8, while in the case of Au-SiO_2-TC (Aerosil 200) the average particle size only slightly increased. The difference between the silicas in the surface Au/Si ratios before glucose oxidation might be again due to their different structure. In the case of Aerosil support, where Au particles are surrounded, covered by SiO_2 particles similar in size, part of them may be hidden for XPS but not for the glucose and O_2 molecules.

In the case of the spent Au–SiO_2–PVA, XPS did not indicate the presence of carbon deposit or organic residue that may cover the Au surface. In that sample the decrease of the Au/Si ratio could be due to metal leaching or sintering during the reaction. In order to elucidate the reasons TEM images were taken and gold content was measured after glucose oxidation. Based on the gold content measurement by ICP-MS leaching of the metal can be excluded. **Figure 5.4 and Figure 5.5** show typical TEM images (a) and particle size distributions (b) of the Au–SiO_2–PVA sample before and after glucose oxidation. Comparing the figures some very large gold particles (aggregates) of 30-40 nm can be observed besides the smaller particles after the reaction. Biella et al. also observed similar change in the particle size and explained by the dissolution and reprecipitation of the particles.[61] In our case Au particle migration due to increased mobility and aggregation may be the reasons of the decrease in the surface Au/Si atomic ratio. However, particle migration into the pores cannot be excluded because Davisil is a porous support. Another aspect that we have to taking into account is that about 1 wt% of Davisil silica dissolves in the reaction media

which may reprecipitate on the gold surface decreasing the Au/Si atomic ratio.

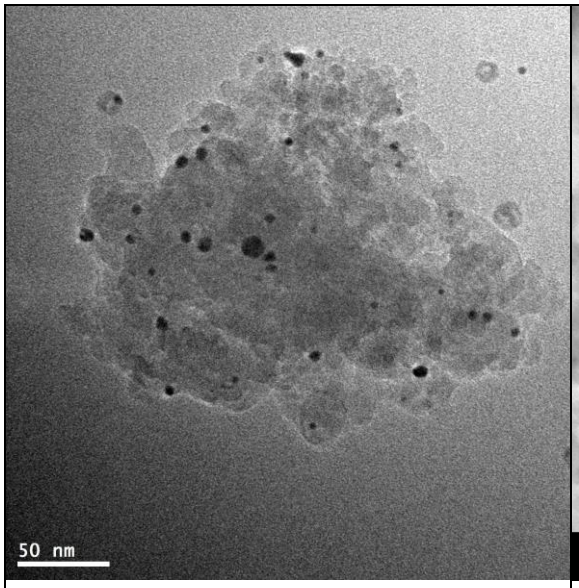

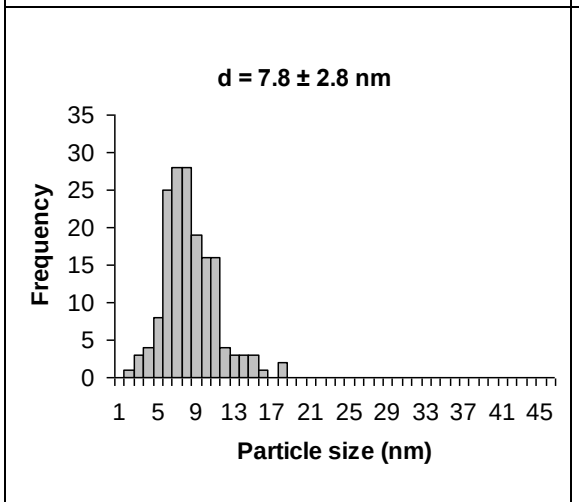

Figure 5.4. TEM image (a) and the size distribution (b) of Au-SiO_2-PVA **before** glucose oxidation.

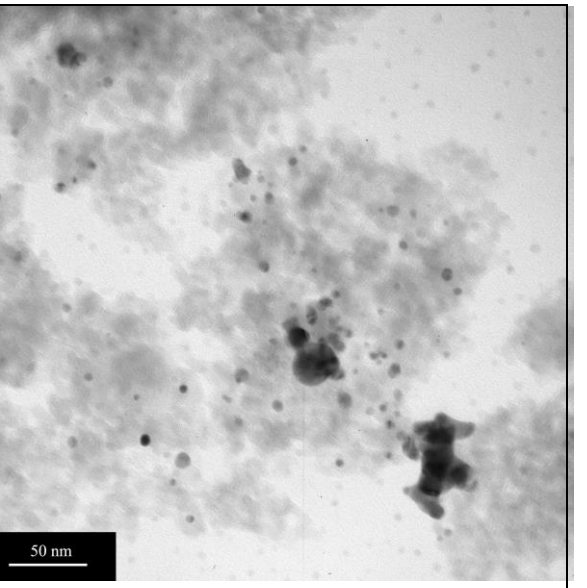

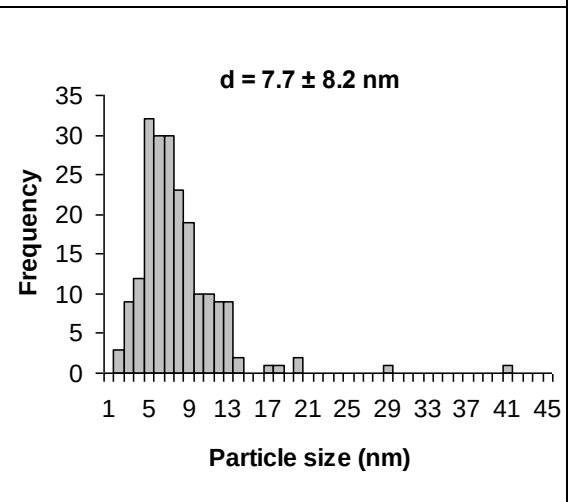

Figure 5.5. TEM image (a) and the size distribution (b) of Au-SiO_2-PVA **after** glucose oxidation.

In the case of Au–TiO_2–TC (Eurotitania supported sample) the results show slight decrease in surface Au/Ti ratio after glucose oxidation that could be due to some sintering or metal leaching again. TEM images were taken after the reaction but no significant change was observed neither in the average particle size nor in the distribution. The particle size of that Au-TiO_2-TC sample was large after calcination and the distribution is quite broad that is why TEM images did not show much changes. It could be possible that the small gold particles migrated into the pores, which causes decrease in surface Au/Ti ratio. Taking into account that in our case Au/Si or Au/Ti ratio decrease was observed only on the porous samples some particle migration into pores is supposed.

Figure 5.6 shows the initial reaction rate of the catalysts in glucose oxidation as the function of particle size. Higher activity was observed over catalysts with larger gold particles on each support.

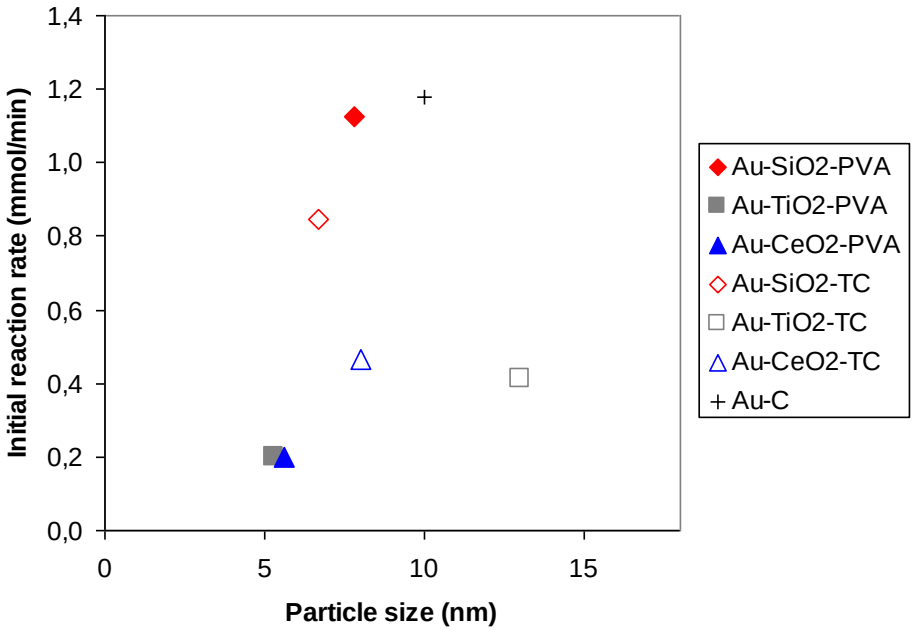

Figure 5.6. Comparison of the catalysts activities in glucose oxidation as the function of Au particle size

Considering the possible explanations of the diverse behavior of the same samples in the CO oxidation and glucose oxidation reactions it is hardly to be expected that the activity is in correlation with the presence of very small c.a. 0.5 nm bilayer clusters as reported by Hutchings and coworkers because the most probable shape of the pre-prepared colloid particles is spherical.[132] The effect of the ionic species is also excluded based on the application of pre-prepared sol and XPS results. The difference between the surface geometry of the small particles and the large particles could be the reason of why the larger particles are more active in glucose oxidation and small ones in CO oxidation. Glucose is a large multifunctional molecule compared to CO. For its adsorption different surface arrangements and sites are needed.

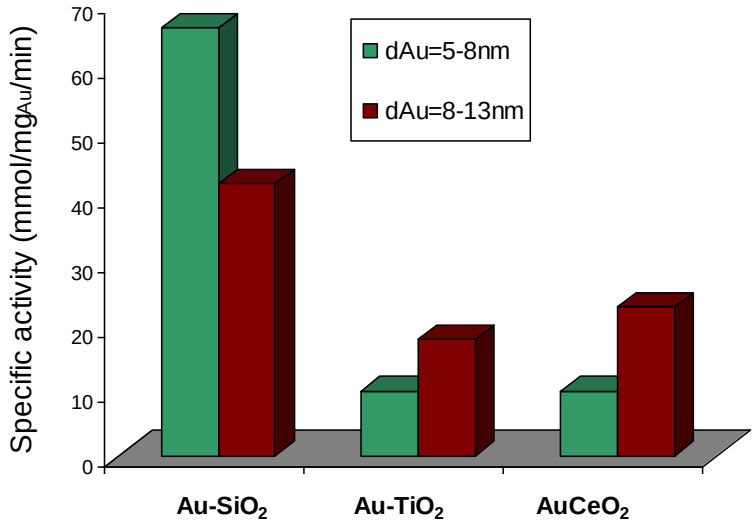

Figure 5.7. Effect of the support on the activity of the catalysts in glucose oxidation

Figure 5.7 clearly shows the higher activity of silica supported samples compared to the reducible oxide ones in the case of both particle size ranges. In this study the Au/C reference catalyst gives higher activity (**Figure 5.6**) however, the silica supported catalysts also work well indicating that weak metal–support interaction and high surface area favour the reaction. The pore structure should also play a role in the accessibility of the smaller particles in the pores by glucose. In our systems Davisil silica, Eurotitania and Activated carbon are porous supports. Davisil silica has 15 nm pore size and gold particles could penetrate into the pores. However, if the stabilized Au particles penetrate into the pores and stabilized there in the calcined sample after the removal of large organic stabilizer there

should be enough accessibility of the much smaller glucose but in this case pore diffusion can occur. Even so the activity of this sample is the highest in glucose oxidation compared to the other samples. Eurotitania is also a porous support with 3.6nm pore size. This support was used with 6–7 nm particle size gold sol considering that most of the particles are outside of the pores but some of them could be small enough to penetrate into the pores. The role of the surface area of the support could be that the support may adsorb the reacting glucose molecule facilitating the reaction as it was discussed by Okatsu et.al.[77]

Deposition of the same Au sol on different supports resulted different particle size after calcination at 400°C depending on the support due to particle aggregation and sintering. This behavior can be observed also at low temperature in the liquid phase reaction in case of Au–SiO_2–PVA sample, where larger particles or aggregates are shown in TEM images (**Figure 5.5)**. Particle migration on the surface is hindered on reducible oxides after calcination in the catalytic reaction because of stabilization of the Au particles by metal–support interaction. On SiO_2 support weak metal–support interaction is supposed compared to ceria or titania.

5.1.5 Conclusions

In gold catalyzed total oxidation reactions as e.g. CO the smaller gold particle size and the reducible oxide supports favor the activity. On the contrary, our results in glucose oxidation using SiO_2, CeO_2 and TiO_2 supported sol derived two different size gold particles show that the SiO_2 supported larger size gold is more active.

The opposite support effect observed in the glucose oxidation as compared in CO oxidation suggests different O_2 activation mechanism in the two reactions and/or the presence of a metal–support interaction in case of reducible oxides that modifies the ability of Au for activating glucose and O_2. The results show that the effect of the support is more significant than the small gold particle size.

5.2 CeO_2–Au/SiO_2 inverse catalysts for CO oxidation

5.2.1 Introduction

It is known and confirmed by our results (Chapter 5.1) that reducible oxides supported gold catalysts provide high activity in CO oxidation. In this chapter the role of CeO_2 was studied with the aim of the preparation of highly active catalysts in the reaction. For this reason Au/SiO_2 powder catalysts modified by different amounts of CeO_2 in a special way, when nanosize Au is decorated with CeO_2 patches were prepared. We wished to investigate the catalytically active Au–CeO_2 interface in CO oxidation.

5.2.2 Catalytic properties

The CeO_2 – doped Au/SiO_2 samples prepared by method A (Ce–Au sol adsorption on SiO_2) or B (Au/SiO_2 impregnated by $Ce(NO_3)_3$) (see Chapter 4.2) with different Ce loadings and the reference samples Au/SiO_2 and Au/CeO_2 were tested in CO oxidation. CO oxidation was used as a highly sensitive tool to test the presence of Au–CeO_2 active interface.

Table 5.4 contains data of metal loading of the samples together with the particle size determined by TEM and the catalytic data. The Au content of the samples agrees reasonably with each other and it is close to the nominal 2 wt%. We are certain that the undetermined Au

loadings are around 2 wt%, too, because the discoloration of liquid phase in the sol adsorption step showed that all Au nanoparticles in sol were attached to the silica.

Table 5.4. Metal loading, temperature of 50% CO conversion and Au particle size of the samples.

Sample	Au content (wt%)	CeO_2 content (wt%)	$T_{50\%}$ (°C)		Au particle size[b] (nm)
			after calc. at 300°C	after calc. at 450°C	
ACe0.04	2.0[a]	0.04		121	6.30±1.45
ACe0.08	1.8	0.08	138	85	-
ACe0.16	1.8	0.16	76	83	8.07±3.44
BCe0.06	2.0[a]	0.06	-	140	-
BCe0.11	2.0[a]	0.11	-	70	-
BCe0.60	2.0	0.60	50	48	5.73±1.92
BCe1.14	1.8	1.14	49	47	-
BCe2.64	1.9	2.64	44	44	6.57±1.65
BCe7.40	1.7	7.40	51	40	7.15±1.75
Au/SiO_2	2.0[a]	0	-	401	6.37±3.78
Au/CeO_2	2.0[a]	98	74	-	8.00±3.81

[a]: nominal value

[b]: determined by TEM after calcination at 450°C followed by catalytic run and only for Au/CeO_2 after calcination at 400°C followed by catalytic run

The catalytic measurements were conducted after calcination treatments at 300°C or 450°C. Carbonaceous deposits remained on catalytic active sites were removed already at 300°C in air, however, when applying 450°C calcination treatment, the CO_2 peak centered at

around 300°C had a negligible tailing above 300°C which means, insignificant organic material may have been remained on the support after the lower temperature calcination.

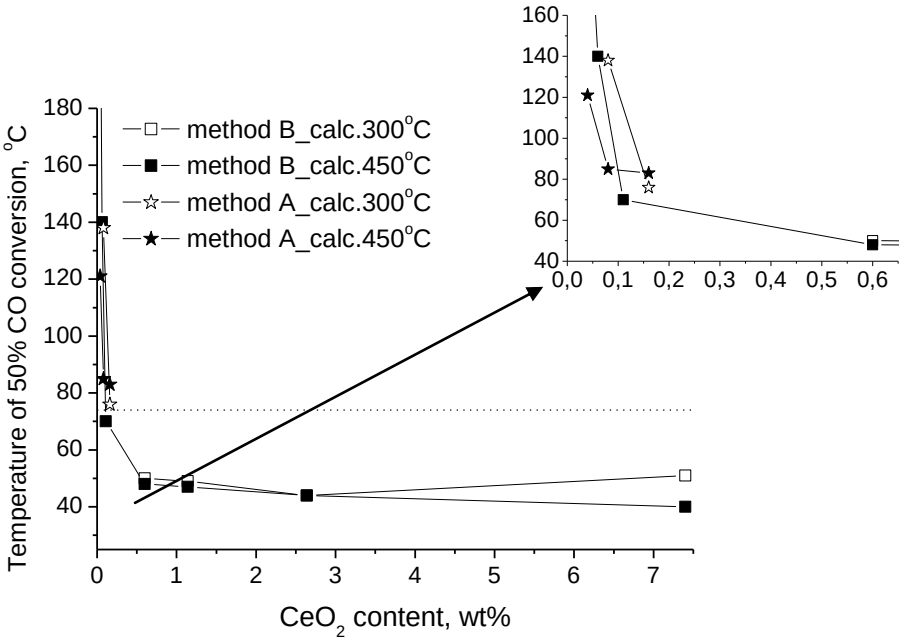

Figure 5.8. CO oxidation activity of the samples prepared by method A and B: the temperatures where 50% CO conversion was achieved ($T_{50\%}$) as a function of ceria content. 300°C calcination/pretreatment temperature is signed with empty, 450°C calcination/pretreatment temperature is signed with full symbols, respectively. Dotted line represents activity of Au/CeO_2 after calcination pretreatment at 300°C. The small inset enlarges the range of 0-0.6 wt% CeO_2 content.

Figure 5.8 summarizes the CO oxidation activity of the samples, viz., the temperatures where 50% CO conversion was achieved ($T_{50\%}$) as a function of ceria content. Data obtained after different calcination temperatures and different preparation methods are distinguished but

surprisingly lay on the same line which sharply increases between 0.2wt% and 0.5wt% CeO_2 meaning the decline of activity. The numeric data are collected in **Table 5.4.** The dotted line at 74 °C in **Figure 5.8** indicates the activity of the reference Au/CeO_2 sample. We can state that enhanced catalytic activity of CeO_2-modified samples was found compared to Au/CeO_2 reference sample at as low as 0.6wt% of CeO_2 loading already. The very little 0.04 wt% CeO_2-content on the other side makes ACe0.04 sample already a more efficient catalyst than the reference Au/SiO_2.

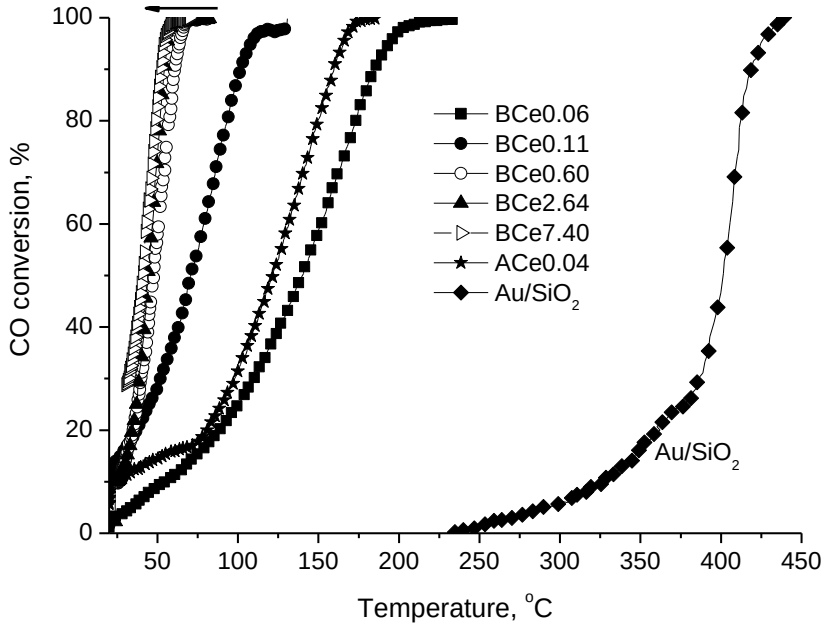

Figure 5.9. Representative conversion curves of samples prepared by method A (Ce–Au sol adsorption on SiO_2) and B (Au/SiO_2 impregnated by $Ce(NO_3)_3$) versus reaction temperature. The data were obtained after calcination pretreatment at 450°C. Note the extremely similar curves at CeO_2 content >0.6wt% for samples prepared by method B.

The difference between the activities of the samples is much better discernable looking at **Figure 5.9** where a few representative conversion curves obtained after calcination pretreatment at 450^{o}C are plotted against temperature. The main issue is that after reaching 0.6wt% CeO_2-content (by method B) there is only a minor difference between the catalysts. Furthermore, there is a slight difference in favor of method A, because ACe0.04 sample exhibits better activity than BCe0.06 in spite of the higher Ce–content of the latter.

Considering the formation of the active Au–CeO_2 species the structural characterization of the catalysts was carried out in order to understand the catalytic behavior of the samples.

5.2.3 Formation of Au–CeO_2 nanostructures on silica support

It is certainly eye-catching (**Table 5.4**) that the final CeO_2 content of samples prepared by method A (Ce–Au sol adsorption on SiO_2) is very low and more than 10 times less than the intended values (0.5wt%, 2.5wt%, 7.5wt%). **Figure 5.10** shows that by method A the attachment of all Ce–containing components to the silica surface was very limited. Thus, we prepared low loaded samples by method B (Au/SiO_2 impregnated by $Ce(NO_3)_3$) as well to be able to compare catalysts synthesized by the two methods at similar or the same Ce loadings. Of course, the success of Ce introduction by method B is obvious since it can be considered as a kind of wet impregnation of Au/SiO_2 by cerium nitrate: all the Ce compounds remain on the surface of the sample after evaporation of water.

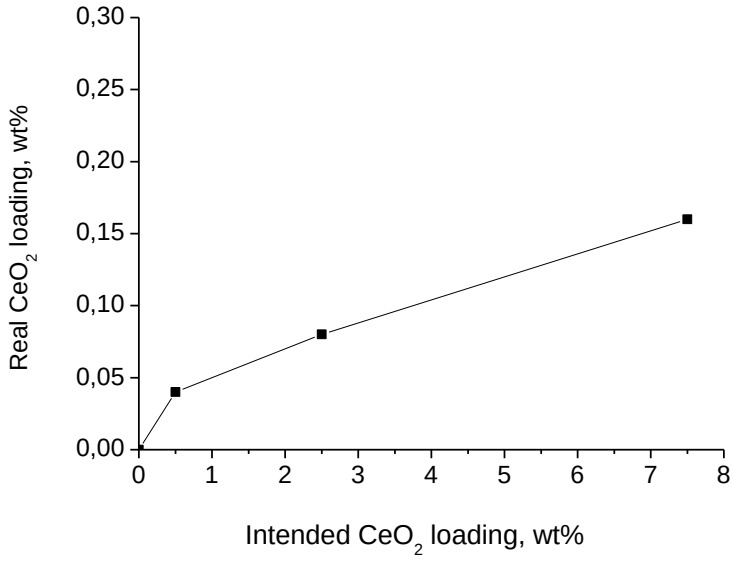

Figure 5.10. Measured CeO_2–content of samples prepared by method A (Ce–Au sol adsorption on SiO_2) versus intended CeO_2–loadings.

Let us consider what happens at the addition of cerium nitrate to the parent Au sol which has a pH=6.5 containing hydrolyzed tannin and citrate and all the byproducts of reduction. For the preparation of crystalline CeO_2 nanoparticles the main synthesis methods are based on solution phase methods such as alcohothermal,[133] hydrothermal, thermolysis processes. In hydrothermal route the starting precursor can be Ce(III), which is usually oxidized to Ce(IV) by the presence of air or other oxidants. Due to the presence of base, provided at higher pH, $Ce(OH)_4$ forms, then $Ce(OH)_4$ nucleation and growth takes place, and finally the $Ce(OH)_4$ particles formed dehydrate into CeO_2 during heat treatment.[134,135,136] Since Ce(IV) is more easily hydrolised than Ce(III), homogeneous precipitation can be initiated by H_2O_2 addition

at low temperature that slowly oxidises Ce(III). Thus, precipitation can be induced by the change in the oxidation state of precursor cation and not by the pH, however, base is needed to complete the hydrolysis. Ce(III)-hydroxide is a definite compound but Ce(IV)-hydroxide which can be described as CeO_2x2H_2O is considered to be a hydrous oxide which dehydrates progressively.[137] Primary particle of hydrous ceria posses at pH<7.2 a positive surface charge thus hydrous ceria is expected to adsorb anions.[138]

From the above references it is evident that the final oxidation state of hydroxide precipitates formed during hydrolysis is mostly Ce(IV). However, Kockrick and co-workers[139] reported the formation of nanoscale $Ce(OH)_3$ particles inside micelle structure of inverse microemulsion using cerium(III) nitrate and aqueous ammonia. Destabilization of microemulsion by acetone, filtrating, washing, drying at 100^{o}C resulted $Ce(OH)_3$ particles of 2–3 nm as was detected by HRTEM (lattice spacing corresponded to Ce(III)-hydroxide).

We should keep in mind that the presence of residual citrate and tannic acid or the hydrolysed byproducts such as gallic acid may play a crucial role in determining the fate of Ce precursor. Both reducing/stabilizing agents present in the Au sol are able to complex metal ions such as Ce(III), or stabilize CeO_2 or Ce-hydroxide particles, as well.[140,141,142] CeO_2 nanoparticles from cerium salt were produced with citric acid as protective agent against particle growth. Cerium-citric acid complex formation was suggested to occur first, and after its hydrolysis cerium hydroxide sol formed where the nanoparticles were covered with citric acid.[143,144] Marcilly and co-workers used also citric acid during ceria preparation while increasing

the pH to the basic region and applying fast evaporation of the solvent at 70^{o}C. The particles formed this way were amorphous and nanosize and contained mainly Ce(III) as was detected by XPS.[145,146] Note that in the above literature data the pH of the liquid phase was basic during preparation and so Ce(III) hydrolysis certainly happened. We believe that the presence of Ce(III) ions in the Au sol can cause particle aggregation and flocculation without hydrolysis based on the work of Oladoja and co-workers.[147] They assumed that positively charged species can strongly adsorb on the negative tannin molecules, can give effective destabilization through neutralization and thus promote flocculation. Complexation or chelation and ion exchange between the metal ion and the polyhydroxylphenol group of the tannin (gallic acid) molecule are assumed to take place simultaneously.

Consequently, it was not ascertained whether or not Ce-nitrate hydrolysed in our reaction conditions. Macroscopic particle aggregation which was observed in our blank experiments and at the highest cerium concentration does not necessarily mean the formation of hydroxide precipitate but it may reflect only charge neutralization and flocculation of Ce(III)-tannin-citrate complexes. The pH of the Au sol was 6.5 which is still acidic so we rather suggest that no or only partial hydrolysis happened to Ce-nitrate in our experiments and most of Ce(III) was bound in a chelate complex with tannin (gallic acid) and citrate. At lower Ce-nitrate concentration complete charge neutralization and so macroscopic precipitation does not happen between the anionic organic molecules and cerium ions. In the subsequent adsorption step, PDDA, a positively charged

polyelectrolyte was used to recharge the SiO_2 surface to be able to bind Au particles covered by negative stabilizing sphere.[17,21] The final low Ce content of samples prepared by method A reflects that Ce species (any kind of them) do not favour the positively charged polyelectrolyte covered solid and they rather remain in liquid phase in the filtrate associated with hydrolyzed negatively charged tannin (gallic acid) and citrate ions. The highest negative charge density and the highest concentration of complexing agents for Ce(III) is located around the Au particles, that is why the relatively low Ce concentration is expected to be concentrated around Au.

In the case of method B (Au/SiO_2 impregnated by $Ce(NO_3)_3$) the gold nanoparticles were located already on silica when Ce(III) nitrate was added. The samples were washed to remove the majority of organic and inorganic residues and dried at 60°C before Ce addition, however, negatively charged residual–shell around the gold can be expected which may localize a part of added Ce–nitrate.

In both methods the final evolution of $Au–CeO_2$ nanostructures takes place during calcination in air when all Ce species transform into CeO_x/CeO_2.

5.2.4 Structure of the catalysts: particle size and distribution of Ce species

In whatever form Ce species are present after drying, calcination pretreatment to remove organic moieties transforms them into Ce-oxide. X-ray diffraction pattern of BCe7.40 and BCe2.64 shown in **Figure 5.11** were taken after calcination at 450°C to check the

presence of crystalline CeO_2 (and Au) phases. Highly dispersed CeO_2 in samples of about 1 wt% CeO_2 and lower cannot be detected by XRD. Crystallite sizes are listed in **Table 5.5**. We could ascertain the presence of cubic CeO_2 fluorite structure with about 5 nm crystallite size in both samples. The intensity ratios of X-ray diffraction peaks for CeO_2 and Au for samples BCe7.40 and BCe2.64 are also shown in **Table 5.5**. As the scattering strengths are different for the various crystalline phases, therefore these values do not give the volume or weight fractions of CeO_2 and Au, it can be used only for comparison purpose between the two samples. Anyway, the four times larger intensity ratio for sample BCe7.40 revealed that a part of the CeO_2 is not visible by XRD in BCe2.64, suggesting the presence of an X-ray amorphous part of CeO_2.

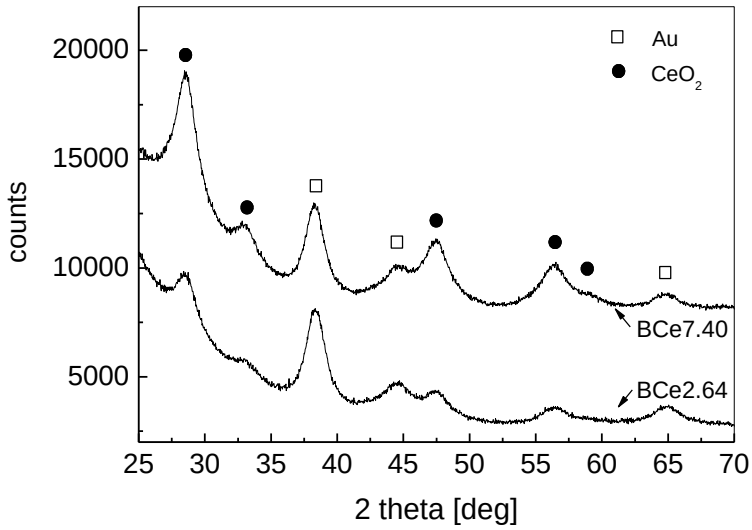

Figure 5.11. X-ray diffraction pattern of BCe7.40 and BCe2.64 after calcination pretreatment at 450^{o}C and catalytic run.

Table 5.5. The crystallite size for Au (d_{Au}) and CeO_2 (d_{ceria}) phases, and the intensity ratio characterizing the volume fraction of the two phases determined by XRD technique.

Sample	d_{Au} (nm)	d_{ceria} (nm)	I_{ceria}/I_{Au}
BCe7.40	5.5±0.6	4.9±0.5	1.79±0.16
BCe2.64	5.2±0.5	5.8±0.6	0.43±0.02

The nice, even distribution of individual Au particles is clearly seen in **Figure 5.12** that depicts the TEM micrograph of Au/SiO_2 after calcination pretreatment at 450^{o}C and catalytic run. The particle sizes of all the samples do not differ significantly, they range between 5.7 nm and 8.1 nm which is not the interval of the usual sudden change in activity with Au dispersion (d_{Au}~0–5 nm). Accordingly, differences in catalytic behavior can be attributed rather to the characteristics of Au/CeO_2 interface than the Au particle size itself. Looking at the particle size distributions of Au/SiO_2 and Au/CeO_2 reference samples it is clearly seen that ceria modification induces a kind of stabilization effect since the $Au\text{-}CeO_2\text{–}SiO_2$ systems have narrower size distribution, except for ACe0.16 which was the sample obtained by the adsorption of previously destabilized Au–Ce composite sol.

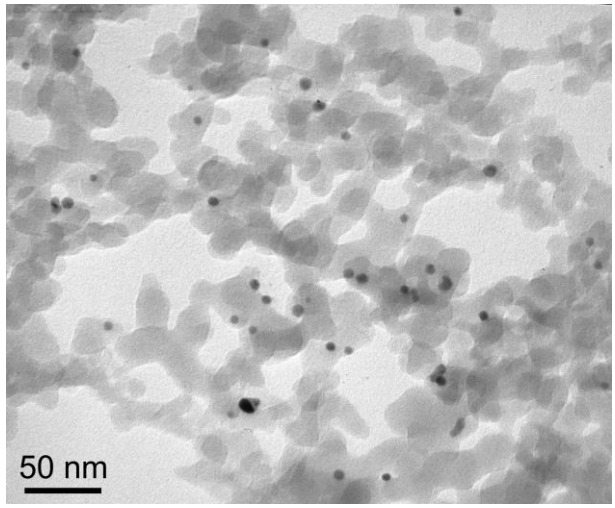

Figure 5.12. TEM image of the sample Au/SiO_2 after calcination pretreatment at 450ºC followed by a catalytic run. Even distribution of Au particles is seen that is characteristic to all investigated samples.

We already know that XRD detected crystalline CeO_2 phase. EDS measurements detected Ce and oxygen, as well, conventional TEM measurements (not shown here) gave us a hint on the existence of CeO_2 particles on silica surface of BCe7.40, but at lower Ce–content only Au particles could be distinguished by TEM.

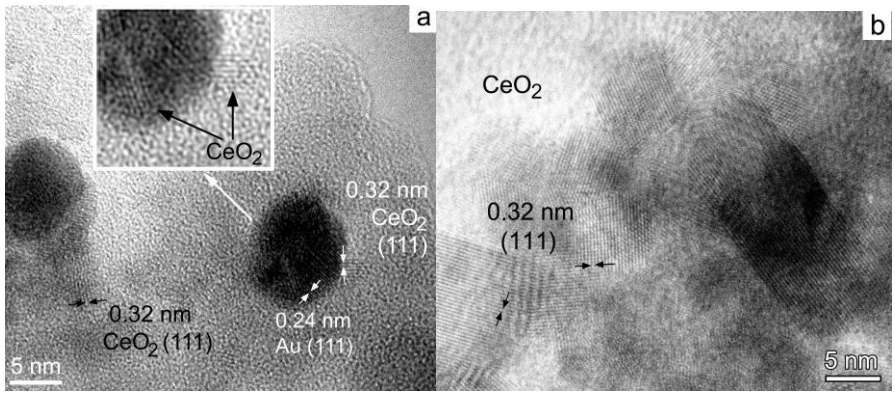

Figure 5.13. HRTEM of BCe7.40 with 7.4 wt% CeO_2. The 0.32nm period lattice fringes represent CeO_2 crystals both attached to the Au particles (a), and located, in large patches, on the SiO_2 (b).

HRTEM provided further information on the location, size, and structure of the promoting oxide in three samples prepared by method B (Au/SiO_2 impregnated by $Ce(NO_3)_3$) and in the one with the lowest Ce–content prepared by method A (Ce–Au sol adsorption on SiO_2). The HRTEM micrographs of sample BCe7.40 are shown in **Figure 5.13**(a) and (b). **Figure 5.13**(a) reveals the presence of nanosize CeO_2 particles, in contact with the Au nanocrystals surfaces. Two thin slabs with fringes can be observed partly covering the Au particles in the inset of the figure. The fringe period (0.32 nm) corresponds to the (111) lattice spacing of cubic CeO_2. Far from the Au particles, the pure SiO_2 surface is also covered by thin CeO_2 particles of 5–15 nm size as seen in **Figure 13**(b) by the lattice fringes characteristic to CeO_2 (111). Note that, although most gold particles are decorated by fringes of CeO_2, we found Au particles with no sign of CeO_2. The absence of fringes does not definitely mean the absence of CeO_2. It may mean that the crystallographic alignment of a CeO_2 crystal is far from a suitable zone, i.e. does not favor lattice imaging. The sample BCe2.64 also contained CeO_2 particles both in contact with and separated from the Au, but the amount of separate CeO_2 was less due to the lower Ce–content. **Figure 5.14** shows the HRTEM and EELS elemental mapping results of BCe2.64. **Figure 5.14**(a) and (b) represent the unfiltered image and the Ce elemental map of the same area, respectively. The arrows in (a) mark medium contrast regions that correspond to bright contrast regions i.e. high Ce concentration in the Ce map (b). **Figure 5.14**(c) and (d) are the enlarged frames from **Figure 5.14** (a) marked with “c” and “d”, respectively. In (d) a CeO_2 crystal is identified by its (111) lattice fringes that is located on the

silica, while, the CeO_2 particle shown in (c) is attached to the Au. As we go further to less Ce-content (BCe0.60), **Figure 5.15** with the enlarged inset shows that the CeO_2 appears mostly on or nearby the Au surface, while the silica is depleted in CeO_2.

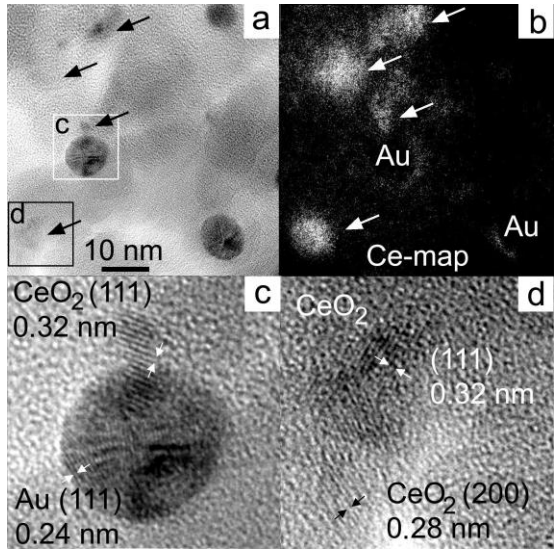

Figure 5.14. Unfiltered HRTEM image (a) and EELS Ce map of the same area (b) of sample BCe2.64 with 2.64 wt% CeO_2. The bright contrast regions in (b) represent presence of Ce that corresponds to the regions with 0.32 nm lattice fringes in (a). (c) and (d) are enlarged frames from (a).

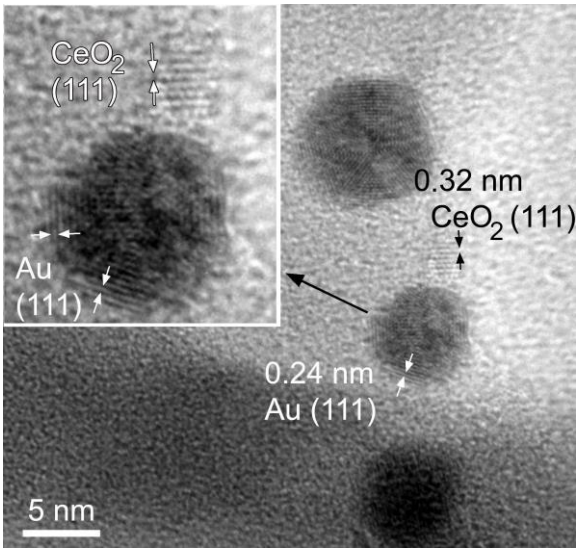

Figure 5.15. HRTEM image of sample BCe0.60 with 0.6 wt% CeO_2 (inset: magnified Au particle and associated Ce-oxide as marked by the arrow) representing that CeO_2 is found mainly as attached to Au and in the vicinity of the Au particles.

To reveal the distribution of CeO_2 at extreme low cerium contents is of crucial importance because theoretically it is very easy to locate this amount of Ce-oxide on the high surface area Aerosil SiO_2 without even any contact with Au particles. With this aim, a sample prepared by method A (0.04wt% Ce) was also investigated. HRTEM and EELS found no trace of Ce-oxide on silica, however, it gave definite proof of CeO_2 associated to Au (the existence of Au–CeO_2 interface) as it is presented in **Figure 5.16. Figure 5.16** (a), (b) and (c) show the unfiltered HRTEM image, the EELS Ce–map and the enlarged frame "c" from (a), respectively. The bright contrast in the Ce map (b) indicates a distribution of Ce exclusively around/on the Au particles (see also the arrows). No remarkable signal of Ce

was detected apart from the Au crystals. Furthermore, in **Figure 5.16 (c)** a single Au particle is seen (enlarged frame from (a)) with the lattice fringes of CeO_2 nanoparticles on its surface.

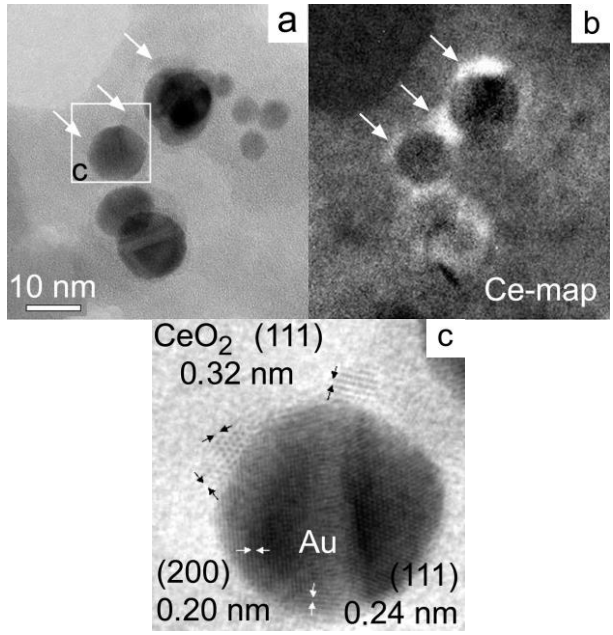

Figure 5.16. Unfiltered micrograph (a) and EELS Ce map (b) of sample ACe0.04 with 0.04 wt% CeO_2. The bright contrast in the Ce map (b) marks regions that contain Ce. The enlarged image (c) shows CeO_2 particles (0.32nm lattice spacing) on the Au crystal (from the center of (a)). Practically no CeO_2 was found apart from Au.

We calculated the possible maximum coverage of CeO_2 exclusively on Au surface assuming 2 wt% Au and 0.0326 wt% Ce content and d_{Au}=6 nm size particles. Using the work of Stanek and co-workers,[148] where the number of Ce atoms on CeO_2(111) surface is given as 2.31 Ce atoms/a_o^2 where a_o=0.5412 nm, and assuming monolayer coverage of CeO_2 on Au (which is not the case), we

obtained that at such a low Ce-content only 17% of the Au surface can be covered by CeO_2. If ceria is present in multiple layers, this number is even smaller. Certainly, our calculation applies several assumptions; however, we get an approximate idea how dispersed CeO_2 must be detectable on the surface of Au particles under the electron beam.

Considering all experimental results, XRD and HRTEM measurements proved the presence of crystalline CeO_2 particles/domains of different size (between about 2 and 15nm, depending on CeO_2 loading) in our samples. Depending on the Ce-loading and preparation method, ceria can be found selectively on the Au nanoparticles or both on Au and on the bare silica surface. The localized oxide promotion of gold is greatly accomplished, since it seems that independent of the preparation method, gold surface is somehow saturated by ceria first, then the increase of Ce-loading causes Ce species spread over the support surface, as well. Full coverage of a single Au particle by ceria, viz. core-shell structures were not detected. **Scheme 2** summarizes the main points and differences of the two preparation methods depicting the assumed interactions and final catalyst structures.

Scheme 2. Main steps of preparation with the suggested structures and interactions.

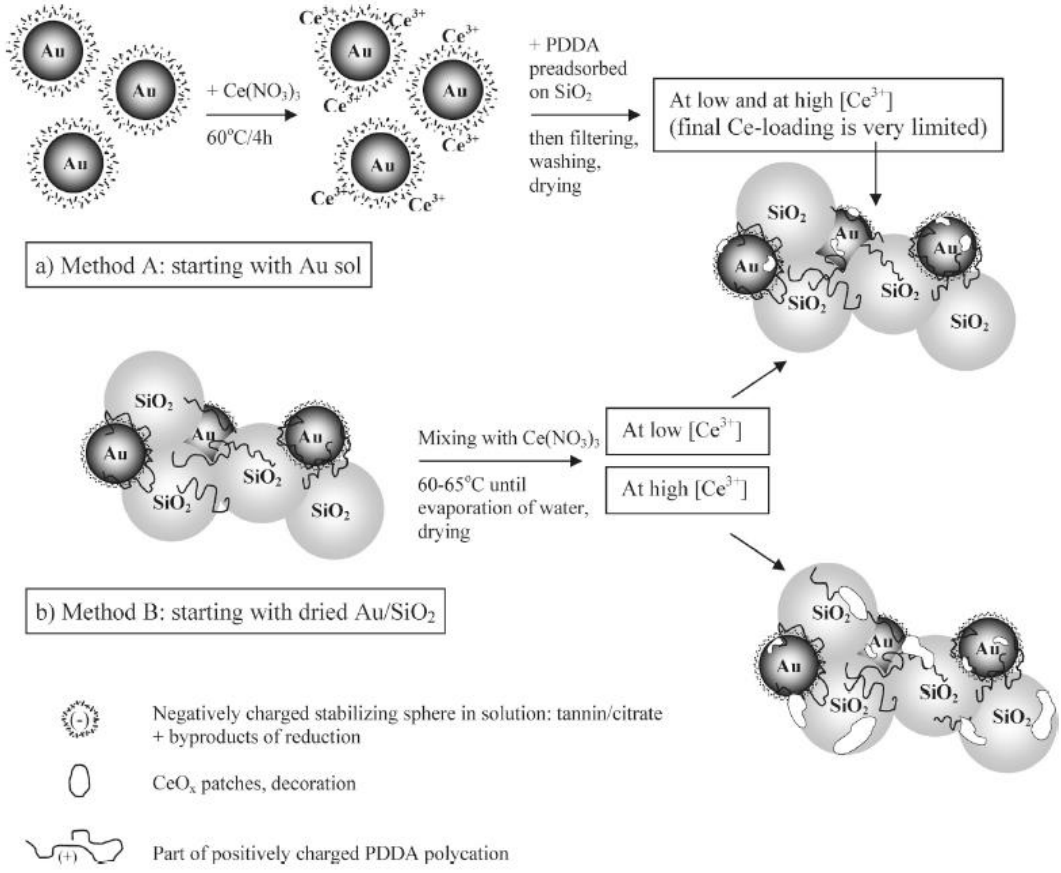

We tentatively suggest that when Ce precursor is added to the sol, the stabilizing sphere around Au is full and attracts more Ce species to be attached and complexed there than the one after washing off most of organic materials and drying (what applies for method B). It is still surprising (but is in accordance with the evolution of CO_2 in calcination resulting from the oxidation of organic residues) that washing leaves a sufficient part of negatively charged stabilizing

sphere on the surface of Au and so when Ce-nitrate added during preparation method B to the suspension, it is bound first to the Au particles as HRTEM and catalytic studies proved. Otherwise, if 0.06 wt% CeO_2 were homogeneously dispersed on silica surface it would not provide a catalyst with $T_{50\%}$=140^oC (note that $T_{50\%}$=401^oC for Au/SiO_2).

Considering the results of XRD and TEM, we are definite to say that nanosize, thin CeO_2 domains which are localized around Au particles play the crucial role in the reaction, and CeO_2 islands far from Au particles are not able to influence or enhance catalytic activity through the well-known oxygen storage and release capacity to a significant extent. The CeO_2 coverage on Au is somewhat limited due to the complexing capacity of stabilizing sphere, this is why at higher Ce–loading even more and more ceria is deposited on the bare silica, additional activity increase cannot be observed or it is only negligible.

Let us consider what the possible reasons of the very high activity of Au–CeO_2 interface can be. Gold particle size difference is not suggested to be the determining factor, because d_{Au} varies between 5.7–8.1 nm for all the samples. The commercial ceria nanopowder which is the support of the reference sample consists of 6–50 nm size particles while our ceria decoration over gold has a particle size of ~2–5 nm. It is known from the literature, that the structure, morphology of ceria can greatly influence catalytic activity.[149] The morphology effects of nanoscale ceria possessing different shape such as rod, polyhedra or cube was investigated in Au/CeO_2 samples, and XRD, TEM, temperature programmed

reduction (TPR), X-ray photoelectron spectroscopy (XPS) and diffuse reflectance Fourier transform infrared studies (DRIFTS) revealed that not the crystallite size but the surface structure, the exposed surface planes are of high importance in achieving good redox ability and catalytic activity: the predominantly exposed {100}/{110}-dominated surface structures of ceria nanorods turned to be the best supports for gold.[60,150] The CeO_2 islands, slabs in our samples seem to be very thin but we could not find distinguished crystal planes in abundance by the characterization methods applied. However, as they formed by calcination treatment at a relatively low temperature from organic complexes or hydroxides arranged around Au particles in liquid phase, they must contain surface defect sites and lots of oxygen vacancies.

CO oxidation on Au/CeO_2 is suggested to take place via the reaction of CO adsorbed on low-coordinated Au sites and oxygen activated on the oxygen vacancies formed along the $Au–CeO_2$ interface (adlineation sites). [151,152,153] There is a certain correlation observed between the presence of oxygen vacancies, the amount of Ce(III) ions and the increased catalytic activity as the following studies reveal. The work of Widmann and co-workers[151] using TAP technique (temporal analysis of products) proved that CO oxidation activity can be enhanced by the removal of about 7% surface oxygen of ceria (reductive activation). Furthermore, model studies showed that the Ce(III) concentration is in line with the oxygen vacancy concentration, and the presence of large amount of oxygen vacancies in the oxide support influences the binding energy of small Au particles with $d<2nm$ and the CO desorption temperature, but these

effects disappear with increase of Au size.[152] According to Qian and co-workers[158] increase in calcination temperature in air annihilates surface oxygen vacancies in CeO_2 (the Ce(III)/Ce(IV) ratio decreases measured by XPS), while Ce(III)/Ce(IV) increases when the support is loaded with Au which means that the loading of Au facilitates the formation of surface oxygen vacancies. Escamilla-Perea and co-workers[159] declared the promoting role of Ce(III) ions in CO oxidation, because the decrease in their surface exposure led to a decrease in activity.

In our case two parameters of ceria might be of high importance concerning the high activity observed, namely the size (dimension) of ceria islands and the preparation medium which is of reducing, with citric acid and gallic acid present. XPS, STEM and IRAS techniques applied on gold deposited on CeO_2{111} thin films and CeO_x nanoparticles revealed that 3+ is the dominating oxidation state of ceria in smaller particles in the nanosize CeO_2. XPS results suggested that ~ 5 nm is the particle size below which ceria exhibits a significant degree of reduction.[154] Tsunekawa and co-workers[155] showed during investigation of ceria sols containing 6.7–2.1 nm particles that electron diffraction lattice parameter changes with size meaning conversion of Ce(IV) near the surface to Ce(III). As for the reducing medium, Chen and co-workers[156] found that ascorbic acid treatment of sol–gel derived Au/CeO_2 might have been the reason for the improvement of the Ce(III)-ion related defect content of ceria and the higher ratio of ionic gold. Ceria that was prepared by Marcilly method in the presence of citric acid after only drying contains mainly Ce(III).[145,146]

According to these literature references it seemed reasonable to carry out XPS measurements on the samples to determine the Ce(III)/Ce(IV) ratio. Unfortunately even at the highest CeO_2 content it did not make sense to fit the broad and unstructured peaks of the cerium region. The only definite result was that BCe7.4 sample does contain Ce(III) component beside Ce(IV) in as prepared state, which upon a 300^oC calcination treatment does not change significantly. This finding means that the Ce(III) component is highly stable. The determination of about 25% Ce(III) concentration is only approximate and was based on the ratio of the total Ce 3d area to the Ce(IV) satellite peak area at about 917eV BE. The Ce 3d intensity in the most interesting samples with low CeO_2 content was extremely low and could hardly be seen on the curved baseline. That is why we had to relay on the literature references of somewhat similar systems and keep in our mind that all the reaction condition (presence of reducing and complexing agents) may help to prevent the early oxidation of Ce^{3+} component as the XPS measurement after calcination treatment proved.

Thus, based on the above literature and the XPS data of BCe7.4, we tentatively suggest that our thin CeO_2 patches in close contact with Au nanoparticles may contain large amount of Ce(III) ions and so many oxygen defect sites, which in turn enhance oxidation ability compared to the bulk, commercial CeO_2 particles. Special electronic interaction may exist between the contacting few layer thick CeO_2 patches and the Au particle. Furthermore, the contact area between Au and nanosize CeO_2 islands must be larger than the interface

between the same Au particles and the bulky ceria particles of ceria nanopowder.

Table 5.6. Initial reaction rate (r_0) was calculated at 30°C when the CO conversion values were below 15%. Calculated TOF values obtained for the structural model assumed. Flat Au surface and hemispherical CeO_2 particles of 3 nm are assumed. Active sites are Au atoms within 1 nm range around the CeO_2 hemispheres, this is called perimeter.

Sample	r_o	TOF
	μmol CO/s/g_{cat}	1/s
BCe0.06	0.262	1.05E-01
ACe0.04	0.674	4.06E-01
BCe0.11	1.016	2.23E-01
BCe0.60	0.886	3.56E-02

Next, theoretical calculation was done to quantify the catalytic data at the extreme low CeO_2 contents. TOF values were calculated using the following model that we know includes several assumptions. Flat Au surface was supposed which is covered by hemispherical CeO_2 particles of 3 nm, and TOF values were calculated related to one active Au site. The active sites (called Au perimeter sites) were supposed to be Au atoms within 1 nm region around the hemispherical CeO_2 particles. Au(111) surface was assumed with $1x10^{15}$ Au atoms/cm^2. Initial reaction rate was calculated at 30°C when the CO conversion values were relatively low, below 15%. The results are summarized in **Table 5.6**. TOF values are in good agreement with the work of Zhou and co-workers,

who did TOF calculation for a model type CeO_2/Au inverse system.[160] The TOF of the sample of the 3 lowest CeO_2 content does not differ significantly, suggesting that the increase of CeO_2 loading in this region results in increasing number of similar active sites. The somewhat lower TOF calculated for BCe0.60 may reflect the appearance of some portion of CeO_2 on SiO_2 instead of Au.

We should consider finally the effect of 150^oC difference in the calcination temperatures applied as pretreatment. Increase in calcination temperature is expected to heal the oxygen vacancies to some extent and increase the crystallization of ceria. Our data, however, do not reflect any significant changes due to the increase of calcination temperature meaning that the Au–CeO_2 interface formed is relatively stable under our reaction conditions. In the work of Beier and co–workers[157] liquid–phase oxidation of alcohols was studied on silver-based catalysts promoted by ceria in a simple way, viz., commercial CeO_2 was mixed and calcined at different temperatures with the 10wt%Ag/Aerosil sample. The mixture that was calcined at 500^oC was highly active and the calcination time had a great influence on activity and selectivity: a medium time (30 min) was the perfect choice, while the particle size determined by XRD did not change with increase in calcination time. Other possible reasons were not discussed. In our case BCe7.40 had an average 6.42 nm particle size after 300°C calcination, whereas that increased to 7.15 nm after 450°C calcination. The difference in particle size is negligible; moreover, the sample calcined at 450°C was more active than the other. This shows that particle size difference indeed is not the reason of the difference in catalytic activity between the samples.

We can conclude that compared to TiO_2–Au/SiO_2 system,[19] where the activity reached the activity of the reference Au/TiO_2 sample only at 4wt% TiO_2-loading, here, in the case of CeO_2–Au/SiO_2 systems a small amount of Ce was enough to reach the activity of the Au/CeO_2 reference sample (0.16wt% CeO_2).

5.2.5 Conclusions

In this chapter work on CeO_2–Au/SiO_2 inverse catalysts is presented. Au/SiO_2 catalysts were promoted by 0.04-7.4 wt% CeO_2 using two different methods based on the application of Au sols. In method A Ce(III) nitrate was added to the Au sol and after a heat treatment at 60°C the adsorption step onto SiO_2 was accomplished using PDDA. In method B the Ce precursor was added to the washed and dried Au/SiO_2 parent catalyst producing a suspension which was kept also at 60°C until the evaporation of water. By method A the introduction of Ce was very limited; the maximum cerium content in the final samples corresponds to 0.16 wt% CeO_2.

XRD showed the presence of CeO_2 nanocrystals at 2.4 wt% and 7.4wt% CeO_2 content (above the detection limit of the technique). HRTEM measurements found thin CeO_2 moieties over gold already at 0.04wt% CeO_2 in the calcined catalysts. This extreme low 0.04 wt% CeO_2 content decreased the temperature of 50% CO conversion by 280°C compared to Au/SiO_2 reference and 0.16wt% CeO_2 was enough to approach closely the activity of the Au/CeO_2 reference sample. The increase of Ce–loading above 0.6 wt% CeO_2 content apparently did not increase the CeO_2 coverage on gold nanoparticles, because the samples had almost the same activity up to 7.4wt% CeO_2.

HRTEM proved that the additional CeO_2 is located on silica surface, when this is the only possibility (method B) or removed by the filtration of liquid phase (method A).

The localization of Ce–species around gold particles in liquid phase must be provided and limited by the interaction with the organic stabilizing shell. This applies for method B, as well.

5.3 SiO_2 supported bimetallic AgAu catalysts for glucose oxidation

5.3.1 Introduction

As seen from the literature cited above in Chapter 2, the Ag modified Au bimetallic catalysts are very promising in oxidation reactions and the origin of their activities is not clear. In Chapter 5.1 we found high activity of the silica supported catalysts in glucose oxidation, so we decided to modify that Au/SiO_2 "parent sample" by Ag addition. Our aim was to produce well characterized truly bimetallic AgAu NPs of various Ag/Au atomic ratios and study the effect of particle composition on glucose oxidation activity. The structure of the AgAu colloidal particles has also been studied.

5.3.2 Catalytic properties

The bimetallic $AgAu/SiO_2$ catalysts with different Ag/Au ratios (preparation method was detailed in Chapter 2) were tested in glucose oxidation. The catalytic activity of the samples was compared in **Figure 5.17**. Synergistic activity increase was achieved with addition of Ag to Au up to Ag/Au=33/67 nominal atomic ratio. At Ag/Au=50/50 nominal ratio no activity was detected as in the case of pure Ag/SiO_2 sample.

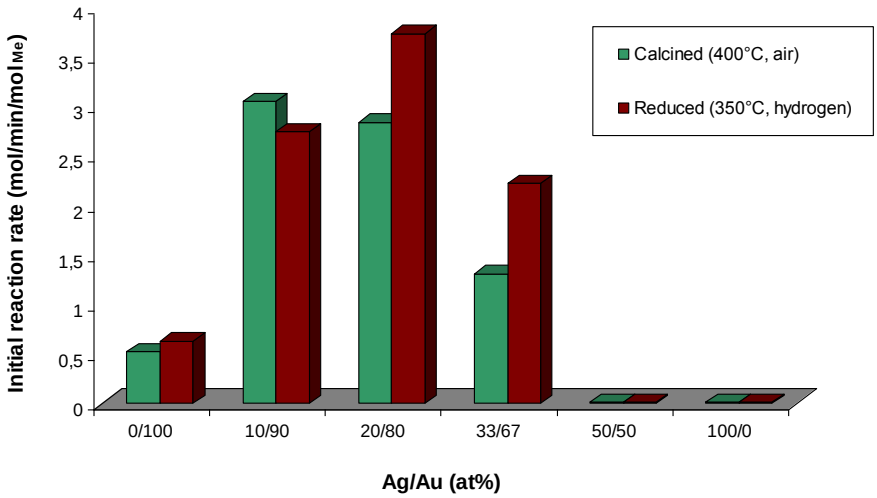

Figure 5.17. Catalytic activities of the $AgAu/SiO_2$ samples in glucose oxidation; T=35°C, pH 9.5, $c_{glucose}$ =0.1M.

The effect of the reduction treatment in H_2 at 350°C of the calcined samples was investigated. The activity reached a maximum value at 20/80 Ag/Au ratio in the case of the reduced sample. The reduction treatment slightly affects the activity of the calcined $10Ag90Au/SiO_2$ and Au/SiO_2 catalysts. The $50Ag50Au/SiO_2$ and Ag/SiO_2 showed no activity even in reduced form. The reduction treatment increased the activity to a higher extent in the case of $33Ag67Au/SiO_2$ and somewhat lower extent in the case of $20Ag80Au/SiO_2$.

Physical mixture of the monometallic Ag/SiO_2 and Au/SiO_2 catalysts in 20% and 80% metal content, respectively, was also tested in the reaction. The activity correlated to the activity of the monometallic Au/SiO_2 as converted to the same amount of metal. Absence of any synergistic effect shows that the Ag of the physical mixture is not involved in the reaction.

In order to understand the structure of the catalysts, characterization of the system was carried out at each step of the preparation process.

5.3.3 Formation of AgAu nanostructures

PVA stabilized Ag sol was formed by reducing $AgNO_3$ with $NaBH_4$. This parent Ag sol was analyzed by HRTEM which provided information on the crystal structure of the sample. Considering our preparation method regular cubic Ag crystal structure was expected.

Figure 5.18a shows a HRTEM image of the Ag sol. We measured the lattice fringes in numerous grains and found distances of 0.250 nm, 0.247 nm, 0.238 nm and 0.232 nm. The 0.238 nm and 0.232 nm lattice periods and the 70.5° interplanar angle measured in particle A refers to the (111) planes of the usual face centered cubic (fcc) phase (PCPDF 040-783) as indicated also in the Fast Fourier Transform (FFT) inset of A. However, in particle B we measured fringe spacings of 0.250 nm and 0.247 nm with an interplanar angle of 60°, that cannot be indexed with fcc structure. Instead, these lattice spacings at an angle of 60° can be indexed as the (10-10) type planes of the hexagonal *4H*–Ag structure (PCPDF 411-402) as represented also in the FFT inset in **Figure 5.18.**B.

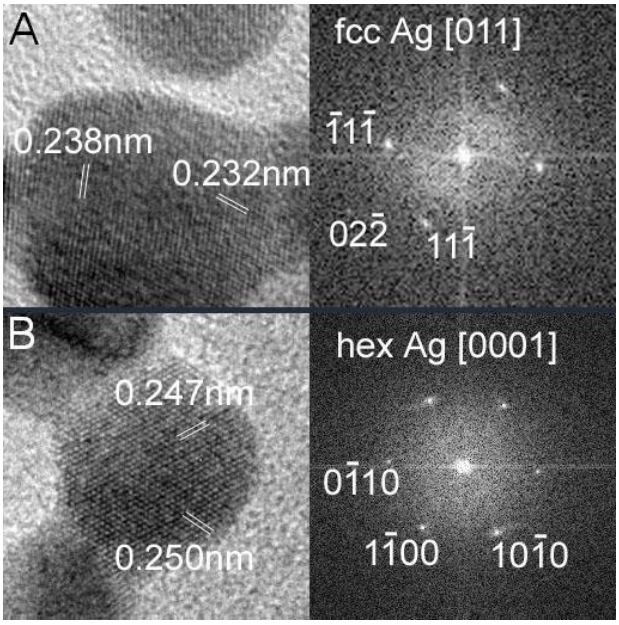

Figure 5.18a. HRTEM image of the Ag sol. The particles marked with A and B with corresponding FFT patterns represent fcc and hexagonal Ag phases, respectively.

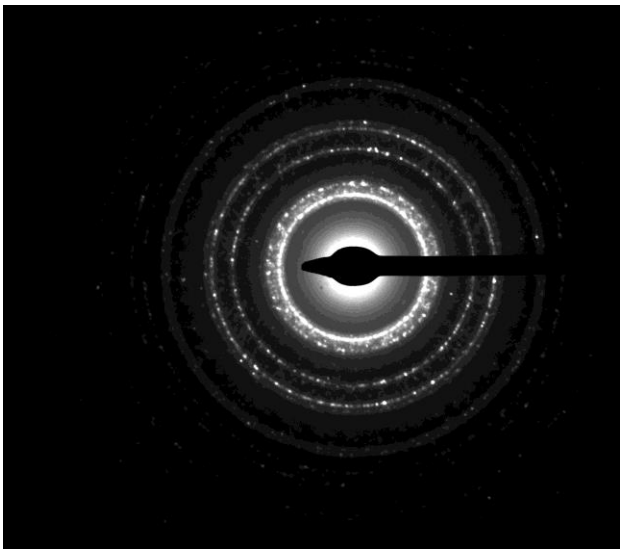

Figure 5.18b. Electron diffraction pattern of several hundreds nanoparticles in Ag sol.

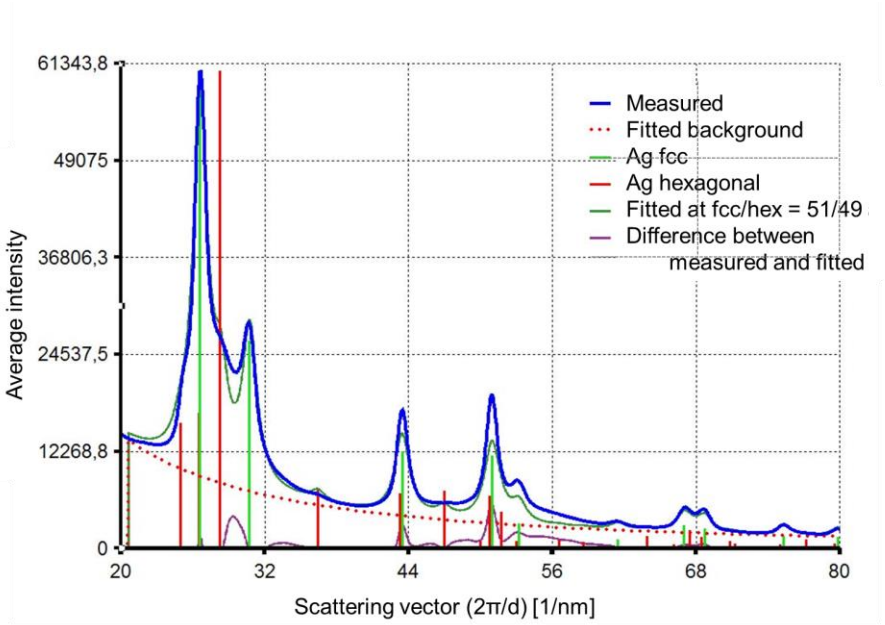

Figure 5.18c. Intensity distribution in electron diffraction pattern shown in Figure 5.18b.

Selected Area Electron Diffraction (SAED) results confirmed the coexistence of the Ag–fcc and Ag–*4H* hexagonal about the same amount in the Ag sol. **Figure 5.18b** shows the electron diffraction pattern of more than 600 nanoparticles in Ag sol and **Figure 5.18c** presents the intensity distribution in that electron diffraction pattern. The measured curve (blue line) fits well with the dark green curve, which was calculated at 51% Ag–fcc and 49% Ag–*4H* hexagonal phase composition. The coexistence of the fcc and *4H* Ag phases was also observed in the case of Ag–nanowires.[161] The equilibrium crystal structure for silver is fcc (a=0.4086 nm),[162] however, three other polytypes of Ag have also been reported: the 9R polytype forming at grain boundaries in polycrystalline Ag,[163] the two-dimensional (*2H*) hexagonal phase of Ag can be grown on glass and

Si by controlled electrochemical deposition[162] and the *4H* hexagonal polytype which, interestingly, to date, has been observed only in nanocrystalline and continuous films[162,164] or nanorods.[161,165,166]

Size–dependent phase stability of silver nanocrystals governing the formation of different Ag polytypes was reported in references.[161,167] Chakraborty et al.[162] underlined the importance of the control of growth kinetics prior to the size effect and concluded that the former is enough to obtain any of the three polytypes of Ag. Huang et al.[168] successfully fabricated belt–like *4H*–Ag and suggested that the reason why *4H*–Ag is rarely observed is probably due to a special combination of synthesis parameters. Similar interpretation of why *4H*–Ag is favored under our experimental condition could be applied. In our preparation method the silver nanoparticles were prepared in aqueous media and $NaBH_4$ was added quickly to the mixture of $AgNO_3$ and PVA. The reduction of the Ag ions happened rapidly. Thermodynamically the fcc structure is favorable while under kinetic control the less stable *4H* hexagonal polytype of silver can be grown. For *4H*–Ag higher chemical activity is supposed because of its higher distance between the planes than in fcc structure Ag. Our simple Ag sol preparation process could be a basis for synthetizing Ag nanoparticles with desired polytype.

HRTEM provided further information on the structure of the bimetallic sol sample prepared by $HAuCl_4$ reduction in the parent Ag sol. A HRTEM image of the bimetallic 33Ag67Au sol is shown in **Figure 5.19.** The enlarged image and the FFT pattern of particle A (insets) show lattice periods and reflections of 0.237nm and 0.206nm positioned at an angle of 71° and 54°, respectively. That obviously

refers to the (111) and (200) planes of fcc Ag(Au) structure as shown by the corresponding indices in the FFT. Contrarily to the 4H of Ag sol, the fcc Ag(Au) structure was found typical in the bimetallic AgAu system.

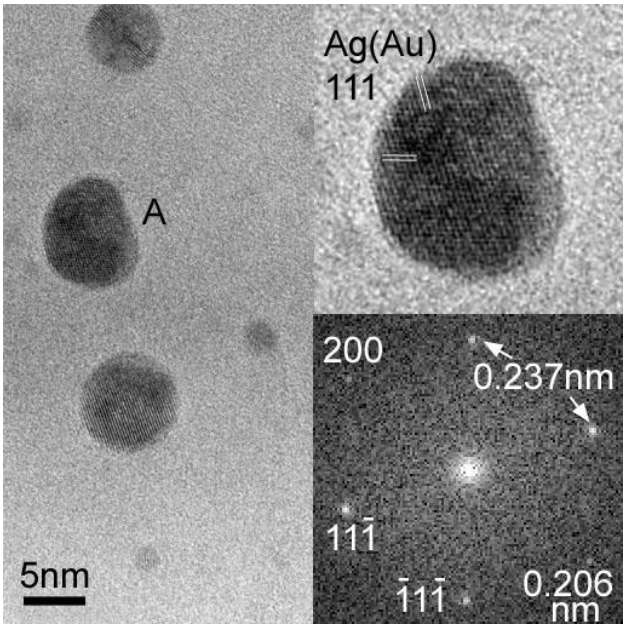

Figure 5.19. HRTEM image of 33Ag67Au sol with the inset of the enlarged particle marked with A and the inset of its FFT pattern. The 0.237nm lattice periods at an angle of 71° and the 0.206nm-period at an additional angle of 54°, correspond to the (111) and (200) planes of fcc Ag(Au), respectively.

The contrast features of the particles in the micrograph suggest that Ag and Au are randomly distributed, i.e. AgAu alloy was formed. It is to mention, that in case of 6nm–size AuPd particles concentric dark/bright contrast could be detected by TEM in our laboratory, earlier, indicating Au_{core}–Pd_{shell} structure.[169] Hodak et al. have shown clear phase boundaries between the Au core and the Ag shell for particles ≥20 nm, but for particles with smaller sizes phase

contrast were not observed. Size-dependent spontaneous alloy formation was concluded by Shibata et al.[170] In the case of alloy structures, e.g. CuAu,[171] ZnAu,[172] PbAu,[169,173] SbAu[174] HRTEM was utilized to determine the change in the lattice parameters resulting from the alloying process. Gold and silver have similar atomic sizes and a face centered cubic (fcc) crystal structure with similar lattice constants of 0.408nm and 0.409nm, respectively;[170] complete miscibility can be obtained by these metals in the bulk at any composition with no change in lattice constants. Therefore the usually observed lattice parameter change in the case of alloy structures is not expected in AgAu system. *4H* Ag hexagonal crystal structure – found in the case of the parent Ag sol – was not detected in the case of alloy sol samples, only the equilibrium fcc crystal structure was observed. The absence of *4H* Ag phase in the alloy could be due to that the NPs can be restructured during the preparation process.

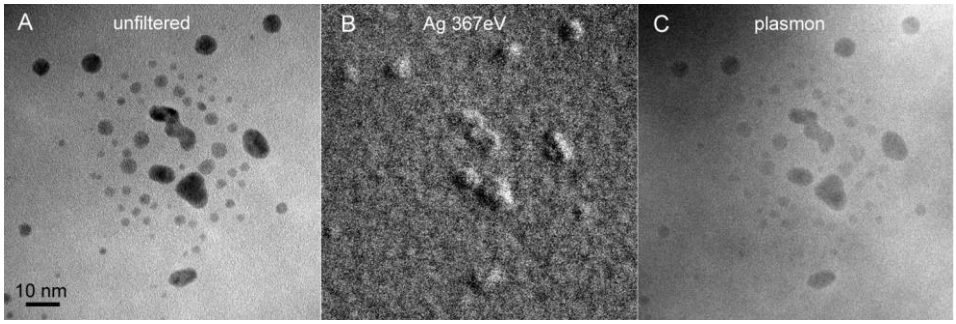

Figure 5.20. TEM image of the of bimetallic 33Ag67Au sol sample (a), EELS Ag elemental map (b) and plasmon image (c) of the same area.

Figure 5.20 a-c shows the unfiltered TEM image of bimetallic 33Ag67Au, the EELS Ag elemental map of the same area and the

plasmon image of the sample sol, respectively. The bright contrast in the Ag map (b) refers to high Ag concentration that indicates the presence of Ag in all particles. Particles smaller than 2 nm cannot be seen in the Ag map because of the ambient noise. We can conclude that every – observable – particle contains Ag, so the particles should be bimetallic. Alloy formation is supported also by the contrast within the particles that is distinct from the appearance of core–shell structure in bimetallic particles. The plasmon image shows dark contrast of the catalyst particles compared to the non–metallic carbon background. That represents metallic feature of the AgAu particles suggesting that all of them are reduced.

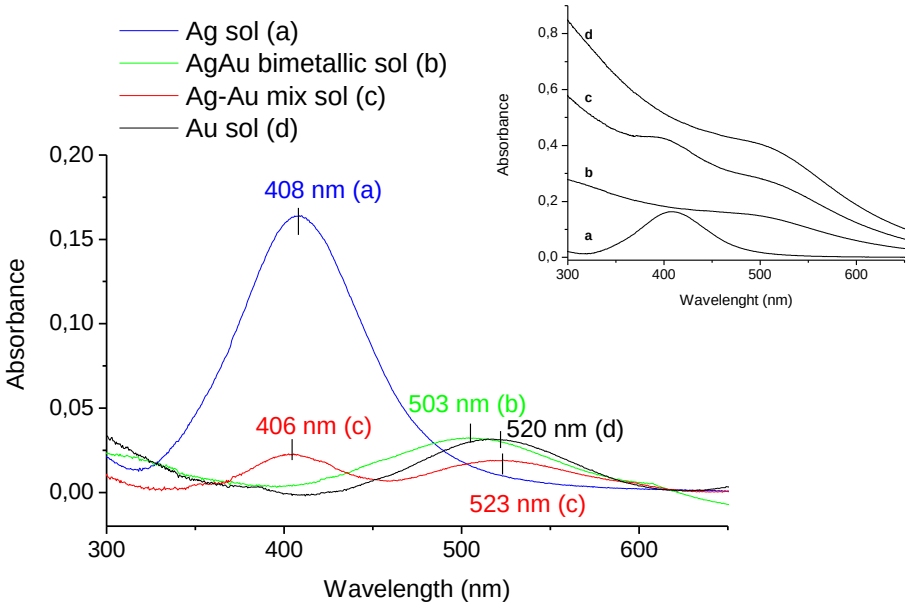

Figure 5.21. UV-visible spectra of Ag sol (a), the bimetallic 20Ag80Au sol (b), the mixture of the monometallic Ag and Au sol in 20/80 volume ratio (c) and Au sol (d) after linear baseline corrections. The inset shows the original spectra of the same sols.

UV–visible spectra of the AgAu nanostructures were recorded to understand the formation of the bimetallic particles. **Figure 5.21** a-d show the baseline corrected absorption curves of (a) the parent Ag sol; (b) the bimetallic 20Ag80Au sol; (c) the mixture of the monometallic Ag and Au sol in 20/80 volume ratio and (d) Au sol prepared by the same way as all of the other sols (see in Chapter 2.2). The inset shows the original spectra of the sols and in **Figure 5.22** the different color of the sols can be observed. As shown in **Figure 5.21** the Au surface plasmon resonance (SPR) appeared at 520 nm and the Ag SPR at 408 nm. The origin of this surface plasmon band is the collective oscillations of free conduction electrons in metal excited by light at a particular wavelength.[175] In the case of the AgAu bimetallic sol a single absorption band appeared at 503 nm.

Figure 5.22. Colors of the monometallic Ag and Au, the mixture of Ag and Au monometallic sol in 20/80 volume ratio and the bimetallic alloy sols.

In order to check the possibility of the formation of separate monometallic particles during the synthesis of AgAu sol, a mixture of Ag and Au monometallic sols were used as a blank experiment. In the case of the mixture sol two distinct surface plasmon bands appeared at 406 nm and 523 nm. The results proved that bimetallic AgAu sol formed and not a mixture of Au and Ag sols. The disappearance of Ag SPR and blue shift of Au SPR suggests that the Au reduced on the surface of Ag. This results proved that the $[AuCl_4]^-$ anion is able to replace the PVA on the surface of the Ag particle and the reduction of Au^{3+} takes place there. According to our preparation process the consecutive reduction of the silver and gold ions should led to Ag–core Au–shell particles, but the single band for the bimetallic particles suggests AgAu alloy formation in the sol, which is in agreement with HRTEM results. Nonalloy, or core–shell AuAg nanoparticles, exhibit two characteristic absorbance peaks.[176] According to theoretical calculations (based on Mie theory) in the case of core–shell structure, gold deposition should result only in damping of the underlying silver surface plasmon band. The blue shift of single Au SPR can correlated with alloy structure and originated from the perturbation of the d–band energy levels.[177] Considering the electrode potential of the metals in the system, it is clear that its relations favor the alloy formation. Ag was in metallic form when Au^{3+} ions were added to the system.

$3Ag + Au^{3+} \rightarrow 3Ag^{+} + Au$ reaction could take place thus the reduction of Au^{3+} was caused by both the BH^{4-} reducing agent and the Ag; and simultaneously the Ag^{+} formed was reduced by $NaBH_4$, which promoted the intermixing of the metals. The reduction of Au

precursor by metallic Ag was confirmed in a separate experiment, when solution of $HAuCl_4$ and PVA was added to the Ag sol without $NaBH_4$ reducing agent. The sudden disappearance of the yellow color of the Ag sol and the slow evolution of the red color of the bimetallic sol indicated that galvanic replacement reaction took place.

Shibata et al. also observed[170] spontaneous alloying of bimetallic core–shell AuAg nanoparticles at ambient temperature, which was explained by the vacancy defects at the boundary between the two metals. Such defects may be caused by the need to replace the stabilizers at the surface of the particle during synthesis of the shell. In our case similar behavior could also be the reason of the alloy formation in the sol. The diffusion of metals is commonly accepted to proceed via migration of atoms into vacancy defects. A single vacancy at the interface is enough to catalyze fast diffusion. This process is reinforced by the decreased melting point of the metals due to small diameter of the particles.[177]

5.3.4 Structure of the AgAu/SiO_2 catalysts

Table 5.7 presents the actual metal contents and the Ag/Au ratios of the catalysts determined by prompt gamma activation analysis (PGAA), and fit well with the nominal values. AgAu particle sizes of the catalyst samples after calcination at 400^{o}C in synthetic air (by that the organic residues can be removed) and after following reductive treatment in H_2 at 350^{o}C were determined by TEM and the standard deviations which are characteristic of the particle size distribution.

Table 5.7. Metal content and particle sizes of the catalysts determined by PGAA and TEM, respectively.

Catalysts	Ag/Au (%)	Metal content		Particle size (nm)	
		Ag (mmol/ $g_{cat.}$)	Au (mmol/ $g_{cat.}$)	after calcination	after reduction
Au/SiO_2	0/100	0	0.190	4.8 ± 2.4	4.0 ± 2.0
$10Ag90Au/SiO_2$	13/87	0.014	0.093	3.5 ± 2.3	3.1 ± 1.6 ($3.5 \pm 2.0^{*}$)
$20Ag80Au/SiO_2$	23/78	0.025	0.085	2.9 ± 1.2	3.5 ± 1.7
$33Ag67Au/SiO_2$	33/67	0.033	0.067	3.4 ± 2.5	3.3 ± 1.2
$50Ag50Au/SiO_2$	51/49	0.049	0.051	5.2 ± 2.2	-
Ag/SiO_2	100/0	0.092	0	4.8 ± 3.5	4.9 ± 3.6

*Particle size after catalytic reaction.

The mean particle size of pure Au/SiO_2 and pure Ag/SiO_2 sample were similar, 4.8 nm. In the case of Ag/SiO_2 sample the particle size distribution was broad (4.8 ± 3.5 nm) due to several much larger particles with 5–16 nm in diameter beside the numerous particles with 3–4 nm size. In the case of the bimetallic samples the mean particle sizes range between 2.9 and 5.2 nm. In the case of Au/SiO_2 the decreased Au particle size after reduction is surprising. Small changes were observed in the particle sizes after reduction treatments (or catalytic reaction), and the resulting sizes were more similar in the different samples than in the calcined state.

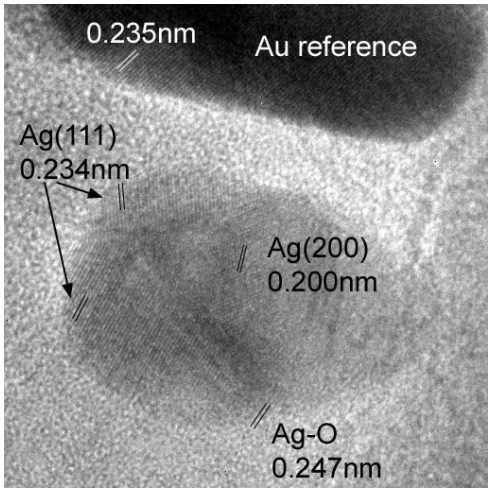

Figure 5.23. HRTEM of Ag/SiO_2 calcined at 400°C. The 0.200nm and 0.234nm fringe periods represent metallic fcc Ag phase. The 0.247 nm period represent Ag–oxide.

HRTEM of monometallic calcined Ag/SiO_2 sample is shown in **Figure 5.23.** Fringe periods of both Ag (0.200 nm and 0.234 nm) and Ag_2O_3 (0.247 nm, PCPDF 72-0607) can be identified in the catalyst particle after calcination in air at 400°C. The precision of this measurement was provided by a comparison with the (111) lattice spacings (0.235 nm) of the Au reference particle visible at the top of **Figure 5.23.** Only a few crystals were found as pure silver-oxide, most part of the particles was in metallic phase. It is worth pointing out that both Ag and Ag–oxide phases were present within one particle (**Figure 5.23)** regardless of the size of the particles in every case where Ag-oxide was observed. HRTEM measurement of $33Ag67Au/SiO_2$ bimetallic catalyst showed mostly metallic Ag(Au) crystals and two-phase contrast was not seen within the particles.

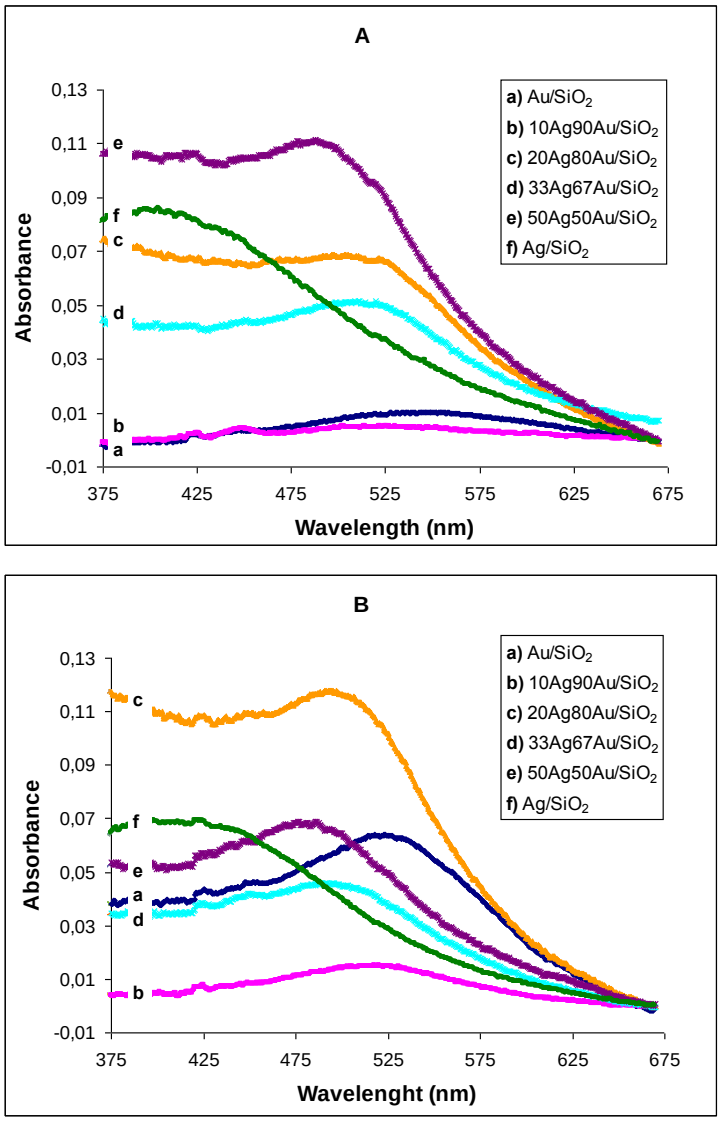

Figure 5.24. UV–visible spectra of $AgAu/SiO_2$ catalysts after calcination in air at 400°C (A), after reduction in H_2 at 350°C (B).

Figure 5.24 shows the UV–visible spectra of the supported catalysts after calcination (A) and after reduction treatment (B). The intensities of the bands are not comparable because – as a

consequence of the measurement method – the catalyst amounts placed on the glass plates were not the same.

Single adsorption bands were detected in the case of all samples after calcination. All surface plasmon resonance (SPR) bands were broad due to the size distribution of the particles. After reduction only single, narrower SPR bands were detected for all catalysts compared to the bands of the calcined samples.

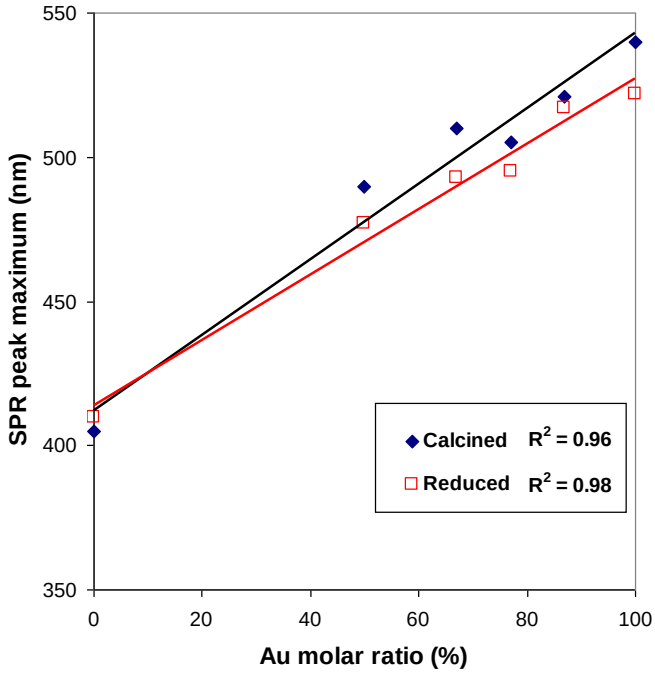

Figure 5.25. UV–visible absorption band maximum of AgAu/SiO_2 catalysts versus Au molar fraction after calcination in air at 400°C and reduction in H_2 at 350°C.

Figure 5.25 shows the correlation between the nominal Au molar ratio and the maximum of surface plasmon bands. The SPR bands shift to higher wavelengths with increasing Au molar ratio. The position of the maximum absorption band is related to the surface

structure and composition beside the particle size.[101,107] In accordance with the literature linear correlation was found in the case of calcined samples and reduced samples showing AgAu alloy structure.

In a recent study[178] on the dependence of the SPR band on the alloy composition the authors found that the correlation between the position of the SPR band and the gold fraction was deviated from linearity and was described by a third–order polynomial function. The composition dependence can be approached by a linear relation between 0.2 and 0.8 gold fraction range only. The authors took into account alloy nanoparticles with diameters between 5 nm and 50 nm as against our work where smaller than 5nm sized particles were studied. The band positions were changed with calcination-reduction treatments in our case. In the calcined samples deviation from linearity can be originated from the somewhat different particle size and may suggest some phase segregation, inhomogeneity of alloy. Reduction pretreatment caused a blue shift of the absorption bands and a diminution of the deviation from linearity suggesting more homogeneous AgAu alloy structures. This effect could be explained by the following: oxygen treatment favors the Ag concentration enhancement on the surface because Ag–oxide formation is thermodynamically favored, but as the temperature raises the decomposition of the preformed oxide is occurred above 250°C.[179] Modification of the surface plasmon of the particles likely reflects this surface structure/geometry change, that can be an important factor affecting the catalytic properties.

The results confirm that the AgAu nanoparticles prepared by our method are AgAu alloy with random distribution of Ag atoms

rather than core–shell AgAu, AuAg or a mixture of Au and Ag nanoparticles.[180]

To determine the oxidation states of the bimetallic nanoparticles close to the surface and the relative surface concentration of Ag and Au XPS spectra were recorded on the catalyst samples after calcination in air at 400°C and after reduction treatment in H_2 at 350°C. **Table 5.8** shows the binding energies of Au $4f_{7/2}$ and Ag $3d_{5/2}$. BE of Au was in the range of 82.9 – 83.2 eV which can be assigned to Au metallic state. Combining Au with Ag the BE of Ag shifts to lower value (366.8 – 367.5 eV) from 368.6 eV measured for calcined Ag/SiO_2 sample. The effect of reduction treatment on the BE was smaller and not really significant in the case of bimetallic catalysts than in the case of pure Ag/SiO_2, in case of that the BE of Ag $3d_{5/2}$ decreased by 1.4 eV.

Table 5.8. XPS data of $AgAu/SiO_2$ catalysts.

Catalysts	**Au binding energy (eV)**		**Ag binding energy (eV)**		**Ag/Au atomic ratio**		
					Bulk*	**Surface**	
	calcined	reduced	calcined	reduced		calcined	reduced
	catalysts		catalysts			catalysts	
Au/SiO_2	83.0	83.0	–	–	–	–	–
$10Ag90Au/SiO_2$	82.9	82.8	367.0	366.8	0.15	0.18	0.17
$20Ag80Au/SiO_2$	82.9	82.8	367.5	367.3	0.29	0.34	0.28
$33Ag67Au/SiO_2$	82.9	83.2	367.0	367.1	0.49	1.14	1.00
$50Ag50Au/SiO_2$	82.9	83.1	367.4	367.3	0.95	1.17	1.17
Ag/SiO_2	–	–	368.6	367.2	–	–	–

* Determined by PGAA.

However, the clear shift of Ag $3d_{5/2}$ band to lower BE in the monometallic Ag/SiO_2 as a result of reducing treatment is in contradiction with the general view about behavior of Ag (according to the literature the BE of Ag $3d_{5/2}$ for metallic Ag is 368.3 eV, while for oxidized Ag varies between 367.3 – 368.0 eV) and our other results. Further experiments are in progress to clarify this unusual behavior of Ag.

The surface atomic ratio of Ag and Au were calculated using sensitivity factors given by the manufacturer and are presented in **Table 5.8**. Surface Ag/Au ratios are only slightly higher than the bulk for the $10Ag90Au/SiO_2$ and $20Ag80Au/SiO_2$ catalysts, but high Ag enrichment on the surface was observed for the $33Ag67Au/SiO_2$.

In the case of $33Ag67Au/SiO_2$ sample the reduction treatment resulted in glucose oxidation activity increase to a higher extent and somewhat lower extent in the case of $20Ag80Au/SiO_2$. Regarding that the mean particle size of the bimetallic particles is the smallest (2.9 nm) in the $20Ag80Au/SiO_2$ sample; it does not mean that the 20/80 is the optimum atomic ratio. These differences might be explained by the decreased surface Ag/Au atomic ratio in the latter reduced **(Table 5.8)** samples compared to the calcined ones, supposing that the optimal Ag/Au surface ratio (at which the activity reached the maximum value) is lower than in calcined $20Ag80Au/SiO_2$.

The inactivity of $50Ag50Au/SiO_2$ cannot be explained only by the different particle size (5.2 nm), the Ag/Au ratio must be a more important factor. Taking into account that the penetration depth of XPS is greater than one monolayer it is possible that the Ag/Au

atomic ratios are higher in the topmost surface layer than the XPS results show and this causes the inactivity of the 50Ag50Au/SiO_2 sample.

5.3.4.1 The role of Ag

The higher activity of the bimetallic samples can be originated from the role of Ag in the oxygen activation during the reaction. Alloying silver with gold induces significant changes in the mode of oxygen adsorption on Ag. Kondarides and Verykios studied[181] the oxygen adsorption properties of α–Al_2O_3 supported silver – gold alloy catalysts using micro–gravimetric and temperature desorption techniques in the temperature range from 30 to 400°C. Three types of adsorbed oxygen species have been proposed on the alloy surface including molecular, atomic and subsurface. Subsurface oxygen diffusion, which is initiated at relatively high adsorption temperatures, inhibited by the presence of Au in the AgAu alloy. The population of atomic oxygen decreases with increasing Au content because of the need of silver multiatom adsorption sites for atomic oxygen adsorption. On pure Au surfaces the dissociative adsorption of O_2 is limited, particle morphology is a key factor influencing O_2 dissociation, it is more favored on low coordinated corner and edge Au atoms highly populated on small particles of about less than 2 nm diameter.[1,182,183,184] In the AgAu alloy molecular oxygen adsorption is favored due to the absence of Ag multiatom sites and the presence of single Ag atoms. In our experimental conditions (at high Au and low Ag content, low temperature, aqueous media) molecular adsorption

could take place on the surface of bimetallic catalysts. The high surface coverage of hydroxide ions in water at high pH also makes difficulties in oxygen dissociation therefore atomic oxygen adsorption is not likely on the surface of our catalysts.

Considering that the ionization potential of Au and Ag is 9.22 and 7.58 eV, respectively; electronic charges could transfer from Ag to Au atoms, but in the case of our bimetallic samples the BE of Au (or Ag) did not depend on the Ag/Au molar ratio. Experimental results with the physical mixture of the monometallic catalysts (no synergistic activity increase was detected in that case) suggested that synergism occurred if Ag atoms were in the vicinity of Au atoms, maximum activity was reached at Ag/Au=20/80. The Ag/Au ratio affected the geometry (size, shape and surface composition) of the particles. Considering the molecular size of glucose (1 nm of diameter[185]) and Ag (or Au) atoms (atomic radius 0.144 nm), the former is much larger than the latter. Consequently for glucose activation multiatom adsorption sites are needed. Considering the size of glucose, oxygen and gold/silver atoms, more space is needed for the surface adsorption of the glucose than the O_2. Oxygen adsorption is preferred on silver rather than on gold and adsorption of other negatively charged species (OH groups, carbonate and bicarbonate species) may be stronger on the positively charged Ag than on Au. The strength of adsorption of these molecules on gold is thought to be weaker compared to silver, therefore the glucose may substitute the pre-adsorbed molecules on the gold surface but not on the silver surface. Thus the O_2, OH adsorption is suggested to be dominant on Ag sites, while glucose adsorption on multiatom Au sites and the

reaction takes place between these species in close vicinity. If the Ag/Au ratio is higher than the ideal one, the adsorption of larger glucose is hindered also on gold. Having not enough extended Au surface lowers the glucose oxidation activity.

5.3.4.2 Hypothetical reaction mechanism

The mechanism proposed for glucose oxidation over our silica supported silver – gold catalysts is consistent with our experimental results and based on previous studies for alcohol oxidation[186] and glucose oxidation on gold catalysts.[69,70,187]

Zope et. al. have studied[186] the oxidation of alcohols over Au/C catalyst with isotopically labeled O_2 or H_2O in order to clarify the origin of oxygen in the product and found that O is originated from hydroxide ions instead of molecular oxygen. Molecular oxygen is thought to be taking part in the reaction by regeneration of the hydroxide through hydrogen peroxide formation and dissociation and by removal of the electrons left on the surface by the OH^- adsorption. The following reaction steps have been suggested (* refers to the surface of the catalyst):

$$[O_2]^* + [H_2O]^* \rightarrow [OOH]^* + [OH]^* \quad \{1\}$$

$$[OOH]^* + [H_2O]^* \rightarrow [HOOH]^* + [HO]^* \quad \{2\}$$

$$[HOOH]^* \rightarrow [OH]^* + [OH]^* \quad \{3\}$$

$$[OH]^* + e^- \leftrightarrow OH^- + {}^* \quad \{4\}$$

Density functional theory calculations[186] on ethanol oxidation over gold surfaces showed the highest activation barriers for the decomposition of peroxide {2} and hydrogen peroxide {3} intermediates. All the other reaction steps showed lower activation barriers.

Study on the decomposition of hydrogen peroxide on silver, gold and silver – gold alloys concluded high activity of silver in this reaction compared to gold.[188] Despite of the activity-reducing effect of gold addition to silver, the alloy showed higher activity than pure gold.

Scheme 3. Suggested reaction scheme for glucose oxidation over $AgAu/SiO_2$ bimetallic catalysts.

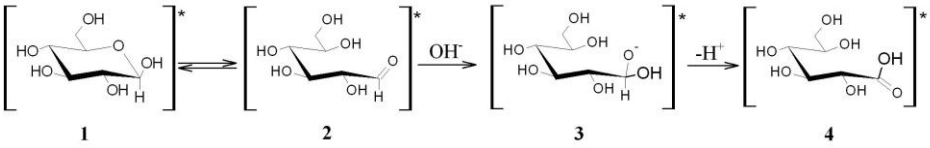

Scheme 3 shows the suggested reaction scheme for glucose oxidation over our bimetallic $AgAu/SiO_2$ catalysts. The glucose adsorbs on the catalysts surface and forms alkoxy intermediate of the geminal diol with adsorbed hydroxide, which is followed by the subsequent elimination of H^+ by the HOO species adsorbed on Ag {5}. This helps the decomposition of the HOOH on silver. The active center of the catalyst should contain Ag and Au in low Ag/Au ratio, where the adsorbed OOH and glucose intermedier **(3)** are close enough to each other to react. **Figure 5.26** shows the schematic

illustration of the active center of the catalyst with the reaction between the adsorbed OOH and glucose.

$$[OOH]_{surf.\ Ag} + [RC\mathit{H}(OH)O]_{surf.\ Au} \rightarrow [\mathit{H}OOH]_{surf.\ Ag} + [RCOOH]_{surf.\ Au} \quad \{5\}$$

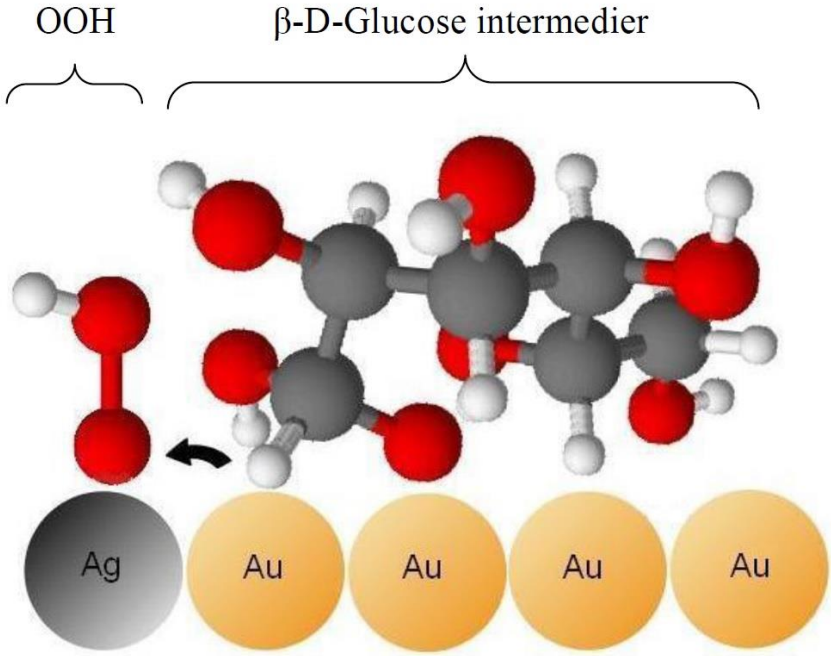

Figure 5.26. Schematic illustration of the reaction between the adsorbed peroxide and the glucose intermedier (**3)** on the catalysts surface.

The higher activity of our bimetallic samples compared to the monometallic Au/SiO_2 catalyst can be explained by the higher decomposition rate of peroxide–species on the surface of the bimetallic catalysts promoted by Ag. Geometry of the metal surface plays an important role in the creation of the active centers.

5.3.5 Conclusions

Ag addition to Au/SiO_2 up to about Ag/Au=33/67 provided synergetic effect in selective glucose oxidation reaction. The AgAu catalysts contained dominantly alloyed metallic particles both after calcination and following reduction treatments. The calcination – reduction pretreatment changes somewhat the particle size and the surface Ag/Au atomic ratio slightly affected the activity of the catalysts, however, the activity order of the samples remained the same. The higher activity of the bimetallic samples could be due to the improved O_2 activating ability provided by Ag sites at optimum surface arrangement The further increase of Ag loading above the ideal concentration may dilute or cover the Au to such an extent that the number of gold ensembles necessary for glucose activation decreases deteriorating the activity.

6 Outlook

Understanding the heterogeneous reactions at molecular level is difficult, because the catalytic activity of a metal is influenced by many parameters such as the dispersion and the morphology of the metal, the electronic structure, the nature and the morphology of the support, the presence of impurities and these are all influenced by each other and may be sensitively depended on the preparation method. That is why the knowledge of the structure – activity relationship is essential to catalyst development. The proper choice of modification of the catalysts can lead us to achieve high performance in a desired reaction.

The reaction specificity of the catalysts was demonstrated by our studies, where the same catalysts were tested in a total oxidation and a selective partial oxidation model reaction. It was surprising that in selective glucose oxidation the small gold particle size does not provide necessarily high activity; the support effect seemed to be a more important factor influencing the activity. It would be worth to carry out further study on the particle size effect on a wider size range in selective glucose oxidation. Moreover understanding the role of the non–reducible oxide support and its most relevant properties determining the catalytic activity would deserve more investigation.

In the case of CeO_2–Au/SiO_2 catalysts the CeO_2 patches were found exclusively on the surface of gold up to 0.6wt% CeO_2 due to the interaction between the Ce species and the stabilizing shell. It would be interesting to apply other stabilizing agents for the preparation of the gold sol, to enhance its attraction towards CeO_2

promotor of larger amount. In this way perhaps more CeO_2 decoration could be deposited on gold and even higher activity could be achieved. The size of the active CeO_2 – Au perimeter could be characterized more precisely using CO–chemisorption measurement followed by infrared spectroscopy.

Significantly higher activity of the bimetallic $AgAu/SiO_2$ catalysts compared to the monometallic ones can be achieved in glucose oxidation. The advantages of our catalysts compared to the previously reported unsupported colloidal catalysts are the organic polymer–free surface of the higher stability NPs and the easy–handling of them. A tentative reaction mechanism was proposed for glucose oxidation over our silica supported silver – gold catalysts. It would be necessary to find further experimental evidences supporting the mechanism advised. Isotopic labeled experiments also would be beneficial. Application of the bimetallic $AgAu/SiO_2$ catalysts would be rewarding in selective oxidation of other oxygen–containing substrates.

During the preparation process of the bimetallic AgAu sols HRTEM and UV-visible spectroscopic measurements showed AgAu alloy formation which is not expected at the temperature of the synthesis (0°C) or at the temperature of storage (ambient temperature). Formation of hexagonal *4H* polytype of Ag was also surprising and that simple synthesis method could be further developed in order to prepare Ag nanoparticles with desired polytype.

The general intention would be to discover the key differences between the required active sites in the total and partial oxidation

processes via the comparison of all the modified catalysts in both types of reactions.

A better fundamental understanding would be achieved with these measurements in the behavior of the studied catalysts described in the previous chapters.

7 Thesis

1. Inverse correlation was found between the activities of supported gold catalysts in CO oxidation and in selective glucose oxidation applying two different size-ranges of reducible oxide (CeO_2 and TiO_2) and non–reducible oxide (SiO_2) supported gold nanoparticles. Both the type of the support and the Au particle size affects the activity of the catalysts in glucose oxidation: the larger–size, non–reducible SiO_2 supported samples showed higher activity, in contrast with the known support and particle size effect of gold catalysts in CO oxidation.

2. CeO_2 decoration on SiO_2 supported Au catalysts derived from Au colloid provided higher CO oxidation activity at already 0.6wt% CeO_2 content compared to the CeO_2 supported Au catalyst, which is caused by the thin, nanosize CeO_2 in contact with gold forming higher activity perimeter than bulk CeO_2 with Au.

3. The activity of the CeO_2 decorated SiO_2 supported Au catalysts did not change above 0.6wt% CeO_2 content. Up to 0.6wt% concentration CeO_2 is attached dominantly onto gold surface and further increase in Ce-loading caused CeO_2 spread over the support surface as well. Strong interaction of limited amount of Ce species with stabilizer ligands around Au nanoparticles is suggested as the reason for CeO_2 localization preferentially on gold up to a given CeO_2 loading.

4. AgAu alloy nanoparticles were proved to be formed during the reduction of $HAuCl_4$ by sodium borohydride in Ag sol at different Ag/Au molar ratios. The alloy structure of the AgAu nanoparticles was retained after adsorption on SiO_2 support and subsequent oxidation and reduction treatments.

5. SiO_2 supported bimetallic AgAu nanoparticles of different Ag/Au molar ratios were applied for the first time in selective glucose oxidation. The catalysts showed synergetic activity increase up to 33/67=Ag/Au molar ratio compared to the monometallic SiO_2 supported Au and Ag catalysts. The activity of the catalysts was similar after oxidation and reduction pretreatments.

6. The nanospherical form of hexagonal *4H*–Ag crystal structure was described for the first time. Reduction of $AgNO_3$ with sodium-borohydride in the presence of polyvinylalcohol results in silver sol with face centered cubic and hexagonal *4H* crystal structured Ag nanoparticles in about the same amount.

8 List of Publications

Related to the Thesis

T. Benkó, A. Beck, K. Frey, D.F. Srankó, O. Geszti, G. Sáfrán, B. Maróti, Z. Schay, *Bimetallic Ag-Au/SiO_2 catalysts: Formation, structure and synergistic activity in glucose oxidation*, Applied Catalysis A: General, 479 (2014) 103-111
IF: 3.410 (2013) C(IC):0(0)

A. Horváth, A. Beck, G. Stefler, **T. Benkó**, G. Sáfrán, Z. Varga, J. Gubicza, L. Guczi, *Silica-Supported Au Nanoparticles Decorated by CeO_2: Formation, Morphology, and CO Oxidation Activity*, Journal of Physical Chemistry C, 115 (42), (2011) 20388-20398
IF: 4.805, C(IC): 7(0)

L. Guczi, A. Beck, **T. Benkó**, Z. Pászti, *Gold Catalysis: Particle Size or Promoting Oxide Morphology?*, MRS Online Proceedings Library, 1351 (2011) mrss11-1351-ff13-02, doi: 10.1557/opl.2011.1168

T. Benkó, A. Beck, O. Geszti, R. Katona, A. Tungler, K. Frey, L. Guczi, Z. Schay, *Selective oxidation of glucose versus CO oxidation over supported gold catalysts*, Applied Catalysis A: General, 388 (2010) 31
IF: 3.383; I(IC): 12(3)

Other publications

A. Beck, G. Magesh, B. Kuppan, Z. Schay, O. Geszti, **T. Benkó**, R. P. Viswanath, P. Selvam, B. Viswanathan, L. Guczi, *Specific role of polymorphs of supporting titania in catalytic CO oxidation on gold*, Catalysis Today, 164(1), (2011) 325-331
IF: 3.407; I(IC): 6(0)

E. Nieddu, L. Mazzucco, P. Gentile, **T. Benkó**, V. Balbo, R. Mandrile, G. Ciardelli, *Preparation and biodegradation of clay composites of PLA*, Reactive and Functional Polymers, 69 (6), (2009) 371-379
IF: 2.461; I(IC): 45(0)

Oral presentations

Hordozós arany-ezüst katalizátorok előállítása és aktivitása glükóz szelektív oxidációjában, **T. Benkó**, A. Beck, K. Frey, G. Sáfrán, D.F. Srankó, Z. Schay,
Tavaszi Szél Konferencia, Debrecen, 21-23 March 2014.

Glükóz szelektív oxidációja hordozós arany katalizátorokon, **T. Benkó**, A. Beck, K. Frey, G. Sáfrán, D.F. Srankó, Z. Schay, XXXVI. Kémiai Előadói Napok, Szeged, 28-30 October 2013.

Research in the Institute of Isotopes, HAS, **T. Benkó**, K. Frey,
Regional Training Course on Nanomaterials and Radiation: Synthesis, Characterization, Applications, University of Reims Champagne Ardenne, Reims, France, 30 November 2009.

Arany nanorészecskék felülethez kötése, Arany katalizátorok előállítása és felhasználása glükóz szelektív oxidációjában, **T. Benkó**, A. Beck, Z. Schay, L. Guczi, Fiatal Kutatók Beszámolója, MTA Kémiai Kutatóközpont, 18 September 2009.

Liquid phase oxidation of glucose over gold catalysts, **T. Benkó**, A. Beck, A. Tungler, L. Guczi, Z. Schay, COST CHEMISRTY D36/003/06 Working Group Meeting, Palermo, 15-16 May 2009.

Posters

Silica-supported bimetallic Ag-Au nanoparticles: Formation, structure and high activity in glucose oxidation, **T. Benkó**, K. Frey, A. Beck, O.Geszti, L. Guczi, Z.Schay, 11th European Congress on Catalysis – EuropaCat-XI, Lyon, France, 1-6 September 2013.

SiO_2 supported Ag-Au alloy nanoparticles with high catalytic activity in selective oxidation of glucose, K. Frey, **T. Benkó**, O. Geszti, L. Guczi, Z. Schay,
Proc. of Final workshop of the COST D36 Action. pp. 39-40., Fuengirola, Spain, 18-20 May 2011.

Supported gold catalysts in selective glucose oxidation and CO oxidation, **T.Benkó**, K. Frey, A. Beck, A. Horváth, L. Guczi, Z. Schay, EFACTS School, Anakara, Turkey, 13-19 September 2010.

Supported gold catalysts in selective oxidation of D-glucose, **T. Benkó**, K. Frey, A. Beck, L. Guczi, A. Tungler, Z. Schay, 10th Pannonian Symposium, Kraków, Poland, 29 August – 2 September 2010.

Selective oxidation of D-glucose versus CO oxidation over supported gold catalysts, **T. Benkó**, A. Beck, A. Horváth, L. Guczi, Z. Schay, The Sixth Tokyo Conference on Advanced Catalytic Science and Technology, Sapporo, Japan, 18-23 July 2010.

Glükóz szelektív oxidációja arany katalizátorokon – hordozó hatás vizsgálata,
T. Benkó, A. Beck, A. Tungler, L. Guczi, Z. Schay, Oláh György Doktori Iskola VII. Konferenciája, 4 February 2010.

Selective d-glucose oxidation over gold catalysts – support effect, **T. Benkó**, A. Beck, L. Guczi, A.Tungler, Z. Schay, COST Chemistry D36 3rd Workshop, Benahavis, Spain, 21-23 October 2009.

Propene total oxidation over gold catalysts: Influence of TiO_2 and CeO_2 decoration on Au / mesoporous SBA-15, **T. Benkó**, A. M. Venezia, L. F. Liotta, G. Pantaleo, A. Beck, L. Guczi , Z. Schay, CLEAR Summer School, Porto Carras, Greece, 24-30 May 2009.

9 References

1. M. Haruta, N. Yamada, T. Kobayashi, S. Iijima, J. Catal. 115 (1989) 301-309.
2. G.C. Bond, C. Louis, D.T. Thompson, Catalysis by Gold; Imperial College Press: London, 2006.
3. T. Mallat, A. Baiker, Annu. Rev. Chem. Biomol. Eng. 3 (2012) 11-28.
4. http://www.gold.org/technology/gold-and-environment
5. M. Haruta, Gold Bull. 37 (2004) 27.
6. P. A. Sermon, G. C. Bond, P. B. Wells, J. Chem. Soc. Faraday Trans. 75 (1979) 385.
7. N. W. Cant, W. K. Hall, J. Phys. Chem. 75 (1971) 2914.
8. W. Vogel, D. A. H. Cunningham, K. Tanaka, M. Haruta, Catal. Lett. 40 (1996) 175.
9. S. D. Lin, M. Bollinger, M. A. Vannice, Catal. Lett. 17 (1993) 245.
10. J. Y. Lee, J. Schwank, J. Catal. 102 (1986) 207.
11. R. Zanella, S. Giorgio, C.R. Henry, C. Louis, J. Phys. Chem. B 106 (2002) 7634.
12. M. Haruta, Catal. Today 36 (1997) 153.
13. L.A. Hermans, J.W. Geus, Stud. Surf. Sci. Catal. 4 (1979) 113.
14. S. Tsubota, D.A.H. Cunningham, Y. Band, M. Haruta, Stud. Surf. Sci. Catal. 91 (1995) 227.
15. B. Bhushan (ed.), Encyclopedia of Nanotechnology, DOI 10.1007/978-90-481-9751-4, Springer: Dordrecht; New York, 2012. pp2621-2630.
16. M.C. Daniel, D. Astruc, Chem. Rev. 104 (2004) 293-346.
17. Beck, A.; Horváth, A.; Stefler, Gy.; Katona, R.; Geszti, O.; Tolnai, Gy.; Liotta, L. F.; Guczi, L. Catal. Today 2008, 139, 180-187
18. L. Guczi, A. Beck, A. Horváth, Z. Koppány, G. Stefler, K. Frey, I. Sajó, O. Geszti, D. Bazin, J. Lynch, J. Mol. Catal. A: Chem. 204-205 (2003) 545-552.
19. A. Beck, G. Magesh, B. Kuppan, Z. Schay, O. Geszti, T. Benkó, R. P. Viswanath, P. Selvam, B. Viswanathan, L. Guczi, Catal. Today, 164(1) (2011) 325-331.

20. F. Porta, L. Prati, M. Rossi, S. Coluccia, G. Martra, Catal. Today 61 (2000) 165.
21. Horváth, A.; Beck, A.; Sárkány, A.; Stefler, Gy.; Varga, Zs.; Geszti, O.; Tóth, L.; Guczi, L. J. Phys. Chem. B 2006, 110, 15417-15425.
22. J.K. Edwards, B.E. Solsona, P.Landon, A.F. Carley, A. Herzing, C.J. Kiely, G.J. Hutchings, J. Catal. 236 (2005) 69-79.
23. J.K. Edwards, B.E. Solsona, P.Landon, A.F. Carley, A. Herzing, M. Watanabe, C.J. Kiely, G.J. Hutchings, J. Mater. Chem. 15 (2005) 4595.
24. G. Riahi, D. Guillemot, M. Polisset-Thfoin, A.A. Khodadadi, J. Fraissard, Catal. Today 72 (2002) 115.
25. A. Sandoval, A. Aguilar, C. Louis, A. Traverse, R. Zanella, J. Catal. 281 (2011) 40-49.
26. R. Brayner, D.d.S. Cunhab, F. Bozon-Verduraz, Catal. Today 78 (2003) 419.
27. M. Bonarowska, J. Pielaszek, W. Juszczyk, Z. Karpinski, J. Catal. 195 (2000) 304.
28. B.D. Chandler, A.B. Schabel, C.F. Blanford, L.H. Pignolet, J. Catal. 187 (1999) 367-384.
29. A.M. Venezia, V.L. Parola, G. Deganello, B. Pawelec, J.L.G. Fierro, J. Catal. 215 (2003) 317.
30. H. Lang, S. Maldonado, K.J. Stevenson, B.D. Chandler, J. Am. Chem. Soc. 126 (2004) 12949.
31. S. Albonetti, T. Pasini, A. Lolli, M. Blosi, M. Piccinini, N. Dimitratos, J.A. Lopez-Sanchez, D.J. Morgan, A.F. Carley, G.J. Hutchings, F. Cavani, Catal. Today, 195(1) (2012) 120-126.
32. L. Liu, X. Guan, Z. Li, X. Zi, H. Dai, H. He, Appl. Catal. B 90 (1–2) (2009) 1-9.
33. G.C. Bond, Gold Bull. 41(3) (2008) 235-241.
34. P.L. Dulong, L.G. Thenard, Ann. Chim. Phys. 23 (1823) 440.
35. P.A. Sermon, Gold Bull. 9 (1976) 129.
36. W.A.Bone, R.V. Wheeler, Phil. Trans. 206A (1906) 1.
37. A.F. Beaton, J.C. Elgin, J.Am.Chem.Soc. 49 (1927) 2426.
38. M. Haruta, T. Kobayashi, H. Sano, N. Yamada, Chem. Lett. 2 (1987) 405.

39. L. Aschwanden, Novel Routes for the Synthesis of Efficient Gold Catalysts in Aerobic Oxidations, PhD dissertation ETH No.19143 Zurich 2010.
40. C.J. Weststrate, A. Resta, R. Westerström, E. Lundgren, A. Mikkelsen, J.N.J. Andersen, Phys. Chem. C 112 (2008) 6900-6906.
41. M. P. Casaletto, A. Longo, A.M. Venezia, A. Martorana, A. Prestianni, Appl. Catal. A: Gen. 30 (2006) 309-316.
42. M. Han, X. Wang, Y. Shen, Ch. Tang, G. Li, R.J. Smith, Phys. Chem. C 114 (2010) 793-798.
43. F. Vindingi, M. Manzoli, A. Chiorino, F. Boccuzzi, Gold Bull. 42 (2009) 106-112.
44. G.C. Bond, D.T. Thompson, Catal. Rev. Sci. Eng. 41 (1999) 319-388.
45. R. Grisel, K.J. Westrate, A. Gluhoi, B.E. Nieuwenuys, Gold Bull. 35 (2002) 39-45.
46. M.M. Schubert, S. Hackenberg, A.C. van Veen, M. Muhler, V. Plzak, R.J. Behm, J. Catal. 197 (2001) 113-122.
47. V. Schwartz, D.R. Mullins, W. Yan, B. Chen, S. Dai, S.H. Overbury, J. Phys. Chem. B 108 (2004) 15782.
48. A. Beck, A. Horváth, Gy. Stefler, M. S. Scurrell, L. Guczi, Top. Catal. 52 (2009) 912-919.
49. F. Somodi, Hordozós arany katalizátorok eliállítása, módosítása és vizsgálata CO oxidációjában, PhD dissertation BME, MTA-KK, Budapest 2009.
50. O.A. Simakova, R.J. Davis, D.Y. Murzin, Biomass Processing over Gold Catalysts, Springer Cham Heidelberg New York Dordrecht London 2013.
51. C.K. Costello, J.H. yang, H.Y. Law, Y. Wang, J.N. Lin, L.D. Marks, M.D. Kung, H.H. Kung, Appl. Catal. A, 243 (2003) 15.
52. L. Fu, N.Q. Wu, J.H. Yang, F. Qu, D.L. Johnson, M.C. Kung, H.H. Kung, V.P. David, J. Phys. Chem. B 109 (2005) 3704.
53. Z.P. Liu, P. Hu, A. Alavi, J. Am. Chem. Soc. 124 (2002) 14770.
54. L. Guczi, D. Horváth, Z. Pászti, L. Toth, Z.E. Horváth, A. Karacs, G. Pető, J. Phys. Chem. B 104 (2000) 3183.
55. G.C. Bond, D.T. Thompson, Gold. Bull. 33 (2000) 41.

56. S.D. Lin, M. Bollinger and M.A. Vannice, Catal. Lett. 17 (1993) 245.
57. M.M. Schubert, S. Hackenberg, A.C.v. Veen, M. Muhler, V. Plzak and R.J. Behm, J. Catal. 197 (2001) 113.
58. A.C. Gluhoi, H.S. Vreeburg, J.W. Bakker, B.E. Nieuwenhuys, Appl. Catal. A: Gen. 291 (2005) 145.
59. A.M. Venezia, G. Pantaleo, A. Longo, G.D. Carlo, M.P. Casaletto, F.L. Liotta, G. Deganello, J. Phys. Chem. B 109 (2005) 2821-2827.
60. G. Yi, Z. Xu, G. Guo, K. Tanaka, Y. Yuan, Chem. Phys. Lett. 479 (2009) 128-132.
61. S. Biella, L. Prati, M. Rossi, J. Catal. 206 (2002) 242-247.
62. S. Biella, G.L. Castiglioni, C. Fumagalli, L. Prati, M. Rossi, Catal. Today 72 (2002) 43.
63. M. Besson, F. Lahmer, P. Gallezot, G. Fleche, J. Catal. 152 (1995) 116–121.
64. M. Besson, P. Gallezot, Catal. Today 57 (2000) 127–141.
65. M. Comotti, C. Della Pina, M. Rossi, J. Mol. Cat. A 251 (2006) 89–92.
66. Y. Önal, S. Schimpf, P. Claus, J. Catal. 223 (2004) 122–133.
67. U. Prüsse, M. Hermann, C. Baatz, N. Decker, Appl. Cat. A 406 (2011) 89.
68. P. Beltrame, M. Comotti, C. Della Pina, M. Rossi, Appl. Catal. A 297 (2006) 1–7.
69. M. Comotti, C. Della Pina, E. Falletta and M. Rossi, Adv. Synth. Catal. 348 (2006) 313-316.
70. C. Della Pina, E. Falletta, M. Rossi, Chem. Soc. Rev. 41 (2012) 350 -369.
71. C. Della Pina, E. Falletta, M. Rossi and A. Sacco, J. Catal. 263 (2009) 92-97.
72. M. Comotti, C. Della Pina, R. Matarrese, M. Rossi, Angew. Chem. Int. Ed. 43 (2004) 5812-5815.
73. A. Stephen, K. Hashmi Chem. Rev. 107 (2007) 3180–3211.
74. M. Comotti, C. Della Pina, M. Rossi, R. Mataresse, Appl. Catal. A 291 (2005) 204-209.
75. P. Beltrame, M. Comotti, C. Della Pina, M. Rossi, J. Catal. 228 (2004) 282-287.
76. T. Ishida, N. Kinoshita, H. Okatsu, T. Akita, T. Takei, M. Haruta, Angew. Chem. Int. Ed. 47 (2008) 9265-9268.

77. H. Okatsu, N. Kinoshita, T. Akita, T. Ishida, M. Haruta, Appl. Catal. A 369 (2009) 8-14.
78. P. Landon, P.J. Collier, A.F. Carley, D. Chadwick, A.J. Papworth, A. Burrows, C.J. Kiely, G.J. Hutchings, Phys. Chem. Chem. Phys. 5 (2003) 1917.
79. N. Macleod, J.M. Keel, R.M. Lambert, Appl. Cat. A: Gen. 261 (2004) 37.
80. D.J. Enache, J.K. Edwards, P. Landon, B. Solsona-Espriu, A.F. Carely, A.A. Herzing, M. Watanabe, C.J. Kiely, D.W. Knight, G.J. Hutchings, Science 311 (2006) 362.
81. X. Wang, N.S. Venkataramanan, H. Kawanami,Y. Ikushima, Green Chem. 9 (2007) 1352.
82. L. Kesavan, R. Tiruvalam, M.H. Ab Rahim, M. Izham bin Saiman, D.I. Enache, R.L. Jenkins, N. Dimitratos, J.A. Lopez, S.H. Taylor, D.W. Knight, C.J. Kiely, G.J. Hutchings, Science 331 (2011) 195.
83. A. Villa, A. Gaiassi, M. Veith, L. Prati, Angew. Chem. Int. Ed. 49 (2010) 4499-4502.
84. D. Liang, J. Gao, J. Wang, P. Chen, Z. Hou, Catal. Commun. 10 (2009) 1586.
85. A. Wittstocks, V. Zielasek, J. Biener, C.M. Friend, M. Baeumer, Science, 327 (2010) 319.
86. C. D. Pina et al., J. Catal., 260 (2008) 384-386.
87. F. Besenbacher, I. Chorkendorff, B.S. Clausen, B. Hammer, A.M. Molenbroek, J.K. Norskov, I. Stensgaard, Science 279 (1998) 1913.
88. J.M Yan, X.B. Zhang, T.Akita, M. Haruta, Q. Xu, J. Am. Chem. Soc. 132 (2010) 5326.
89. L.C. Liu, X. Guan, Z.M. Li, X.H. Zi, H.X. Dai, H. He, Appl. Catal. B: Environ. 90 (2009) 1.
90. A. Gomez-Cortes, J. Phys. Chem, 113 (2009) 9710-9720.
91. T. Streethawong, Catalysis Letters, 138 (2010) 160-170.
92. X. Huang, X. Wang, X. Wang, X. Wang, M. Tan, W. Ding, X. Lu, J.Catal. 301 (2013) 217-226.
93. S. Tokonami, N. Morita, K. Takasaki, N. Toshima, J. Phys. Chem. C 114 (2010) 10336-10341.
94. M. C. Daniel, D. Astruc, Chem. Rev. 104 (2004) 293-346.
95. H. Shi, L. Zhang, W. Cai, J. Appl. Phys. 87(3) (2000) 1572-1574.

96. X. Liu, A. Wang, L. Li, T. Zhang, C. Y. Mou, J. F. Lee, Prog. Nat. Sci. Mat. Int. 23(3) (2013) 317-325.
97. A. Wang, X. Y. Liu, C.Y. Mou, T. Zhang, J. Catal. 308 (2013) 258-271.
98. C. W. Yen, M. L. Lin, A. Wang, S. A. Chen, J. M. Chen, C. Y. Mou, J.Phys.Chem.C. 113 (2009) 17831-17839.
99. Z. Qu, Guozhou Ke, Y. Wang, M. Liu, T. Jiang, J. Gao, Appl. Surf. Sci. 277 (2013) 293-301.
100. A. Sandoval, A. Aguilar, C. Louis, A. Traverse, R. Zanella, J. Catal. 281 (2011) 40-49.
101. A. Q. Wang, C. M. Chang, C. Y. Mou, J. Phys. Chem. B 109 (2005) 18860-18867.
102. A. Q. Wang, J. H. Liu, S.D. Lin, T. S. Lin, C. Y. Mou, J. Catal. 233 (2005) 186-197.
103. M. Comotti, C. Della Pina, M. Rossi: J. Mol. Cat. A 251 (2006) 89-92.
104. S. Hermans, A. Deffernez, M. Devillers, Catal. Today 157 (2010) 77–82.
105. H. Zhang, T. Watanabe, M. Okumara, M. Haruta, N. Toshima, Nat. Mater. 11 (2012) 49-52.
106. H. Zhang, N. Toshima, J. Colloid Interface Sci. 394 (2013) 166-176.
107. H. Zhang, N. Toshima, App. Cat. A 447-448 (2012) 81-88.
108. H. Zhang, M. Okumura, N. Toshima, J. Phys. Chem. C 115 (2011) 14883-14891.
109. H. Zhang, N. Toshima, App. Cat. A 400 (2011) 9-13.
110. H. Zhang, N. Toshima, Catal. Sci. Technol. 3 (2013) 268-278.
111. A. Beck, A. Horváth, A. Sárkány, L. Guczi, Current Appl. Phys. 6 (2) (2006) 200-204.
112. G. Pető, G.L. Molnár, Z. Pászti, O. Geszti, A. Beck and L. Guczi, Mat. Sci. and Eng. C 19 (2002) 95.
113. L. Guczi, G. Pető, A. Beck, K. Frey, O. Geszti, G. Molnár and C. Daróczi, J. Am. Chem. Soc., 125(14) (2003) 4332-4337.
114. G. Pető, O. Geszti, G. Molnár, Cs. Daróczi, A. Karacs, L. Guczi, A. Beck and K. Frey, Mat. Sci. Eng. *C* 23 (2003) 733-736.
115. L. Guczi, G. Pető, A. Beck, Z. Pászti, Topics in Catalysis 29 (2004) 129-138.
116. L. Guczi, K. Frey, A. Beck, G. Pető, Cs. Daróczi, N. Kruse, S. Chenakin, Appl. Catal. A 291 (1-2) (2005) 116-125.
117. K. Frey, A. Beck, G. Pető, G. Molnár, O. Geszti, L. Guczi, Catal. Commun. 7 (2) (2006) 64-67.

118. L. Guczi, Z. Pászti, K. Frey, A. Beck, G. Pető, Cs. Daróczy, Topics in Catal. 39 (3-4) (2006) 137-143.
119. K. Frey, G. Pető, K.V. Josepovits, L. Guczi, Vacuum, 86 (6) (2012) 745-749.
120. A.M. Venezia, F.L. Liotta, G. Pantaleo, A. Beck, A. Horváth, O. Geszti, A. Kocsonya, L. Guczi, Appl. Catal. A 310 (2006) 114-121.
121. L. Guczi, A. Beck, K. Frey, Gold Bulletin 42 (2009) 5-12.
122. A.M. Venezia, L. F. Liotta, G. Pantaleo, V. La Parola, G. Deganello, A. Beck, Zs. Koppány, K. Frey, D. Horváth and L. Guczi, Appl. Catal. A 251 (2003) 359-368.
123. A. Beck, A. Horváth, Z. Schay, G. Stefler, Z. Koppány, I. Sajó, O. Geszti, L. Guczi, Topics in Catal. 44 (1-2) (2007) 115-121.
124. I. Szalóki, J. Osán, R.E. Van Grieken, Analytical Chemistry**,** 76 (2004) 3445-3470.
125. P.V. Espen, K. Janssens, J. Nobels, J. Chemometrics and Intell. Labor System **1985,** *1*, 109-114
126. Zs. Révay, T. Belgya: Principles of PGAA method, in: Handbook of Prompt Gamma Activation Analysis with Neutron Beams, (G.L. Molnár ed.), Kluwer Academic Publishers, Dordrecht/Boston/New York, 2004, pp.1–30.
127. L. Szentmiklósi, T. Belgya, Zs. Révay, Z. Kis, J. Radioanal. Nucl. Chem. 286 (2010) 501–505.
128. Zs. Révay, T. Belgya, G.L. Molnár, J. Radioanal. Nucl. Chem. 265 (2005) 261–265.
129. Zs. Révay, Anal. Chem. 81 (2009) 6851–6859.
130. Zs. Révay, R. B. Firestone, T. Belgya, G. L. Molnár, Catalog and Atlas of Prompt Gamma Rays, in: Handbook of Prompt Gamma Activation Analysis with Neutron Beams, (G.L. Molnár ed.), Kluwer Academic Publishers, Dordrecht/Boston/New York, 2004, pp. 173–364.
131. D.R. Lide, CRC Handbook of Chemistry and Physics, 88th edition, 2007-2008.
132. A.A. Herzing, C.J. Kiely, A.F. Carley, P. Landon, G.J. Hutchings, Science 321 (2008) 1331-1335.
133. D. Andreescu, E. Matijevic, D.V. Goia, Coll. Surf. A: Physicochem. Eng. Aspects 291 (2006) 93-100.
134. Q. Yuan, H.H. Duan, L.L. Li, L.D. Sun, Y.W. Zhang, C.H. Yan, J. Coll. Int. Sci. 335 (2009) 151-167.
135. M.H. Oh, J.S. Nho, S.B. Cho, J.S. Lee, R.K. Singh, Materials Chem. Phys. 124 (2010) 134-139.

136. A.A. Athawale, M.S. Bapat, P.A. Desai, J. Alloys and Compounds 484 (2009) 211-217.
137. B. Djuricic, S. Pickering, J. European Ceram. Soc. 19 (1999) 1925-1934.
138. F. Zhang, S.P. Yang, H.M. Chen, X.B. Yu, Ceram. Int. 30 (2004) 997-1002.
139. E. Kockrick, Ch. Schrage, A. Grigas, D. Geiger, S. Kaskel, J. Sol. State Chem. 181 (2008) 1614-1620.
140. T.S. Anirudhan, P.S. Suchithra, Appl. Clay Sci. 42 (2008) 214-223.
141. A. Ohyoshi, E. Ohyoshi, H. Ono, S. Yamanaka, J. Inorg. Nucl. Chem. 34 (1972) 1955-1960.
142. H. Holness, Anal. Chim. Acta 3 (1949) 290-294.
143. T. Masui, H. Hirai, N. Imanaka, G. Adachi, T. Sakata, H. Mori, J. Mat. Sci. Lett. 21 (2002) 489-491.
144. V.K. Ivanov, O.S. Polezhaeva, A.S. Shaporev, A.E. Baranchikov, A.B. Shcherbakov, A.V. Usatenko, Russian J. Inorg. Chem. 55 (2010) 328-332.
145. J. Rebellato, M. Natile, A. Glisenti, Appl. Catal. A 339 (2008) 108-120.
146. C. Marcilly, P. Courty, B. Delmon, J. Am. Ceram. Soc. 53 (1970) 56-57.
147. N.A. Oladoja, Y.B Alliu, Ofomaja, A. E.; Unuabonah, I. E. Desalination 271 (2011) 34-40.
148. C.R Stanek, A.H. Tan, S.L Owens, R.W. Grimes, J. Mater. Sci. 43 (2008) 4157-4162.
149. F. Niu, D. Zhang, L. Shi, X. He, H. Li, H. Mai, T. Yan, Mat. Letters 63 (2009) 2132-2135.
150. X.S. Huang, H. Sun, L.C. Wang, Y.M. Liu, K.N. Fan, Y. Cao, Appl. Catal. B: Environmental 90 (2009) 224-232.
151. D. Widmann, R. Leppelt, R.J. Behm, J. Catal. 251 (2007) 437-442.
152. C.J. Weststrate, R. Westerström, E. Lundgren, A. Mikkelsen, J.N. Andersen, A.J. Resta, J. Phys. Chem. C 113 (2009) 724-728.
153. V. Shapovalov, H.J. Metiu, J. Catal. 245 (2007) 205-214.
154. M. Baron, O. Bondarchuk, D. Stacchiola, S. Shaikhutdinov, H.J. Freund, J. Phys. Chem. C 113 (2009) 6042-6049.
155. S. Tsunekawa, R. Sivamohan, S. Ito, A. Kasuya, T. Fukuda, Nanostructured Materials 11 (1999) 141-147.

156. Z. Chen, Q. Gao, Appl. Catal. B 84 (2008) 790-796.
157. M.J. Beier, T.W. Hansen, J.D. Grunwaldt, J. Catal. 266 (2009) 320-330.
158. K. Qian, S. Lv, X. Xiao, H. Sun, J. Lu, M. Luo, W. Huang, J. Mol. Cat. A : Chem. 306 (2009) 40-47.
159. L. Escamilla-Perea, R. Nava, B. Pawelec, M.G. Rosmaninho, C.L. Peza-Ledesma J.L.G. Fierro, Appl. Catal. A 381 (2010) 42-53.
160. Z. Zhou, M. Flytzani-Stephanopoulos, H. Saltsburg, J. Catal. 280 (2011) 255-263.
161. X. Liu, J. Luo, J. Zhu, Nano Lett. 6 (3) (2006) 408-412.
162. I. Chakraborty, D. Carvalho, S. N. Shirodkar, S. Lahiri, S. Bhattacharyya, R. Banerjee, U. Waghmare, P. Ayyub, J. Phys.:Condens. Matter 23 (2011) 325- 401.
163. F. Ernst, M.W. Finnis, D. Hofmann, T. Muschik, U. Schönberger, U. Wolf, and M. Methfessel, Phys. Rev. Lett. 69 (1992) 620-623.
164. P. Taneja, R. Banerjee, P. Ayyub, R. Chandra, G. K. Dey, Phys. Rev. B 64 (2001) 033 405.
165. A. Singh, A. Ghosh, J. Phys. Chem. C 112 (2008) 3460-3463.
166. C. Liang, K. Terabe, T. Hasegawa, M. Aono, Jpn. J. Appl. Phys. 45 (2006) 6046-6048.
167. C. C. Yang and S. Li, J. Phys. Chem. C 112 (2008) 16400–16404.
168. T.K. Huang, T.H. Cheng, M.Y. Yen, W.H. Hsiao, L.S. Wang, F.R. Chen, J.J. Kai, C.Y. Lee, H.T. Chiu, Langmuir 23 (2007) 5722-5726.
169. A. Sárkány, O. Geszti, G. Sáfrán, App. Cat. A 350 (2008) 157-163.
170. T. Shibata, B. A. Bunker, Z. Zhang, D. Meisel, C. F. Vardeman II, J. D. Gezelter, J. Am. Chem. Soc. 124 (2002) 11989-11996.
171. H. Yasuda, H. Mori, M. Komatsu, K. Takeda, J. Appl. Phys. 73 (1993) 1100-1103.
172. H. Yasuda, H. Mori, Phys. Rev. Lett. 69 (1992) 3747-3750.
173. H. Yasuda, H. Mori, Philos. Mag. A 73 (1996) 567-573.
174. H. Mori, H. Yasuda, Mater. Sci. Eng. A 217/218 (1996) 244-248.

175. V. Abdelsayed, K.M. Saoud, M. Samy El-Shall, J. Nanopart. Res. 8 (2006) 519-531.
176. M. P. Mallin, C. J. Murphy, Nano Letters 2(11) (2002) 1235-1237.
177. P. Mulvaney, Langmuir 12 (1996) 788-800.
178. S. W. Verbruggen, M. Keulemans, J. A. Martens, S. Lenaerts, J. Phys. Chem. C 117 (2013) 19142-19145.
179. S. Karski, I. Witońska, J. Rogowski, J. Gołuchowska, J. Mol. Catal. A 240 (2005) 155-163.
180. Y. Iizuka, A. Kawamoto, K. Akita, M. Daté, S. Tsubota, M. Okumura, M. Haruta, Catal. Lett. 97(3-4) (2004) 203-208.
181. D. I. Kondarides, X. E. Verykios, J. Catal. 158 (1996) 363–377.
182. M. Boronat, A. Corma, Dalton Trans. 39 (2010) 8538-8546.
183. B. Hvolbaek, T.V.W. Janssens, B.S. Clausen, H. Falsig, C.H. Christensen, J. K. Norskov, Nano Today 2 (4) (2007) 14-18.
184. X. Deng, B.K. Min, A. Guloy, C.M.Friend, J. Am. Chem. Soc 127 (2005) 9267-9270.
185. W. G. Ferrier, Acta Cryst. 13 (1960) 678-679.
186. B. N. Zope, D. D. Hibbitts, M. Neurock, R. J. Davis, Science 330 (2010) 74-78.
187. T. Mallat, A. Baiker, Chem. Rev. 104 (2004) 3037-3058.
188. K. Goszner, H. Bischof, J.Catal. 32 (1974) 175-182.

10 Appendix

Table A.1. List of the investigated catalysts

Catalysts	Support	Modification	Preparation method
Au-SiO_2-PVA	SiO_2	–	Au sol adsorption
Au-TiO_2-PVA	TiO_2	–	Au sol adsorption
Au-CeO_2-PVA	CeO_2	–	Au sol adsorption
Au-SiO_2-TC	SiO_2	–	Au sol adsorption
Au-TiO_2-TC	TiO_2	–	Au sol adsorption
Au-CeO_2-TC	CeO_2	–	Au sol adsorption
ACe0.04	SiO_2	0.04 wt% CeO_2	(Ce – Au) sol adsorption
ACe0.08	SiO_2	0.08 wt% CeO_2	(Ce – Au) sol adsorption
ACe0.16	SiO_2	0.16 wt% CeO_2	(Ce – Au) sol adsorption
BCe0.06	SiO_2	0.06 wt% CeO_2	Au/SiO_2 imp. by $Ce(NO_3)_3$
BCe0.11	SiO_2	0.11 wt% CeO_2	Au/SiO_2 imp. by $Ce(NO_3)_3$
BCe0.60	SiO_2	0.60 wt% CeO_2	Au/SiO_2 imp. by $Ce(NO_3)_3$
BCe1.14	SiO_2	1.14 wt% CeO_2	Au/SiO_2 imp. by $Ce(NO_3)_3$
BCe2.64	SiO_2	2.64 wt% CeO_2	Au/SiO_2 imp. by $Ce(NO_3)_3$
BCe7.40	SiO_2	7.40 wt% CeO_2	Au/SiO_2 imp. by $Ce(NO_3)_3$
Au/SiO_2	SiO_2	–	Au sol adsorption
Au/CeO_2	CeO_2	–	Au sol adsorption
Ag/SiO_2	SiO_2	–	Ag sol adsorption
10Ag90Au/SiO_2	SiO_2	10% Ag–90% Au	(Ag – Au) sol adsorption
20Ag80Au/SiO_2	SiO_2	20% Ag–80% Au	(Ag – Au) sol adsorption
33Ag67Au/SiO_2	SiO_2	33% Ag–67% Au	(Ag – Au) sol adsorption
50Ag50Au/SiO_2	SiO_2	50% Ag–50% Au	(Ag – Au) sol adsorption
Au/SiO_2	SiO_2	–	Au sol adsorption

NYILATKOZAT

Alulírott Benkó Tímea kijelentem, hogy ezt a doktori értekezést magam készítettem és abban csak a megadott forrásokat használtam fel. Minden olyan részt, amelyet szó szerint, vagy azonos tartalomban, de átfogalmazva más forrásból átvettem, egyértelműen, a forrás megadásával megjelöltem.

Budapest, 2014. augusztus 27.

Benkó Tímea